Understanding Structure-Rheology Relationships of Biopolymer Solutions

Raja, A.

DOI
10.4233/uuid:e9e803ad-37b0-4d36-8bf8-3aba796bc173

Publication date
2025

Document Version
Final published version

Citation (APA)
Raja, A. (2025). *Understanding Structure-Rheology Relationships of Biopolymer Solutions*. [Dissertation (TU Delft), Delft University of Technology]. https://doi.org/10.4233/uuid:e9e803ad-37b0-4d36-8bf8-3aba796bc173

Understanding Structure-Rheology Relationships of Biopolymer Solutions

Anand Raja

Propositions

accompanying the dissertation

Understanding Structure-Rheology Relationships of Biopolymer Solutions

by

Anand RAJA

1. Osmotic pressure would be a good benchmark to measure a biopolymer's molar mass. (*Chapter 2*)
2. Power laws do not capture the physical phenomena at the intersection of relevant concentration scales for polymers. (*Chapter 3*)
3. Even minute changes to the inorganic composition of extracellular "polymeric" substances can have major impacts to their properties. (*Chapter 4*)
4. All foams are gels, whereas all gels are not foams. (*Chapter 5*)
5. Theories come and go, but experiments stay forever. (*Henk Lekkerkerker*)
6. Our deepest fear is not that we are inadequate. Our deepest fear is that we are powerful beyond measure. (*Marianne Williamson*)
7. Humanity managed to harness the elements before actually understanding them. By analogy engineering comes naturally, but science does not.
8. The closing of "Pandora's box", through the sequestration of CO_2 emissions from the atmosphere, challenges the second law of thermodynamics.
9. The unwritten expectation of Dutch proficiency makes research universities across The Netherlands less socially safe. (*Based on - Plan for change: towards a socially safe TU Delft - 15 May 2024*)
10. To become a good principal investigator (PI) in the field of science, one must first become a good technician.

These propositions are regarded as opposable and defendable, and have been approved as such by the promotor Prof. dr. Stephen J. Picken and copromoter Dr. Philipp K. Wilfert.

Understanding Structure-Rheology Relationships of Biopolymer Solutions

UNDERSTANDING STRUCTURE-RHEOLOGY RELATIONSHIPS OF BIOPOLYMER SOLUTIONS

Dissertation

for the purpose of obtaining the degree of doctor
at Delft University of Technology
by the authority of the Rector Magnificus, Prof. dr. ir. T.H.J.J. van der Hagen;

Chair of the Board for Doctorates
to be defended publicly on
Monday, 23 June 2025 at
10:00 o'clock

by

Anand RAJA

Master of Science, Delft University of Technology, The Netherlands
born in New Delhi, India

This dissertation has been approved by the promotors.

Composition of the doctoral committee:

Rector Magnificus,	chairperson
Prof. dr. S. J. Picken,	Delft University of Technology, *promotor*
Dr. P. K. Wilfert,	Delft University of Technology, *copromotor*
Independent members:	
Prof. dr. ir. P. D. Anderson,	Eindhoven University of Technology
Dr. P. E. Boukany	Delft University of Technology
Dr. C. Chassagne	Delft University of Technology
Prof. dr. J. H. van Esch	Delft University of Technology
Prof. dr. ir. J. T. Padding	Delft University of Technology

Dr. C. Chassagne, as an external member, participated in the initial discussions pertaining to Subsection 3.7.2 in Chapter 3.

This research was funded by Top consortium for Knowledge and Innovation Chemistry (Topsector Chemie) and Royal HaskoningDHV under the collective framework to characterise biopolymers from waste streams.

Keywords: Biopolymers, Extracellular Polymeric Substances, Charge, Rheology, Intrinsic Viscosity, Herschel-Bulkley model, Yield Stress

Printed by: Proefschriftspecialist, The Netherlands

Cover by: Anand Raja

ISBN 978-94-6384-798-8

An electronic copy of this dissertation is available at
https://repository.tudelft.nl/.

Everything flows,
And so too should biopolymers.

CONTENTS

SAMENVATTING

De term *biopolymeer* kan worden gebruikt om macromoleculen te beschrijven die afkomstig zijn uit een breed scala van biologische bronnen. In het licht van de groeiende bezorgdheid over het gebruik van niet-biologisch afbreekbare synthetische polymeren, dienen ze als ideale vervanging voor een breed assortiment aan technische toepassingen. Gezien de veelzijdigheid van de (geladen en ongeladen) verbindingen die met elkaar een biopolymeren vormen, is er een aanzienlijke onzekerheid bij het vaststellen van de exacte chemische structuur. De aanwezigheid van geladen groepen in de structuur van het biopolymeer bemoeilijkt de zaken nog verder aangezien ze gevoelig zijn voor parameters zoals zuurgraad (pH) en concentratie van ionen (geleiding). Dit vormt een uitdaging voor de traditionele fysische modellen die polymeren beschrijven in specifieke oplosmiddelen.

Het werk dat in dit proefschrift wordt gepresenteerd, probeert deze beperkingen te overwinnen door middel van een abstracte en geïdealiseerde beschrijving van de structuur. De specifieke kennis over het type ladingen aanwezig in het biopolymeer en parameters zoals pH en ionische geleidbaarheid worden hiervoor gebruikt. Bovendien worden opzettelijke veranderingen aangebracht in de pH en de geleidbaarheid door specifieke (tegen)ionen toe te voegen waarvan bekend is dat zij de thermodynamische stabiliteit van het biopolymeer in oplossing beïnvloeden. Deze veranderingen omvatten zowel aanpassingen aan de conformatie van de biopolymeer kluwens, door elektrostatische interacties als intermoleculaire interacties, tussen naburige biopolymeer kluwens, door de vorming van (zwakke → sterke) fysische bindingen. Uiteraard hebben de bijbehorende veranderingen in structurele conformaties een voorspelbare invloed op de eigenschappen van biopolymeer-oplossingen, wat in dit geval wordt vastgelegd met behulp van *rheologie*, d.w.z. de studie van de vervorming van (vaste, vloeibare en viscoelastische) materialen onder invloed van een externe mechanische spanning.

Rheologie wordt specifiek gebruikt om veranderingen in de volgende parameters te bepalen, de *intrinsieke viscositeit*: wat een maat is voor de grootte van de opgeloste macromoleculen; de *Herschel-Bulkley consistency index*: wat een maat is voor de viskeuze dissipatie van geconcentreerde biopolymeer-oplossingen, de *opslagmodulus* en tenslotte de *vloeispanning*. Deze laatste twee parameters bieden gezamenlijk kwantitatief inzicht in de pakking van zwakgebonden biopolymeer deeltjes. Deze veranderingen in de rheologische eigenschappen van verschillende representatieve biopolymeer systemen, worden vervolgens gebruikt om relevante structuur-eigenschapsrelaties af te leiden die kunnen worden benut voor technisch relevante toepassingen.

De gezamenlijke inzichten die zijn verkregen door het vaststellen van deze structuur-

eigenschapsrelaties, worden gecombineerd om een eenvoudige rheologische test te ontwerpen. Dit eenvoudige experiment is praktisch relevant om de kwaliteit van nieuwe biopolymeer formuleringen in een productie omgeving te faciliteren en om geschikte aanpassingen aan de bestaande extractie protocollen mogelijk te maken.

SUMMARY

The term *biopolymers* may be used to describe macromolecules that are obtained from a wide variety of biological sources. In the wake of growing concerns surrounding the use of non-biodegradable synthetic polymers, they serve as ideal replacements for a wide range of engineering applications. However, given the versatility of (charged or uncharged) chemical species that form biopolymers, there are considerably large uncertainties in determining their exact chemical structure. The presence of charged species in biopolymers further complicates matters, as they remain sensitive to parameters such as acidity (pH) and ionic strength (conductivity), thereby challenging the traditional physical models that describe polymer dissolved within specific solvents.

The work presented in this thesis tries to overcome these limitations through an abstract and idealised description of their structure, using both, specific knowledge about the type of charges present within the biopolymer, as well as parameters such as pH and conductivity. Further, intentional changes are made to the pH and conductivity by introducing specific (counter) ions that are known to influence the thermodynamic stability of the biopolymer in solution. These include both, changes to the conformation of the biopolymers coils due to electrostatic interactions, as well as intermolecular interactions between neighbouring biopolymer coils due to the formation of (weak → strong) physical bonds. Naturally, the accompanying changes to the structural conformations has an predictable influence on the properties of the biopolymer solution, which in this case is captured using *rheology*, i.e. the deformation of (solid, liquid and viscoelastic) materials due to the application of a load.

Specifically, rheology is used to track changes to the following parameters, the *intrinsic viscosity*: which is a measure for the size of the dissolved macromolecules, the *Herschel-Bulkley consistency index*: which is a measure for the viscous dissipation of concentrated biopolymer solutions, and the *storage modulus* and the *yield stress*. These latter two parameters collectively provide quantitative insight about the packing of weakly bonded biopolymer gel particles. In turn this information, i.e. changes to the rheological properties of a wide variety of representative biopolymer systems, is used to derive relevant structure-property relationships that may be exploited for engineering applications.

Finally, the collective insight gained by establishing these structure-property relationships is condensed to provide a simple rheology experiment. This simple experiment is practically relevant to ensure the on site quality of novel biopolymer formulations, as well as to aid suitable modifications to the existing extraction protocol.

1

INTRODUCTION

I would like to describe a field, in which little has been done, but in which an enormous amount can be done in principle. This field is not quite the same as the others in that it will not tell us much of fundamental physics (in the sense of, "What are the strange particles?") but it is more like solid-state physics in the sense that it might tell us much of great interest about the strange phenomena that occur in complex situations. Furthermore, a point that is most important is that it would have an enormous number of technical applications.

What I want to talk about is the problem of manipulating and controlling things on a small scale.

Richard P. Feynman

1

1.1. WHAT IS A POLYMER ?

THE interdisciplinary field of materials science is heavily reliant on the characterisation of a material's structure-property relationships, thereby enabling a variety of engineering applications [1]. Owing to its interdisciplinary nature however, it equally masks the distinction between multiple branches of natural sciences. Hence, when trying to formulate a formal definition for polymer materials, it is worthwhile to provide both, a physical as well as a chemical definition. From the perspective of physics, polymers are linear or branched, nanoscale (at least in one spatial dimension), molecular chains that are susceptible to *soft* thermodynamic interactions in the order of $k_B T$ [2]. Here, k_B refers to the Boltzmann constant (only ~ 1.38 x 10^{-23} J/K or ~ 3.30 x 10^{-27} kcal/°C) and T refers to (room) temperature. The nature of these interactions are between (segments of) a polymer chain and its surrounding medium, i.e. a solvent or other polymer chains, or indeed between segments of the same chain. Based on the favourability of these interactions, the polymer may either be flexible, semi-flexible, or rigid [2]. By contrast, the International Union of Pure and Applied Chemistry (IUPAC) define a polymer (or macromolecule) as "a molecule of high relative molecular mass, the structure of which essentially comprises the multiple repetition of units derived, actually or conceptually, from molecules of low relative molecular mass" [3]. Given the somewhat ambiguous use of the term "high" and "low", IUPAC further clarify that if the addition (or removal) of further repeating units has a negligible effect on the molecular properties, then it may be considered as having a "high relative molecular mass".

In the discussion presented here, as well as the subsequent chapters, the term *polymer* is used interchangeably to reference both, the physical as well as the chemical system. However, as the physical structure-property relationships of (bio)polymers are of predominant interest, it is worth highlighting that the former definition takes precedence, and is therefore used more widely within this thesis.

1.2. WHAT IS A BIOPOLYMER ?

Broadly speaking, it is possible to draw a distinction between polymers that are manufactured synthetically, and those that are available from natural sources [2]. Certainly, upon surveying the surroundings of an individual's household, it is possible to identify the synthetically produced polymers. These include plastics that may be found in consumer healthcare products, electronic devices and furniture, food and grocery packaging films, the painted walls of a house, the synthetic fabrics found within shoes and clothing, etc.

On the other hand, polymers obtained from natural sources have been used for centuries, and include materials such as natural rubber [2], as well as the cellulose found within the paper sheets of this thesis. The term "natural" refers to the fact that the latter subset of polymers are produced by biological sources. They are therefore also referred to as *biopolymers*. Certainly then, these biopolymers need not be limited to commonplace items, and may be present in a wide variety of

biological sources. Indeed, important biomolecules such as deoxyribonucleic acid (DNA), proteins, and polysaccharides such as starch are also biopolymers [4].

Among these biopolymers, it is possible to identify a subset that possess charged sites (or functional groups) along the length of their chains. Some ubiquitous examples of such biopolymers include polynucleotides such as DNA, polypeptides such as gelatin, and polysaccharides such as alginate. It is important to assert that unlike the permanent and *strong* charges present in the case of some synthetic polymers (strong polyelectrolytes), the charges typically found within biopolymers are non-permanent and *weak*, and are therefore sensitive to parameters such as the acidity of the solution (or pH) and salt (or ionic strength) [2, 4, 5]. In many cases, the interaction energy due to these *weak* charges are also in the same order of magnitude as $k_B T$ [4]. Thus, although both synthetic polymers and biopolymers are sensitive to temperature effects, the structure and properties of a wide variety of biopolymers are further sensitive to intramolecular and intermolecular charge interactions.

1.3. WHY STUDY BIOPOLYMER SOLUTIONS ?

The importance of biopolymers can be derived by addressing the elephant in the room. Presently, a majority of the polymer products produced for a wide variety of engineering applications utilise non-biodegradable synthetic polymers [6]. Although these synthetic polymers are largely recyclable, less than 10% (by weight) of the plastic products produced from these polymers are typically recycled [7]. Despite this, recent estimates place the current global plastic production between 50 to 60 kg per capita, per year [6]. To aid interpretation, each person would be required to recycle an equivalent of up to 3000, 1.5 L polyethylene terephthalate (PET) bottles per year to ensure that all plastic products produced globally are efficiently recycled [8, 9]. Although modern methods are being developed to aid the biodegradability of synthetically produced polymer products, they alone cannot support the mammoth effort of managing the plastic (or polymer) waste generated on a global scale [10]. Thus, it is favourable to substitute a wide variety of existing polymer products with sustainable alternatives.

Owing to the fact that biopolymers may be found within naturally occurring biodegradable sources, they serve as likely candidates to replace the synthetically produced polymer materials. As such, biopolymers remain highly relevant within the biomedical and food industries. Indeed, it is difficult to imagine rapid vaccination strategies against widespread global pandemic diseases [11], and alternative food products that utilise plant based recipes [12], without the use of biopolymers. However, these selective applications do not necessarily capture the wide ranging utility of biopolymers. Based on relevant research conducted in the recent years, biopolymers can also be used as hydrogels, foams, coatings, composite and flame retardant materials within the agricultural, construction and even the aerospace industries [13–18].

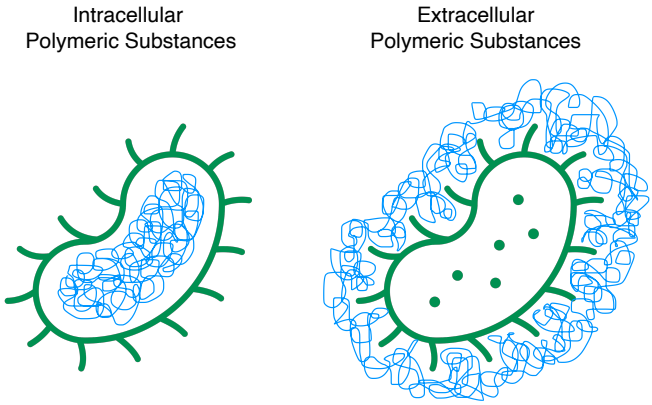

Figure 1.1: A schematic representation of intracellular and extracellular polymeric substances that are produced by bacterial species found within waste streams.

In equal respect, novel biopolymers can also be extracted from relatively unexplored sources such as biomass and wastewater [19, 20]. As shown in Figure 1.1, these waste based polymers are typically produced by bacterial species; either as intracellular polymeric substances in the case of polyhydroxyalkanoates (e.g. PHBV) [19], or as extracellular polymeric substances (EPS) in the case of wastewater biopolymers [20]. When disposed improperly, such *low value* sources also present significant environmental hazards and limited societal utility. Therefore, it is worthwhile to *upscale* biopolymers that can be suitably extracted from these sources. Indeed, it is possible to imagine, that biopolymers from waste streams may not be appealing within the biomedical and food industries. However, by identifying new areas where materials such as PHBV or EPS may be applied, it is possible to expand the number of engineering applications utilising biopolymers.

The challenge in growing the utility of biopolymers however, is limited by the convenience of establishing relevant structure-property relationships. In biopolymers such as PHBV and EPS, there is a large variability in the choice of molecules / molecular species that repeatedly bond together to form the polymer [19, 21]. Thus, it remains extremely difficult to establish the exact chemical structure of these biopolymers. Using some crude approximations, it can be shown that the search space needed to sift through all potential chemical structures in complex biopolymer systems, is bigger than the number of atoms available within the observable universe (upto 10^{82} atoms [22]). For instance, by using just two different *monomers* (the repeating unit in a polymer) with different levels of charge, and by assuming that all favourable combinations are allowed between these two monomers, only 273 repeating units are needed to create ~ 1.52 x 10^{82} unique chemical structures. As such, the idealisation in this illustrative example is not entirely unrealistic, and may be successful in modelling alginate, a negatively charged polysaccharide

rich in *carboxylic* groups (see Figure 1.2 a). Despite the large variability in its potential chemical structure, the specificity of any particular alginate structure is not necessarily important in describing its relevant properties. Instead the molar (or mass) ratio of the two unique monomers, relating to the relative charge levels, is sufficient in capturing the structure-property relationships of alginate [23]. This abstracted structure can be used further to explain structure-property relationships that are relevant during the extraction and processing of biopolymers.

Typical extraction methods for biopolymers, including those for complex systems such as EPS [20, 26, 27], involves the use of acids and bases (or alkali) to dissolve the desired biopolymer, and to subsequently separate it from other undesired biomass / chemicals (discussed in further chapters). Certainly then, the presence of charged functional groups helps in determining the solubility of a polymer in the presence of an acid or a base. Alginate, for instance, is soluble in water under neutral pH conditions. However, upon sufficient acidification (pH ~ 3.7, carboxylic group's acid strength / pK_a [4]) through the addition of H^+ ions, it is possible to *protonate* these carboxylic groups, thereby leading to the formation of intermolecular *hydrogen bonds* (see Figure 1.2 - b and e). As shown in Figure 1.2 e, through the dropwise addition of 37% w/w HCl, the formation of these *hydrogen bonds* reduces the solubility of alginate, and leads to the formation of a gel structure that is susceptible to separation.

Figure 1.2 also illustrates how other counter ions can be introduced to control the solubility of the polymer, and hence its physical properties. For instance, upon adding 0.36 M of Na^+ in place of H^+, no changes are noted in the solubility of alginate. This is due to the inability of Na^+ ions to form bonds between neighbouring chains. Despite this, the positively charged Na^+ ions expectedly neutralise (or *screen*) the repulsive electrostatic interactions between neighbouring negative charges, and therefore influence the conformational flexibility of polymer chains in solution (see Figure 1.2 c) [28]. By contrast, adding just 0.1 M of Ca^{2+}, it is possible bridge negative charges from neighbouring chains via the formation of crosslinks [25]. As expected, the chemical structure of the Ca-alginate system is significantly different compared to the H-alginate system, and it therefore forms a different type of gel (see Figure 1.2 - b, d and e). When trying to replicate the same *crosslinking* mechanism using 0.1 M of Mg^{2+} ions, it is evident that despite the use of a divalent ion, the same degree of *crosslinking* is not obtained in the latter case; although some turbidity is noticeable through strenuous observation (see Figure 1.2 e). Upon surveying a relevant literature source [29], it is clear that while Mg^{2+} has the capacity to *crosslink* with alginate, it is much slower and highly dependent on the presence of *guluronic acid* blocks within the polymer.

Certainly then, a close control of the pH and ionic strength of the solution, and the associated changes to the physical properties of biopolymers, remains highly relevant in the effort to develop biopolymer systems for the engineering applications discussed earlier. Further still, new insights gained about the behaviour of biopolymer systems is instrumental in advancing the field of *polymer physics*. As

1

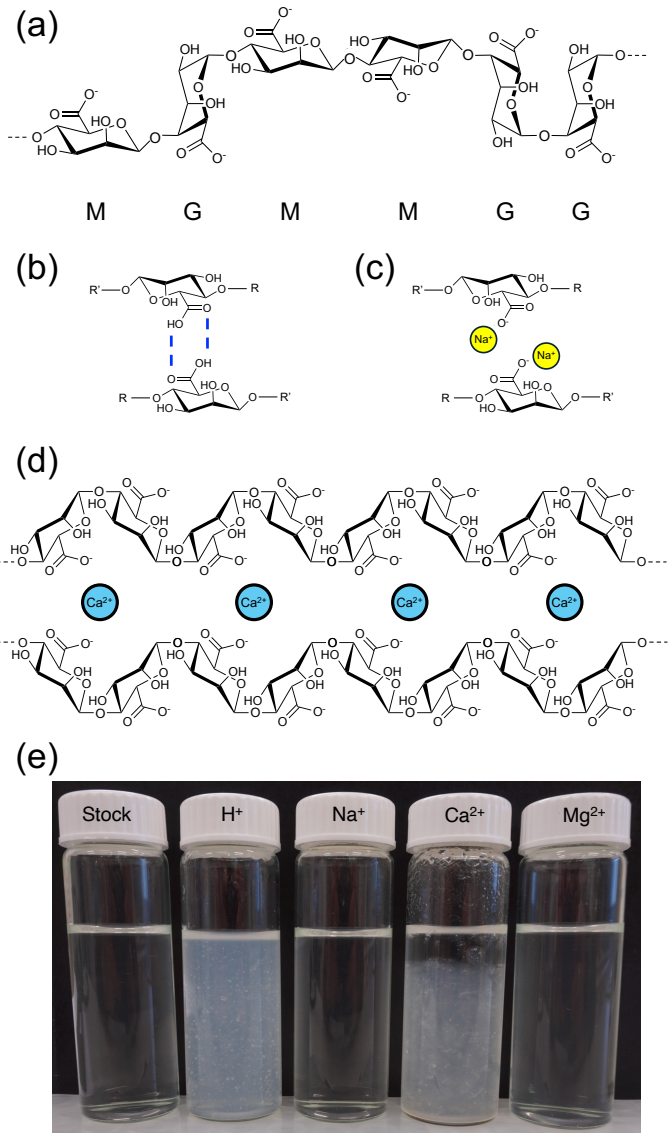

Figure 1.2: Representations of (a) the chemical structure of alginate - M: mannuronic acid, G: guluronic acid [24], (b) intermolecular hydrogen bonds between the carboxylic groups of alginate, (c) neutralisation of electrostatic charge by Na^+ ions, (d) the *egg box* structure representing mannuronic alginate crosslinked by Ca^{2+} ions [25], and (e) sodium alginate solutions containing different ions. Note that the solvent for the stock solution is deionised water.

acknowledged by Rubinstein and Colby, a relevant and highly cited literature source, the physical understanding of polymers with (reversibly) associating groups, i.e. *weak* polyelectrolytes such as biopolymers, remains "far from complete" [2]. Thus, it is equally important to assess if the established physical models for synthetic polymers, and the associated characterisation methodologies, are extendable to biopolymer systems. In addition, existing biochemical advancements such as the development of modern vaccines / medical treatments for diseases, can also benefit from the physical understanding gained about biopolymer systems [30]. However, a mere qualitative description of the properties, such as the example described in Figure 1.2, is not sufficient in developing the physical understanding about biopolymer systems. What is required is a characterisation methodology that can quantitatively capture changes to the physical properties of biopolymers in a variety of solutions.

1.4. HOW TO STUDY BIOPOLYMER SOLUTIONS

In a broad sense, *rheology* may be described as the study of materials under deformation, with the overarching philosophy that "everything flows" ($\tau\alpha\ \pi\acute{\alpha}\nu\tau\alpha\ \rho\epsilon\acute{\iota}$), i.e. all forms of matter are susceptible to deformation [31]. As this definition leaves ample room for misinterpretation, it is worthwhile to motivate the reasons for using rheology as a characterisation tool within this thesis. When changes are made to the pH and ionic strength, it is noticeable through Figure 1.2 that they have a severe effect on the *solid-like* or *liquid-like* characteristics of the biopolymer system. For instance, when associative intermolecular links are formed within the biopolymer system, it forces a transition towards a *solid-like* gel structure. Expectedly, these gel structures are more *resistant* to deformation, under a variety of loading conditions, when compared to the native *liquid-like* dissolved state. Likewise, changes to the inherent flexibility of a dissolved biopolymer chain is also capable of creating variability in the *resistance* to deformation.

It is exactly this *resistance* to deformation that rheology tries to quantitatively capture. In the case of solids, this *resistance (or stiffness)* is measured using a term called the *modulus* (E or G); whereas in the case of liquids, this resistance is measured using a term called the *viscosity* (η) [2]. In intermediate cases, both parameters may be used to describe systems that switch from a *solid-like* to a *liquid-like* behaviour, or vice versa (see *storage and loss modulus* in [2, 32]). Certainly, changes to these parameters are closely influenced by the ability of individual biopolymer chains to occupy a certain (*pervaded*) volume due to their flexibility, or indeed due to associative linkages between neighbouring chains [2]. Thus, by closely controlling the pH and ionic strength, it is possible to parametrically vary the conditions of the system, and therefore influence the rheological parameters such as *modulus* and *viscosity*.

Specifically, these *structure-rheology* relationships may then be used to develop biopolymers for relevant engineering applications. For instance, the *modulus* is relevant in describing the stiffness of biopolymer systems such as gels, coatings,

foams and (nano)composite materials. In the case of gels and foams, the modulus is particularly useful in describing the *elasticity* of the delicate structure, analogous to the *elasticity* of a rubber band [2]. By contrast, the *viscosity* is particularly relevant during the extraction and processing phase, and describes the ease with which biopolymer systems can be pumped, sprayed or extruded by means of conventional engineering apparatus. In the case of (fibre reinforced) coatings and composite materials, it is equally important to assess the ultimate failure of the product, when used for high performance engineering applications such as flame retardant materials, or as aeroelastic structures. In such cases, relevant relationships between viscosity, the molar mass, and the mechanical strength of the (bio)polymer [2], can be used to design engineering solutions that have a well defined "performance envelope" [33]. Finally, relevant relationships between the *modulus* and *viscosity*, relating to the *sagging* observed within complex fluids, can also be used to fine tune the formulations of coatings, inks, food products, cosmetics, medicines, household goods, etc. This *sagging* ability may also be countered, either by changing the time dependent recovery of the the complex fluid's microstructure (known as *thixotropy* [34]), or by intentionally modyfying this microstructure, which stays virtually undeformed below a critical threshold value called the *yield stress* [35].

1.5. SUMMARY OF CONTENTS

Based on the relevant knowledge gaps identified above, intentional changes were made to the relative charge levels, using pH and ionic strength, to suitably modify the underlying structure of the biopolymer system(s) in question. The impact of changes is assessed using the rheology parameters described above, in an effort to establish relevant structure-rheology relationships.

In Chapter 2, the *screening* effects of monovalent counter ions on individual biopolymer chains is studied closely. Changes to the flexibility of these chains, and thus their *pervaded* volume, are relayed using changes to the *viscosity* of the biopolymer solution. This is analogous to studying the effects of Na^+ in Figure 1.2.

In Chapter 3, a methodology is provided to track changes to the *viscosity* as a function of concentration for *unscreened, screened,* as well as *hydrogen bonded* biopolymer solutions. Further, all datasets are collapsed onto a set of universal curves to describe the specific influence of *screening* and *hydrogen bonding*. This is analogous to comparing the Stock, H^+ and Na^+ systems in Figure 1.2.

In Chapter 4, a case study is provided on EPS from wastewater. Particularly, the specific effects of several counter ions in governing the properties of EPS is studied closely. This is analogous to comparing the Na^+, Ca^{2+} and Mg^{2+} systems in Figure 1.2.

In Chapter 5, the moduli of cross-linked and/or jammed hydrogel systems (including EPS) are compared, to highlight the specific influence of microstructure

and concentration of the hydrogel particles on the *yield stress* of the suspensions. This is analogous to comparing the H^+ and Ca^{2+} systems in Figure 1.2.

In Chapter 6, a consolidated outlook from Chapters 2 - 5 is used to describe variations in the rheological properties of EPS; specifically due to intentional changes to the extraction process. The quantitative inferences that may be gained, using a single type of rheological measurements, are also discussed. Additionally, it is described how these rheological measurements are easily implementable, and therefore practically relevant for ensuring the desired properties of biopolymer products, during their extraction and processing for desired applications. Finally, a few key messages are provided to stimulate future research in the field of biopolymers.

1

REFERENCES

[1] W. Callister Jr and D. Rethwisch. *Materials Science and Engineering: An Introduction*. Hoboken, NJ, USA: John Wiley & Sons, 2020.

[2] M. Rubinstein and R. Colby. *Polymer Physics*. Oxford, UK: Oxford University Press, 2003.

[3] A. Jenkins, P. Kratochvíl, R. Stepto, and U. Suter. "Glossary of basic terms in polymer science (IUPAC recommendations 1996)". In: *Pure and Applied Chemistry* 68 (1996), pp. 2287–2311. DOI: https://doi.org/10.1351/pac199668122287.

[4] D. Nelson, M. Cox, and A. Hoskins. *Lehninger Principles of Biochemistry*. New York, NY, USA: Macmillan Learning, 2021.

[5] C. Lopez, A. Matsumoto, and A. Shen. "Dilute polyelectrolyte solutions: Recent progress and open questions". In: *Soft Matter* 20 (2023), pp. 2635–2687. DOI: https://doi.org/10.1039/D3SM00468F.

[6] R. Geyer, J. Jambeck, and K. Law. "Production, use, and fate of all plastics ever made". In: *Science Advances* 3 (2017), e1700782. DOI: https://doi.org/10.1126/sciadv.1700782.

[7] OECD. *Global Plastics Outlook: Policy Scenarios to 2060*. Paris, France: OECD Publishing, 2022.

[8] F. Welle. *The Facts about PET*. URL: https://www.petcore-europe.org/images/news/pdf/factsheet_the_facts_about_pet_dr_frank_welle_2018.pdf.

[9] M. Islam, M. J. Uddin, and K. Alshehri. "Plastic waste and carbon footprint generation due to the consumption of bottled waters in Saudi Arabia)". In: *Research & Development in Material Science* 5 (2018). DOI: http://dx.doi.org/10.31031/RDMS.2018.05.000604.

[10] L. Filiciotto and G. Rothenberg. "Biodegradable plastics: Standards, policies, and impacts". In: *ChemSusChem* 14 (2021), pp. 56–72. DOI: https://doi.org/10.1002/cssc.202002044.

[11] N. Pardi, M. Hogan, F. Porter, and W. D. "mRNA vaccines — a new era in vaccinology". In: *Nature Reviews Drug Discovery* 17 (2018), pp. 261–279. DOI: https://doi.org/10.1038/nrd.2017.243.

[12] Y. He, V. Meda, M. Reaney, and R. Mustafa. "Aquafaba, a new plant-based rheological additive for food applications". In: *Trends in Food Science & Technology* 111 (2021), pp. 27–42. DOI: https://doi.org/10.1016/j.tifs.2021.02.035.

[13] S. Van Vlierberghe, P. Dubruel, and E. Schacht. "Biopolymer-based hydrogels as scaffolds for tissue engineering applications: A review". In: *Biomacromolecules* 12 (2011), pp. 1387–1408. DOI: https://doi.org/10.1021/bm200083n.

[14] S. Zhao, W. Malfait, N. Guerrero-Alburquerque, and G. Koebel M.M.; Nyström. "Biopolymer aerogels and foams: Chemistry, properties, and applications". In: *Angewandte Chemie International Edition* 57 (2018), pp. 7580–7608. DOI: https://doi.org/10.1002/anie.201709014.

[15] T. Xu, C. Ma, Z. Aytac, X. Hu, K. Ng, J. White, and P. Demokritou. "Enhancing agrichemical delivery and seedling development with biodegradable, tunable, biopolymer-based nanofiber seed coatings". In: *ACS Sustainable Chemistry & Engineering* 8 (2020), pp. 9537–9548. DOI: https://doi.org/10.1021/acssuschemeng.0c02696.

[16] J. Zlopasa, B. Norder, E. Koenders, and S. Picken. "Origin of highly ordered sodium alginate/montmorillonite bionanocomposites". In: *Macromolecules* 48 (2015), pp. 1204–1209. DOI: https://doi.org/10.1021/ma502147m.

[17] P. Kanmani and J.-W. Rhim. "Properties and characterization of bionanocomposite films prepared with various biopolymers and ZnO nanoparticles". In: *Carbohydrate Polymers* 106 (2014), pp. 190–199. DOI: https://doi.org/10.1016/j.carbpol.2014.02.007.

[18] A. Raja. "Cellular Solids Based on Biopolymer Nanocomposites: For Hypersonic Heat Shields Aboard Sounding Rockets". Masters' Thesis. Delft University of Technology, 2020. URL: http://resolver.tudelft.nl/uuid:1b4598f6-124d-40f8-9228-d98f8aba31cc.

[19] C. M. Vermeer, M. Nielsen, V. Eckhardt, M. Hortensius, J. Tamis, S. J. Picken, G. M. H. Meesters, and R. Kleerebezem. "Systematic solvent screening and selection for polyhydroxyalkanoates (PHBV) recovery from biomass". In: *Journal of Environmental Chemical Engineering* 10 (2022), p. 108573. DOI: https://doi.org/10.1016/j.jece.2022.108573.

[20] S. Felz, S. Al-Zuhairy, O. Aarstad, M. van Loosdrecht, and Y. Lin. "Extraction of structural extracellular polymeric substances from aerobic granular sludge". In: *Journal of Visualized Experiments* 115 (2016), e54534.

[21] T. Seviour, N. Derlon, M. Dueholm, H.-C. Flemming, E. Girbal-Neuhauser, H. Horn, S. Kjelleberg, M. van Loosdrecht, T. Lotti, and M. Malpei. "Extracellular polymeric substances of biofilms: Suffering from an identity crisis". In: *Water Research* 151 (2019), pp. 1–7. DOI: https://doi.org/10.1016/j.watres.2018.11.020.

[22] P. Kiernan. *Which is greater? The number of atoms in the universe or the number of chess moves?* URL: https://www.liverpoolmuseums.org.uk/stories/which-greater-number-of-atoms-universe-or-number-of-chess-moves#.

[23] H. Grasdalen, B. Larsen, and O. Smisrod. "^{13}C-NMR studies of monomeric composition and sequence in alginate". In: *Carbohydrate Research* 89 (1981), pp. 179–191. DOI: https://doi.org/10.1016/S0008-6215(00)85243-X.

[24] P. Yan, W. Lan, and J. Xie. "Modification on sodium alginate for food preservation: A review". In: *Trends in Food Science & Technology* 143 (2024), p. 104217. DOI: https://doi.org/10.1016/j.tifs.2023.104217.

[25] L. Cao, W. Lu, A. Mata, K. Nishinari, and Y. Fang. "Egg-box model-based gelation of alginate and pectin: A review". In: *Carbohydrate Polymers* 242 (2020), p. 116389. DOI: https://doi.org/10.1016/j.carbpol.2020.116389.

[26] V. Kontogiorgos. *Pectin: Technological and Physiological Properties*. Cham, Switzerland: Springer International, 2020.

[27] J. O'Mahony and P. Fox. "Milk Proteins: Introduction and Historical aspects". In: *Advanced Dairy Chemistry: Volume 1A: Proteins: Basic Aspects*. New York, NY, USA: Springer, 2013, pp. 43–85.

[28] C. Lopez. "Entanglement of semiflexible polyelectrolytes: Crossover concentrations and entanglement density of sodium carboxymethyl cellulose". In: *Journal of Rheology* 64 (2020), pp. 191–204. DOI: https://doi.org/10.1122/1.5127015.

[29] F. Topuz, A. Henke, W. Richtering, and J. Groll. "Magnesium ions and alginate do form hydrogels: a rheological study". In: *Soft Matter* 8 (2012), pp. 4877–4881. DOI: https://doi.org/10.1039/c2sm07465f.

[30] J. Pathak, S. Nugent, M. Bender, C. Roberts, R. Curtis, and J. Douglas. "Comparison of Huggins coefficients and osmotic second virial coefficients of buffered solutions of monoclonal antibodies". In: *Polymers* 13 (2021), p. 601. DOI: https://doi.org/10.3390/polym13040601.

[31] C. Macosko. *Rheology: Principles, Measurements, and Applications*. Hoboken, NJ, USA: John Wiley & Sons, 1996.

[32] T. Osswald and N. Rudolph. *Polymer Rheology: Fundamentals and Applications*. Munich, Germany: Carl Hanser Verlag GmbH, 2015.

[33] M. F. Ashby and D. Cebon. "Materials selection in mechanical design". In: *Le Journal de Physique IV* 3.C7 (1993), pp. 1–9. DOI: https://doi.org/10.1051/jp4:1993701.

[34] M. Agarwal, S. Sharma, V. Shankar, and Y. Joshi. "Distinguishing thixotropy from viscoelasticity". In: *Journal of Rheology* 65 (2021), pp. 663–680. DOI: https://doi.org/10.1122/8.0000262.

[35] A. Malkin, V. Kulichikhin, and S. Ilyin. "A modern look on yield stress fluids". In: *Rheologica Acta* 56 (2017), pp. 177–188. DOI: https://doi.org/10.1007/s00397-016-0963-2.

2

CHARGE MEDIATED CHANGES TO THE INTRINSIC VISCOSITY

A theoretical approach is presented to quantify the effect of ionic strength on the swelling and shrinkage of the hydrodynamic coil size of a generic biopolymer. This was conducted in view of extraction methods that often utilise acids and alkali combinations and, therefore, invariably impact the levels of salt found in commercially available biopolymers. This approach is supplemented by intrinsic viscosity measurements for the purpose of validation across a variety of biopolymer architectures, type of functionalisation, as well as the quoted molar mass. By accurately capturing the magnitude of change in the coil size, it is discussed how a biopolymer coil size is far more sensitive to changes in the ionic strength than it is to the molar mass (or contour length) itself. In turn, it is highlighted why the current characterisation strategies that make use of weight-averaged molar mass are prone to errors and cannot be used to establish structure-property relationships for biopolymers. As an alternative, the scope of developing an accurate understanding of coil sizes due to changes in the "soft" interactions is proposed, and it is recommended to use the coil size itself to highlight the underlying structure-property relationships.

This chapter has been published as: A. Raja, P.K. Wilfert, and S.J. Picken, "Charge Mediated Changes to the Intrinsic Viscosity of Biopolymer Systems Polymers", *Polymers*, **2024**, 16(20), 2894.

2.1. INTRODUCTION

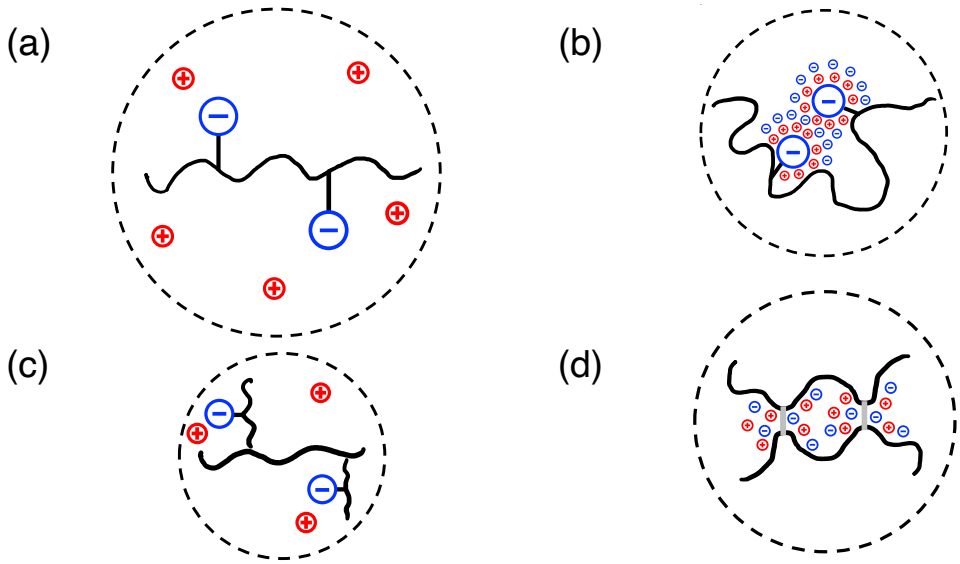

Figure 2.1: Expected coil conformations for different conditions: (a) unscreened linear biopolymer coil, (b) screened linear biopolymer coil, (c) unscreened branched biopolymer coil with the same molar mass as the linear coil, and (d) screened biopolymer coil that forms physical crosslinks. The dashed lines schematically represent the hydrodynamic (pervaded) volumes occupied by the coils.

From a generic point of view, most biopolymers may be described as polymers that are decorated by functional groups [1]. These groups exhibit thermodynamically favourable "soft" interactions and may, therefore, present variations in their levels of protonation due to changes in the pH [2, 3]. Moreover, screening effects due to changes in the ionic strength and favourable bridging (via physical crosslinks) based either on the composition of counter ions in solution or intramolecular interactions such as H-bonding with other functional groups are critically important [1–3]. Certainly, in some cases, the specific effects of these interactions on both the structure as well as the properties have been studied in more detail. One such recent and widely cited example includes the prediction of the folded conformation of proteins through the knowledge of their polypeptide sequence [4].

However, the specificity of such approaches largely overlooks the general trends that may be observed in the structure and properties of all biopolymers, which occur due to changes in the pH or ionic strength. Although there are examples that adopt such a generic methodology [5, 6], the effort to develop such approaches further remains absent. Thus, there is sufficient scope to extend the generic physical understanding on the structure and properties of a biopolymer. Based on the

methods outlined by Picout et al. [6], a choice was made to extend the rheological understanding of biopolymers further, and thus, an attempt to map changes in the hydrodynamic coil size of a generic biopolymer is presented below.

In Figure 2.1, a schematic map of some expectable differences in coil sizes by varying the pH and ionic strength is shown. However, these schematics merely present a coarse-grained physical interpretation of the coil size. What is lacking, then, is a theoretical and quantitative measure for changes in the coil size due to functional group interactions. However, it is clearly not possible to map the effect of all these changes at once. Thus, this study is limited to predominantly cover the effects of ionic strength on the hydrodynamic size of charged biopolymer coils.

As such, substantial ionic strength levels are to be anticipated in biopolymer systems in view of the extraction (or isolation) methods that utilise techniques such as alkaline dissolution followed by acid precipitation (or vice versa) [2, 7]. The large changes in the pH that are used invariably introduce salts within the system and substantially increase the ionic strength. Further, downstream processing steps may be employed to remove the excessive levels of salts [7] in order to meet the yields and purities expected, and these steps, therefore, are instrumental in reducing the ionic strength. Moreover, for the application of such biopolymer systems, the rheological processing behaviour and, indeed, the final properties will critically depend on the ionic strength of the system. Thus, for the purposes of extraction, processing, and applicability of biopolymers, it is important to establish the sensitivity to variations in ionic strength within these systems.

Before highlighting the theoretical approach, a brief outlook on the choice of a measure for the quantitative coil size is provided. Whilst the size of coils may be calculated conveniently using size exclusion chromatography (SEC) or light scattering, the intention was to map the coil sizes using intrinsic viscosity. As it was impractical to account for a variety of standards representative of biopolymer systems under consideration [8], it would have been necessary to deal with inaccuracies in the SEC results depending on the level of screening. Equally, the inaccuracies associated with curve-fitting protocols in commercially viable light-scattering techniques were taken into consideration [9]. In contrast, it has been established that the (intrinsic) viscosity may be precisely measured across a wide variety of polymer systems [10].

As elucidated by Lopez and coworkers in their extensive review [11], the modelling of polyelectrolytes (in this case, biopolymers as weak polyelectrolytes) using worm-like chains allows for the estimation of the intrinsic viscosity and, thus, serves as the basis of the theoretical approach. This is covered extensively in Section 2.2. In Section 2.3, the list of biopolymers and methodology are presented. The results are reported in Section 2.4, and the major findings and drawbacks of estimating a biopolymer's molar mass using the size (or length) of coils are highlighted in Section 2.5. Finally, in Section 2.6, a general outlook for future work in this direction is provided.

2.2. THEORETICAL REVIEW

The intrinsic viscosity may be calculated using the Einstein equation for very dilute polymer systems, where they are traditionally known to behave as a Newtonian fluid [10]:

$$\eta = \eta_S(1 + 2.5\phi) = \eta_S(1 + [\eta]c) \tag{2.1}$$

Here, η represents the viscosity of the bulk system, η_S represents the solvent viscosity, ϕ represents the volume fraction of polymer coils, $[\eta]$ represents the intrinsic viscosity of the polymer coils, and c represents the (mass) concentration of the polymer in solution. The intrinsic viscosity is typically represented in the inverse units of mass concentration and, therefore, should be recognised as a measure of the coil mass density, or, indeed, the macromolecular mass density if the architecture is more complex than a linear chain. Further, as discussed by Rubinstein and Colby [10], the end-to-end distance of a (sufficiently long) worm-like chain may be approximated using the following relation:

$$\langle R^2 \rangle = 2L_pL_c \tag{2.2}$$

Here, $\langle R \rangle$ is the (average) end-to-end distance, and L_p is the persistence length of the chain. L_c in Equation 2.2 is the contour length of the chain and may be calculated by taking the product of the number of repeating units (N) and the single monomer projected length (l). As discussed by Lopez [12], Norisuye and coworkers have provided extensive experimental evidence to show that the radius of gyration of polyelectrolytes in the excess salt limit can be described using the worm-like chain model. Thus, the end-to-end distance may then be used to calculate the radius of gyration [10]:

$$\langle R_g^2 \rangle = \frac{\langle R^2 \rangle}{C} \tag{2.3}$$

Here, $\langle R_g \rangle$ is the radius of gyration. C in Equation 2.3 is an integer whose value depends on the persistence length. For example, in the case of linear chains, $C = 6$ for an ideal chain (coil limit), whereas $C = 12$ for a rod-like chain. In a simplified approach, the Fox-Flory equation [10] can be used to calculate the intrinsic viscosity:

$$[\eta] \approx \frac{\langle R_g^3 \rangle}{M} \tag{2.4}$$

where M is the molar mass of the polymer chain. However, no particular attention is paid to the hydrodynamics of the worm-like cylindrical chain, as the radius of gyration (in place of the hydrodynamic radius) is used, as is, to calculate the intrinsic viscosity. Yamakawa and Fujii [13], specifically account for this by using the Oseen-Burgers procedure, and make an approximation for the value of the intrinsic viscosity. However, in their effort to do so, they only provide analytical solutions for the rod limit as well as the coil limit. For all intermediate conformations, they only provide a numerical (or approximate) solution that is dependent on the length of the stretched-out chain (contour length):

$$[\eta] \approx \phi_{YF} \frac{L_c^{3/2}}{M} \tag{2.5}$$

ϕ_{YF} in Equation 2.5 above is a function [$m^{3/2}$] whose value depends on the contour length. Although well intended, the solution provided by Yamakawa and Fujii reduces the subtle details about the stiffness of chains at relevant intermediated conformations using the semi-empirically calculated values of ϕ_{YF}. Additionally, this model does not provide a means of estimating the intrinsic viscosity at various ionic strengths.

Another drawback of the Fox-Flory approach is the use of molar mass. As highlighted in Section 2.3, this information may not be readily available from the manufacturer for all biopolymer systems. Additionally, the molar mass of commercially available (bio)polymers is typically reported using weight-averaged molar mass [14] (M_w). As M_w determination is dependent on the size (or length) of the polymer coils, variations may be expected in its value depending on the pH and ionic strength of the solution. It is also worth noting that the current study is limited to biopolymer systems whose chemical structure is (somewhat) well defined. However, it is expectable that the chemical structure of the biopolymer system under consideration is not well defined at all [2, 7], and thus, the molar mass as such may not be readily ascertained. Therefore, changes in the intrinsic viscosity may instead be relayed using changes into the persistence lengths in the screened vs. unscreened case. By doing so, it is equally possible to address the limitations surrounding the Yamakawa and Fujii approach.

As discussed by Dobrynin [15], Odijk, Skolnick, and Fixman (OSF) introduced the concept of the electrostatic persistence length for (semi) stiff polyelectrolyte chains. According to their approach, the persistence length of a polymer backbone may be written as the sum of the bare persistence length (referred to above as L_p) and the electrostatic persistence length (L_p^{OSF}):

$$L_p^+ = L_p + L_p^{OSF} \approx L_p + \frac{L_B f^2}{4(\kappa l)^2} \tag{2.6}$$

Here, L_B represents the Bjerrum length, f represents the fraction of monomers that are charged, and κ^{-1} represents the Debye length. By virtue of measuring the conductivity of the dilute unscreened polymer solutions, the concentration of NaCl in solution is estimated to be ~ 1 mM (See Section 2.3). This value can be used to calculate the value of κ^{-1} (9.621 nm). Equally, it is possible to estimate the L_B value of water at 298 K (0.714 nm). Therefore, the unscreened persistence length value may be calculated for different systems using Equation 2.6.

From Equations 2.2 and 2.3, it is clear that $\langle R_g \rangle \approx \langle R \rangle \approx \sqrt{L_p}$. Thus, upon substituting for $\langle R_g^3 \rangle$ in Equation 2.4, it is clear that $[\eta] \approx L_p^{3/2}$. It further follows from Equation 2.6 that, the ratio of the intrinsic viscosity in the unscreened case (subscript U) to that in the completely screened case (subscript S) may in term be

represented as $[\eta]_U/[\eta]_S \approx (L_p^+/L_p)^{3/2}$. By substituting the full expression for L_p^+ from Equation 2.6, the following relation is obtained:

$$[\eta]_R = \frac{[\eta]_U}{[\eta]_S} \approx \left(\frac{L_p^+}{L_p}\right)^{3/2} = \left(\frac{L_p + L_p^{OSF}}{L_p}\right)^{3/2} = \left(1 + \frac{L_p^{OSF}}{L_p}\right)^{3/2} = \left(1 + \Theta_p\right)^{3/2} \tag{2.7}$$

Here, $[\eta]_R$ is termed as the "relative intrinsic viscosity" and represents the ratio of the intrinsic viscosities (unscreened to screened). The term Θ_p represents the expansion to the bare persistence length and is, therefore, labelled as the "expansion factor". Thus, the experimentally obtained relative intrinsic viscosity values are compared to the ones presented theoretically using Equation 2.7. The study is limited to polysaccharides and polypeptides, and Equation 2.7 is, therefore, employed for these two cases.

Lopez reports that there is some contention about the bare persistence length (L_p) of cellulosic backbones [12]. This may be attributed to the fact that cellulose itself remains insoluble in water, and so, it's persistence length may only be calculated via soluble (or charged) derivates [16], where the charged systems additionally will have multiple f values. Thus, the uncertainty surrounding the exact value for the bare persistence length (L_p) of polysaccharides is recognisable. Calculations are, therefore, performed using multiple values. Equally, the fraction of charged monomers (f) is largely governed by the degree of substitution of the sugar rings. In specific cases, such as alginate or pectin, a further reduction in the f value may be expected. In the case of alginate, this is attributable to intramolecular H-bonding effects within the guluronic blocks [17], and in the case of pectin, this may be attributed to the methylation of the galacturonic acid fractions [2]. Thus, the f values were carefully selected for each polysaccharide system. Finally, there may be potential differences in monomer size (l) amongst different sections of the chain in cases such as alginate [18]. However, for the purposes of the calculations, a single value of monomer size [19] (l = 1 nm) is retained.

Unlike polysaccharides, polypeptides are mostly polyampholytes and, thus, show a reversal in swelling phenomena in the screened vs. unscreened cases. Not only this, in the unscreened and fully charged case (+ and −), the oppositely charged moieties have a greater affinity to each other and could, thus, lead to coil contraction or even collapse, frequently leading to the characteristic secondary structures, such as "folding" and "helix" formation, within the coils. Additionally, the f value is far more variable in the case of polypeptides. This is because the fraction of charged monomers is governed by the amino acid fractions that possess a charged side group and is, therefore, unique to each polypeptide sequence. This f value is further variable due to protonation of the different functional groups at different pH ranges (e.g., carboxylic groups vs. amine groups). Thus, it is not very easy to compare the swelling of multiple polypeptides directly with the theoretical approach that is highlighted, unless there is clear a-priori knowledge of the chain conformation. Nevertheless, it is worth analysing the theoretical calculations for an idealised (purely) anionic/cationic polypeptide and to comparing it to polysaccharides. Such a system

may be found under the correct levels of screening and/or (elevated) temperature [7]. Equally, it is worthwhile to compare experimentally obtained pH-associated coil swelling/compaction for fully screened polypeptides to screening-associated coil swelling/compaction in the case of polypeptides. Thus, theoretical calculations are presented for different f values in the case of polypeptides.

2.3. MATERIALS AND METHODS

2.3.1. MATERIALS

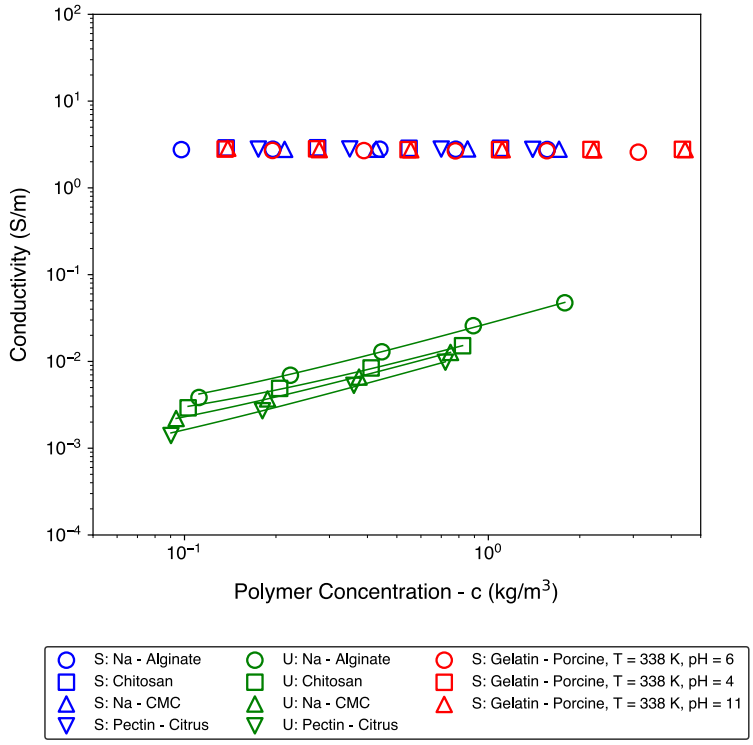

Figure 2.2: Conductivity of the biopolymer systems studied. S = screened, U = unscreened. Guides to the eye are also provided for the unscreened samples to highlight the differences in the values of their conductivity as well as the (almost) linear dependence with respect to concentration.

All the biopolymers used in this study were procured from Sigma-Aldrich (Zwijndrecht, The Netherlands). The list of polymers that were chosen is tabulated

Table 2.1: List of polymers and their salient properties: type of functionalisation, architecture, and molar mass. Note: The (range of) molar masses reported here are the ones provided by the manufacturer.

Polymer Name	**Salient Properties**
Sodium Alginate (Na-Alginate), CAS Number: 9005-38-3	Polyanion: Carboxyl group, High mannuronic acid content, Linear copolymer.
Chitosan, CAS Number: 9012-76-4	Polycation: Amine group, Linear homopolymer, M_w ~ 50 to 190 kg/mol.
Sodium Carboxy Methyl Cellulose (Na-CMC), CAS Number: 9004-32-4	Polyanion: Carboxyl group, Degree of Substitution = 0.9, Linearly substituted homopolymer, M_w ~ 250 kg/mol.
Pectin from Citrus Peels (Pectin-Citrus), CAS Number: 9000-69-5	Galacturonic acid ≥ 74.0%, Degree of methylation ≥ 6.7%, Branched heteropolymer.
Gelatin from Porcine Skin (Porcine-Gelatin), CAS Number: 9000-70-8	Polyampholyte: Carboxyl and amine group, Linear - collagen derivative.

in Table 2.1 along with the information provided by the supplier and their salient features. The specific choice of biopolymers allows the comparison of results for polyanionic, polycationic, as well as polyampholytic polymers. It was equally possible to compare the influence of salient chemical features such as blocks and branching. Additionally, there is also considerable variation in the molar mass (at least in cases where it is documented) across all biopolymers listed. Note that the (range of) molar masses reported here are the ones provided by the manufacturer. No additional measurements were performed to assess the accuracy of the quoted molar mass. As such, none of the quoted values were required for the theoretical calculations presented in the main text.

All biopolymer systems were prepared by stirring a desired concentration of the polymer in deionised water for a period of 24 h (86,400 s) in a sealed conical flask at 293 K. When not in use, the samples were stored in a refrigerator at 277 K to prevent degradation. The conductivity was increased, in the case of the screened samples, by adding the desired amounts (0.2-0.3 M) of NaCl to each individual biopolymer system. The pH changes within the gelatin sample were achieved using 1M HCl and 1M NaOH solutions in deionised water. Finally, the desired dilutions of the individual biopolymer systems were made using deionised water, whilst an effort

was made to maintain the desired pH and ionic strength. All values of conductivity were measured at a temperature of 293 K and 50% RH in the lab environment.

Figure 2.2 shows the conductivity of the samples. In view of the extraction methods for biopolymers, such as dissolution followed by precipitation, the conductivity of the unscreened samples could correspond to residual (surplus) salts that may be present within the samples. Alternatively, the measured conductivity values for some datasets are also in line with the expected values based on the counter ion concentration along the polymer backbone [20, 21] (see Supplementary Material Subsection 2.7.1). Regardless, as noticeable, upon subsequent dilution from higher concentrations, the conductivity dropped in a predictable and almost linear fashion. Thus, the polymer concentrations being represented on the x-axis of all Figures are believed to be within a relative error margin of 11% or 0.0453 decades.

2.3.2. METHODS

The dilute biopolymer systems were tested for their intrinsic viscosity using a stress-controlled TA Instruments Discovery Hybrid Rheometer 3 (DHR-3, TA Instruments-Waters, Etten-Leur, The Netherlands). Due to the low polymer concentration and, therefore, viscosity, all measurements were performed using a concentric cylinder setup. A stainless-steel cup of diameter 30.36 mm and a stainless-steel DIN bob rotor with a diameter of 28.00 mm and a height of 42.07 mm were used. The DIN bob was maintained at a height of 5917.1 μm from the bottom surface of the cup.

All tests were performed at a temperature of 298 K, except in the case of the gelatin samples, where the temperature was increased to 338 K to break the secondary and tertiary structure interactions within the polypeptide chain [22]. As the solutions behaved as Newtonian fluids, measurements at a suitable stress value ($\leq$ 0.1 Pa) were sufficient. Because of the low viscosity, a low stress value was chosen to mitigate flow instabilities resulting from high shear rates. The samples were held under these conditions for a period of 600 s to ensure the development of the plateau value in the viscosity, free from any inertial effects. This setup was also used to obtain the reference viscosity of deionised/saline water under the following conditions: at 298 K with no added NaCl, at 298 K with added NaCl, and at 338 K with added NaCl.

2.4. RESULTS

Table 2.2: Experimentally obtained solvent viscosities. (S.D. = Standard Deviation)

Solvent	η_S **(mPa·s)** $\pm$ **S.D.**
Water, 298 K - No Added Salt	0.871 $\pm$ 0.005
Water, 298 K - Added Salt	0.880 $\pm$ 0.006
Water, 338 K - Added Salt	0.489 $\pm$ 0.002

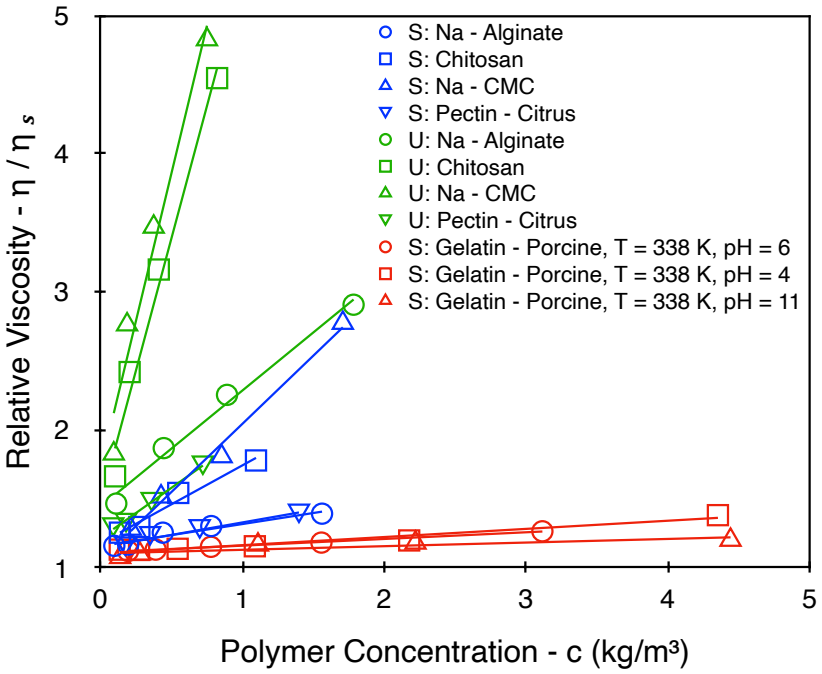

Figure 2.3: Experimentally obtained relative viscosity as a function of polymer concentration. S = screened, U = unscreened. These curves were subsequently used to calculate the intrinsic viscosity values from Equation 2.1. The straight lines act as guides to the eye to point out the linear slopes of each dataset.

Table 2.3: Experimentally obtained values for the intrinsic viscosity. (S.D. = Standard Deviation)

Biopolymer System	$[\eta]$ **(m^3/kg) ± S.D.**
Screened: Na-Alginate	0.308 ± 0.065
Screened: Chitosan	0.795 ± 0.100
Screened: Gelatin-Porcine, T = 338 K, pH = 6	0.102 ± 0.024
Screened: Na-CMC	1.034 ± 0.037
Screened: Pectin-Citrus	0.332 ± 0.064
Unscreened: Na-Alginate	1.183 ± 0.157
Unscreened: Chitosan	4.636 ± 0.379
Unscreened: Na-CMC	5.624 ± 0.626
Unscreened: Pectin-Citrus	1.152 ± 0.175
Screened: Gelatin-Porcine, T = 338 K, pH = 4	0.095 ± 0.017
Screened: Gelatin-Porcine, T = 338 K, pH = 11	0.060 ± 0.017

Table 2.4: Experimentally obtained values for $[\eta]_R$ vs. the range of theoretically calculated values of $[\eta]_R$ for polysaccharides. Θ_p Theory was calculated using L_p values of 10 nm and 5 nm respectively. The column labelled f provides a brief description of the values that were chosen for the theoretical calculations.

Biopolymer	$[\eta]_R$ **Expt.**	Θ_P **Expt.**	$[\eta]_R$ **Theory**	Θ_p **Theory**	f
Sodium Alginate	3.84	1.45	3.13–5.93	1.14–2.28	0.83
Chitosan	5.83	2.24	4.32–8.93	1.65–3.30	1.00
Sodium Carboxy Methyl Cellulose	5.44	2.09	3.58–7.05	1.34–2.68	0.90
Pectin from Citrus Peels	3.48	1.30	2.39–4.13	0.79–1.57	0.69

Table 2.5: Experimentally obtained values for $[\eta]_R$ - gelatin at different pH values vs. theoretically obtained values for $[\eta]_R$ - polypeptides at different f values.

Label	$[\eta]_R$	Θ_p
Experiment: Gelatin pH = 6/Gelatin pH = 4	1.07	0.05
Experiment: Gelatin pH = 6/Gelatin pH = 11	1.71	0.43
Theory: f = 0.05	1.25	0.16
Theory: f = 0.10	2.11	0.65
Theory: f = 0.25	11.3	4.05

Figure 2.3 represents the experimental datasets that were used to calculate the intrinsic viscosity. The y-axis of Figure 2.3 was obtained by dividing a particular system's viscosity with that of the corresponding solvent. As elucidated earlier, these solvent viscosities were also experimentally obtained and are tabulated in Table 2.2. The intrinsic viscosity of all datasets in Figure 2.3 is calculated using Equation 2.1. These are tabulated individually for each dataset in Table 2.3 (conversion to the frequently used dL/g may be obtained upon multiplying all values by 10).

It is noticeable from Table 2.3 (as well as Figure 2.3) that, across multiple biopolymer systems, the intrinsic viscosity spans roughly two orders of magnitude: from 0.06 m^3/kg in the case of gelatin (pH = 11 with screening) up to 5.62 m^3/kg in the case of unscreened CMC. As expected, the transition from the screened to unscreened state (in the case of polysaccharides) is accompanied by an increase in the intrinsic viscosity (green datasets vs. blue datasets). Large differences in the value of the intrinsic viscosity may also be observed across various polysaccharide systems, irrespective of screening effects. For instance, the intrinsic viscosities of CMC and chitosan are significantly larger than the intrinsic viscosities of alginate and pectin to suggest an overall larger coil size in the former cases. In contrast, gelatin presents a much smaller intrinsic viscosity value overall, with very limited changes in its value across multiple gelatin systems. This is roughly in line with what one might expect for a more flexible polypeptide backbone.

The values from Table 2.3 are further used to calculate the relative intrinsic viscosity ($[\eta]_R$) and compared to the theoretical models. To facilitate this comparison, both sets of values are tabulated against each polysaccharide in Table 2.4. The results for gelatin are tabulated separately in Table 2.5.

2.5. DISCUSSION

2.5.1. THEORY VS. EXPERIMENTS

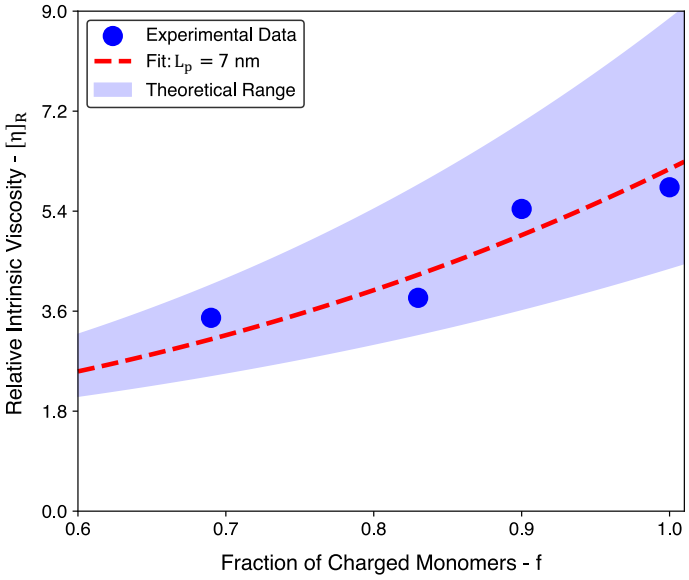

Figure 2.4: The dependence between the relative intrinsic viscosity and the fraction of charged monomers for polysaccharides. The data points represent the experimentally measured values for different polysaccharide systems (see Table 2.4). The shaded region corresponds to the theoretically estimated range that is calculated using L_p values from 5 nm up to 10 nm (see Equation 2.7). The dashed red line represents the optimal L_p value (7 nm) used to fit the experimental results.

As highlighted in Section 2.2, there appears to be some uncertainty surrounding the exact value of the bare persistence length of cellulosic backbones. Thus, the theoretical results in Table 2.4 are presented for L_p values from 5 to 10 nm. Lopez's argument [12] that $L_p <$ 10 nm is supported by the rheological measurements presented here. Despite the somewhat large uncertainty, it is worth remarking that a fit for the experimental data is possible using an L_p value of 7 nm (see Figure 2.4),

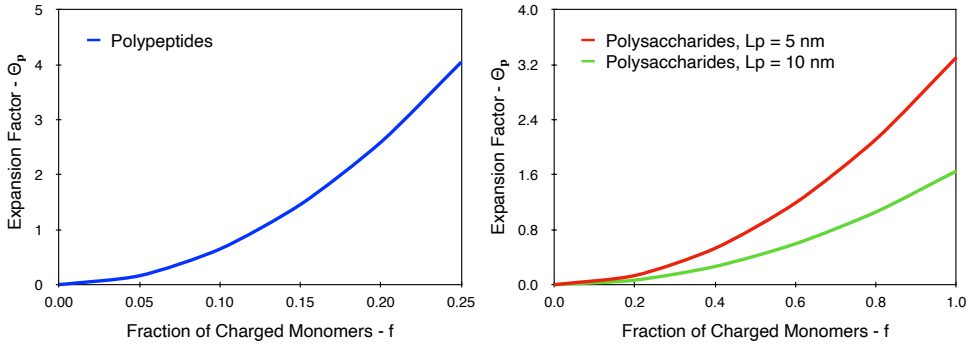

Figure 2.5: The dependence between the expansion factor Θ_p and the fraction of charged monomers (f) for both —polypeptides (left) and polysaccharides (right). The curves were obtained from Equations 2.6 and 2.7 for both cases.

and that this value is comparable with Lopez's proposed range from 5 to 6 nm.

A clarification for the f values presented in Table 2.4 is also provided. To begin, with, an f value of 0.69 is used for pectin based on the information provided by the supplier for the galacturonic acid content and the degree of methylation (74% w/w and 6.7% w/w, respectively, yielding $\approx$ 69%). Similarly, an average f value of 0.83 is used for sodium alginate based on the guluronic acid content found in multiple commercially available sodium alginates [23] (reported range between 0.80 and 0.86). In the case of sodium carboxymethyl cellulose, an f value of 0.9 is used, which corresponds to the degree of substitution stated by the supplier. Finally, for the chitosan system, an f value of 1.0 is used by virtue of every sugar ring possessing an amine group. Based, on the range of L_p values stated earlier, and the range of f values, it is possible to gauge an expectation for the value of $[\eta]_R$ (Figure 2.4). Thus, the quantitative agreement between the OSF model and the experimental results is largely satisfactory (see the Supplementary Material Subsection 2.7.2 for the scaling approach [24]).

The discussion for polypeptides begins with a clarification of the values presented in Table 2.5. The theoretical calculation for polypeptides is performed using a monomer length (l) of 0.371 nm. This is based on estimations for the polypeptide bond length by Corey and Pauling [25]. Additionally, an L_p value of 1.855 nm is used for the theoretical calculations (based on the common approximation [26] that $L_p \approx 5l$). From the experimental results, it is observable that there is a minimal shrinkage/swelling to the coil size of gelatin upon changing the pH. As discussed in Section 2.2, screening via salt addition within a polyampholyte system leads to an overall swelling within the system. In the case of the gelatin system, the polymer coils are further denatured by heating the system to 338 K. Thus, not only does it lose its ability to refold, it also is expectedly invariant to changes in the

pH (or overall charge), thereby leading to very little variation in intrinsic viscosity (Figure 2.3 and Table 2.5). This hypothesis is further confirmed upon comparing the experimental results to the theoretical estimations for screening-related coil expansion in Table 2.5. It is observed that the pH-related changes in the screened system are comparable with the changes into coil conformations for a weakly charged polypeptide chain (f = 0.05 to 0.10). However, upon increasing the value of f to 0.25, there is a dramatic increase in the value of Θ_p by virtue of a quadratic dependence between Θ_p and f (Equations 2.6 and 2.7). This dependence is shown in Figure 2.5 for both cases, i.e., polysaccharides and polypeptides.

It is clear from Figure 2.5 that polypeptides exhibit a more marked quadratic dependence compared to polysaccharides. This is attributable to the fact that the size of a saccharide monomer is approximately 2.7 times larger than the size of a peptide monomer (Equation 2.6). Further, for polysaccharides, $5l \leq L_p \leq 10l$; whereas, for polypeptides, $L_p \approx 5l$, and thus, the denominator term diminishes further in Equation 2.7 for polypeptides.

As highlighted earlier, the charge density of a polypeptide is lower when compared to a polysaccharide. Thus, the results are restricted to an f value of 0.25 (i.e., at most, one in every four amino acids are charged). Even at such low charge densities, it is observable that a polypeptide chain is likely to swell more rapidly when compared to a fully charged polysaccharide chain. However, it is worth bearing in mind that the size of the coil is still strongly dependent on the persistence length of the polymer in question, and thus, as shown in Figure 2.3, the polysaccharides still exhibit much larger intrinsic viscosity values when compared to polypeptides, such as gelatin.

2.5.2. MOLAR MASS DEPENDENCE

Traditionally, the determination of the intrinsic viscosity is of interest to calculate a polymer's molar mass (M) using the Mark-Houwink equation [10]:

$$[\eta] = KM^a \tag{2.8}$$

where K and a are experimentally derived variables that depend on the polymer-solvent interactions. This expression may then be suitably rewritten to calculate the relative intrinsic viscosity term ($[\eta]_R$):

$$[\eta]_R = (M_2/M_1)^a \tag{2.9}$$

Here, M_1 and M_2 represent two distinct values of molar mass. For multiple unscreened polysaccharide systems in good solvents, the value of a is reportedly around 1 [27, 28]. However, in all other cases, the biopolymer chains are expectedly more flexible, and thus, $0.5 < a < 1$ (in the good solvent limit) [29]. Thus, it is noticeable that, in the best-case scenario, Equation 2.9 becomes a linear relationship. In all other cases, it is a sublinear power law dependence. In contrast, it is observable from Equation 2.7, that screening-mediated changes into $[\eta]_R$ take on a superlinear

power law dependence $\left([\eta]_R \approx (1+\Theta_p)^{3/2}\right)$.

It is, therefore, worth highlighting that screening effects are considerably more influential in changing the overall hydrodynamic coil size compared to changes in the molar mass in the case of (charged) biopolymers. Further still, biopolymers of the same molar mass can show dramatic changes in their coil size due to charge-mediated swelling. This latter point is of relevance in the estimation of a polymer's molar mass. As discussed earlier, the molar mass of biopolymers is typically represented using M_w. However, M_w is dependent on the size of coils in solution and is, therefore, highly sensitive to both the pH and ionic strength of the system. As such, typical acid-base (or base-acid) precipitation methods [2, 7] used to extract biopolymers impact both parameters and, thus, introduces considerable variability in the size and solubility of biopolymer coils. Additionally, it also brings into question the traditional approach of relating physical properties, such as the viscosity, to the molar mass [10, 14]. The intention of relating properties to the molar mass is to highlight underlying mechanisms of chain relaxation [10, 14]. However, it is equally accepted that there are multiple methods to determine the molar mass, and that the various techniques respond differently to the change in the molar mass distribution [10]. An argument may yet be made that it is still possible to carefully assess the molar mass using multiple techniques for a particular polymer-solvent system. However, this approach fails in the case of biopolymers where the exact chemical structure is unknown, and might be nearly impossible to establish [7]. In these cases, there is still the possibility to represent trends in viscosity using the intrinsic viscosity (or the size of the macromolecular entity) as the point of reference. This is also the subject of the authors' interest and is discussed in an alternate publication (see Chapter 3) [30].

2.6. CONCLUSIONS

To summarise, it is found that the OSF model is quite suitable to model screening-mediated variations in the hydrodynamic size of a generic biopolymer system. The approach, based on this model, is successful in providing an accurate prediction for a number of polysaccharide architectures, charge levels, and types of functionalisation using a bare persistence length of 7 nm. This value is closely comparable with the recently reported range of persistence lengths for cellulosic backbones. Equally, as expected (both theoretically and experimentally), completely screened polyampholytic polypeptide chains show minimal changes into their intrinsic viscosity despite changes into the pH. However, it is recognised that this study is limited to a few polysaccharides and only one polypeptide. Thus, the inclusion of other (bio)polymers that are relevant for biomedical applications, food and agriculture, and potentially other industries can further establish the validity of the current approach. Extending this study to include purely cationic/anionic polypeptides and DNA, for instance, provides the scope to investigate a wider range of persistence lengths and charge levels due to a single type of charge (+ or −). In contrast, the inclusion of RNA allows for a similar comparison with ampholytic (and

even zwitterionic) polypeptides such as gelatin. Certainly, such comparisons may also be facilitated using synthetic weak polyelectrolytes. In addition, the potential difficulties of estimating a biopolymer's molar mass based on coil size are worth emphasising, as this is somewhat prone to errors due to charge. Moreover, in case the precise molecular structure is unknown, the use of the size of the macromolecular object (or $[\eta]$) as a direct internal reference still allows for underlying trends in the physical properties of biopolymer systems to be established. Although the role of screening-mediated variations in the hydrodynamic size remains the primary focus of the current study, variations in "soft" interactions due to changes into the pH or temperature are equally relevant in the context of biopolymers, which, as such, also remains underdeveloped. It is, therefore, encouraged to extend the current approach to these cases to cover a wider range of structure-property relationships for not only biopolymers, but also for other weak polyelectrolytes, which may help in developing the physical understanding of charged (bio)polymers overall.

2.7. DATA AND SUPPLEMENTARY MATERIAL

The data from the rheology measurements is publicly accessible using the following link: https://doi.org/10.4121/f1ab8cce-67ec-4a8d-8f3b-4471db5d372e.

2.7.1. CONDUCTIVITY DUE TO COUNTER ION CONDENSATION

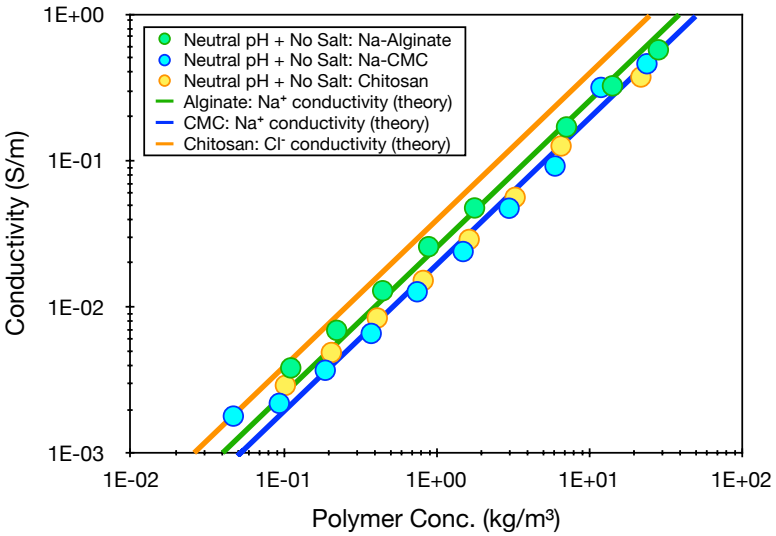

Figure 2.6: This figure represents both, the measured conductivity values of the "Neutral pH – No Salt" samples as well as the estimation of the counterion contributions (expressed in brackets as theory) to the electrical conductivity of the system.

Calculations are presented here for there biopolymer systems where the chemical structure remains well established: Na-Alginate, Na-CMC, and Chitosan. Although no specific information about the counter ion is provided in the case of Chitosan, it is assumed to be Cl^- by virtue of using an HCl solution to adjust the pH. Based on this information, the mass of counter ion present per unit mass of polymer is calculated. This is summarised in Table 2.6.

As highligted in the main text, there is a linear dependence between conductivity and concentration. Therefore, the conductivity is estimated at different polymer concentrations using the limiting molar conductivity values (at 25 °C) for Na^+ and Cl^-, i.e., 0.005 S·m^2/mol and 0.008 S·m^2/mol respectively [20]. The results are depicted graphically in Figure 2.6.

In Figure 2.6, the estimated values of the conductivity are in good agreement with the measured values for Na-Alginate as well as Na-CMC. However, it is observed that the estimations in the case of Chitosan over predicts the expected conductivity. Further, based on the evidence provided in literature [21], the dependence on the concentration is not linear and in fact, a reduction in the conductivity of the polymer may be expected in the concentrated regime. Based on these considerations, it is suspected that the approach here merely provides an initial estimation for the contribution made by the counter ions, and that an investigation into this matter remains outside the scope of the current work.

Table 2.6: This table summarizes the calculations for the mass of counter ion per unit mass of polymer.

Biopolymer	**Mass of Counter Ion / Mass of Monomer**	**Moles of Counter Ion per kg of polymer**
Na-Alginate	0.116	5.051
Na-CMC	0.088	3.846
Chitosan	0.180	5.091

2.7.2. SCALING APPROACH

In the theoretical approach highlighted within the main text, a semi-flexible “worm like” idealisation is used to represent biopolymer chains. Alternatively, Dobrynin, Colby & Rubinstein (DCR) propose the possibility to model polyelectrolytes using a scaling approach that utilises electrostatic blobs [24]. When dissolved in a good solvent, electrostatic interactions of each blob are of the order of the thermal energy. Therefore, the size of each electrostatic blob is governed by L_B. Further, as proposed by the DCR model, on length scales larger than the size of the blob, the electrostatic repulsions start to dominate and thus, the chain may be considered as a rodlike assembly of electrostatic blobs with length L (good solvent limit):

$$L = Nl\left(\frac{u}{A^2}\right)^{2/7} \tag{2.10}$$

Where $u = L_B/l$ and A is the average number of monomers between charges. Thus, it is possible to approximate the radius of gyration for this rod like chain as being:

$$R_g = \frac{L}{\sqrt{12}} = \frac{Nl}{\sqrt{12}}\left(\frac{u}{A^2}\right)^{2/7} \tag{2.11}$$

Similarly, Equations 2.2 and 2.3 (from main text) may be simplified further to yield an R_g in the screened limit (for a linear chain):

$$R_g = \sqrt{\frac{L_c L_p}{3}} = \sqrt{\frac{NP}{3}} \cdot l \tag{2.12}$$

Where $P = L_p/l$. Thus, from Equations 2.11 and 2.12, it is possible to approximate $[\eta]_R$ as follows:

$$[\eta]_R \approx \frac{1}{8} \cdot \left(\frac{N}{P}\right)^{3/2} \cdot \left(\frac{u}{A^2}\right)^{6/7} \tag{2.13}$$

It is worth noting that an equivalence between the hydrodynamic radius and the radius of gyration is assumed in Equation 2.13, and the limitations addressed earlier (see Section 2.2) are not necessarily overcome. Additionally, as Equation 2.13 demands prior knowledge of the molar mass (through N), the comparison is limited to the CMC system (Table 2.7).

It is clear from Table 2.7 that the rod like approximation provided by the DCR model is much larger when compared to both, the OSF approach as well as the experimental value. Thus, the scaling approximation of the polymer chains in the unscreened case may be a very coarse interpretation for the conformation (at least in the case of polysaccharides). The DCR approach highlights that $u/A^2 < 1$ typically, and thus suggests that there is still some flexibility on length scales smaller than the electrostatic blob size [24]. However, it is believed that this approach is valid only when $A^2 >> 1$. In the case of CMC, $A^2 \approx 1.23$ and thus, although the DCR approach captures some flexibility within the polysaccharide chain, the chain is still modelled as an inherently stiff rod like object. In the case of polypeptides $A^2 >> 1$ and thus, the scaling approach may yet be successful in capturing the flexibility within the charged chain.

Table 2.7: A comparison between experimental results, the worm-like chain approach, and the rod like chain approach for sodium carboxymethyl cellulose (L_P = 7nm, refer to Figure 2.4 in main text).

Approach	$[\eta]_R$
Experimental, CMC	5.441
OSF Approach	4.969
DCR Approach	57.21

REFERENCES

[1] D. Nelson, M. Cox, and A. Hoskins. *Lehninger Principles of Biochemistry*. New York, NY, USA: Macmillan Learning, 2021.

[2] V. Kontogiorgos. *Pectin: Technological and Physiological Properties*. Cham, Switzerland: Springer International, 2020.

[3] J. O'Mahony and P. Fox. "Milk Proteins: Introduction and Historical aspects". In: *Advanced Dairy Chemistry: Volume 1A: Proteins: Basic Aspects*. New York, NY, USA: Springer, 2013, pp. 43–85.

[4] J. Jumper, R. Evans, A. Pritzel, T. Green, M. Figurnov, O. Ronneberger, K. Tunyasuvunakool, R. Bates, A. Žídek, and A. Potapenko. "Highly accurate protein structure prediction with AlphaFold". In: *Nature* 596 (2021), pp. 583–589. DOI: https://doi.org/10.1038/s41586-021-03819-2.

[5] K. te Nijenhuis. "On the nature of crosslinks in thermoreversible gels". In: *Polymers Bulletin* 58 (2007), pp. 27–42. DOI: https://doi.org/10.1007/s00289-006-0610-7.

[6] D. Picout and S. Ross-Murphy. "Rheology of biopolymer solutions and gels". In: *The Scientific World Journal* 3 (2003), pp. 105–121. DOI: https://doi.org/10.1100/tsw.2003.15.

[7] S. Felz, S. Al-Zuhairy, O. Aarstad, M. van Loosdrecht, and Y. Lin. "Extraction of structural extracellular polymeric substances from aerobic granular sludge". In: *Journal of Visualized Experiments* 115 (2016), e54534.

[8] D. Some, H. Amartely, A. Tsadok, and M. Lebendiker. "Characterization of proteins by size-exclusion chromatography coupled to multi-angle light scattering (SEC-MALS)". In: *Journal of Visualized Experiments* 148 (2019), e59615.

[9] N. Farkas and J. Kramar. "Dynamic light scattering distributions by any means". In: *Journal of Nanoparticle Research* 23 (2021), p. 120. DOI: https://doi.org/10.1007/s11051-021-05220-6.

[10] M. Rubinstein and R. Colby. *Polymer Physics*. Oxford, UK: Oxford University Press, 2003.

[11] C. Lopez, A. Matsumoto, and A. Shen. "Dilute polyelectrolyte solutions: Recent progress and open questions". In: *Soft Matter* 20 (2023), pp. 2635–2687. DOI: https://doi.org/10.1039/D3SM00468F.

[12] C. Lopez. "Entanglement of semiflexible polyelectrolytes: Crossover concentrations and entanglement density of sodium carboxymethyl cellulose". In: *Journal of Rheology* 64 (2020), pp. 191–204. DOI: https://doi.org/10.1122/1.5127015.

[13] H. Yamakawa and M. Fujii. "Intrinsic viscosity of wormlike chains. Determination of the shift factor". In: *Macromolecules* 7 (1974), pp. 128–135. DOI: https://doi.org/10.1021/ma60037a024.

[14] R. Sayko, M. Jacobs, and A. Dobrynin. "Quantifying properties of polysaccharide solutions". In: *ACS Polymers Au* 1 (2021), pp. 196–205. DOI: https://doi.org/10.1021/acspolymersau.1c00028.

[15] A. Dobrynin. "Electrostatic persistence length of semiflexible and flexible polyelectrolytes". In: *Macromolecules* 38 (2005), pp. 9304–9314. DOI: https://doi.org/10.1021/ma051353r.

[16] K. Kamide, M. Saito, and H. Suzuki. "Persistence length of cellulose and cellulose derivatives in solution". In: *Die Makromolekulare Chemie, Rapid Communications* 4 (2003), pp. 33–39. DOI: https://doi.org/10.1002/marc.1983.030040108.

[17] W. Mackie, S. Perez, R. Rizzo, F. Taravel, and M. Vignon. "Aspects of the conformation of polyguluronate in the solid state and in solution". In: *International Journal of Biological Macromolecules* 5 (1983), pp. 329–341. DOI: https://doi.org/10.1016/0141-8130(83)90056-9.

[18] W. Astbury. "Structure of alginic acid". In: *Nature* 155 (1945), pp. 667–668. DOI: https://doi.org/10.1038/155667a0.

[19] F. Dri, S. Shang, L. Hector, P. Saxe, Z.-K. Liu, R. Moon, and P. Zavattieri. "Anisotropy and temperature dependence of structural, thermodynamic, and elastic properties of crystalline cellulose Iβ: A first-principles investigation". In: *Modelling and Simulation in Materials Science and Engineering* 22 (2014), p. 085012. DOI: https://doi.org/10.1088/0965-0393/22/8/085012.

[20] R. Robinson and R. Stokes. *Electrolyte Solutions*. Mineola, NY, USA: Dover Publication Inc., 2002.

[21] F. Bordi, R. Colby, C. Cametti, L. De Lorenzo, and T. Gili. "Electrical conductivity of polyelectrolyte solutions in the semidilute and concentrated regime: The role of counterion condensation". In: *The Journal of Physical Chemistry B* 106 (2002), pp. 6887–6893. DOI: https://doi.org/10.1021/jp020262i.

[22] A. Veis. *The Macromolecular Chemistry of Gelatin*. New York, NY, USA: Academic Press, 1964.

[23] W. Jiao, W. Chen, Y. Mei, Y. Yun, B. Wang, Q. Zhong, H. Chen, and W. Chen. "Effects of molecular weight and guluronic acid/mannuronic acid ratio on the rheological behavior and stabilizing property of sodium alginate". In: *Molecules* 24 (2019), p. 4374. DOI: https://doi.org/10.3390/molecules24234374.

[24] A. Dobrynin, R. Colby, and M. Rubinstein. "Scaling theory of polyelectrolyte solutions". In: *Macromolecules* 28 (1995), pp. 1859–1871. DOI: https://doi.org/10.1021/ma00110a021.

[25] R. Corey and L. Pauling. "Fundamental dimensions of polypeptide chains". In: *Proceedings of the Royal Society B: Biological Sciences* 141 (1953), pp. 10–20.

[26] J. Bright, T. Woolf, and J. Hoh. "Predicting properties of intrinsically unstructured proteins". In: *Progress in Biophysics and Molecular Biology* 76 (2001), pp. 131–173. DOI: https://doi.org/10.1016/S0079-6107(01)00012-8.

[27] M. Masuelli and C. Illanes. “Review of the characterization of sodium alginate by intrinsic viscosity measurements: Comparative analysis between conventional and single point methods”. In: *International Journal of Biomaterials Science and Engineering* 1 (2014), pp. 1–11.

[28] T. Eremeeva and T. Bykova. “SEC of mono-carboxymethyl cellulose (CMC) in a wide range of pH Mark–Houwink constants”. In: *Carbohydrate Polymers* 36 (1998), pp. 319–326. DOI: https://doi.org/10.1016/S0144-8617(97)00259-2.

[29] M. Masuelli. “Mark-Houwink parameters for aqueous-soluble polymers and biopolymers at various temperatures”. In: *Journal of Polymer and Biopolymer Physics Chemistry* 2 (2014), pp. 37–43.

[30] A. Raja, P. Wilfert, and S. Picken. “Using the Herschel–Bulkley consistency index to characterise complex biopolymer systems—The effect of screening”. In: *Polymers* 16 (2024), p. 2822. DOI: https://doi.org/10.3390/polym16192822.

3

SYSTEMATIC TRENDS USING THE HERSCHEL-BULKLEY CONSISTENCY INDEX

The use of the consistency index, as determined from fitting rheological data to the Herschel–Bulkley model, is described such that it may yield systematic trends that allow a very convenient description of the dissipative flow properties of linear and branched (bio)polymers in general, both in molecular and weakly associated supramolecular solutions. The effects of charge-mediated interactions by the systematic variation of the ionic strength and hydrogen bonding by a systematic variation in pH, using levels that are frequently encountered in systems used in practice, is investigated. These effects are then captured using the associated changes in the intrinsic viscosity to highlight the above-mentioned trends, while it also acts as an internal standard to describe the data in a concise form. The trends are successfully captured up to 100 times the polymer coil overlap and 100,000 times the solvent viscosity (or consistency index). These results therefore enable the rapid characterisation of biopolymer systems of which the morphology remains unknown and may continue to remain unknown due to the wide-ranging monomer diversity and a lack of regularity in the structure, while the macromolecular coil size may be determined readily.

This chapter has been published as: A. Raja, P.K. Wilfert, and S.J. Picken, "Using the Herschel–Bulkley Consistency Index to Characterise Complex Biopolymer Systems—The Effect of Screening", *Polymers*, **2024**, 16(19), 2822.

3.1. INTRODUCTION

The prevalent strategy to characterise biopolymers using a range of different spectroscopy techniques is predicated upon the effort to understand their underlying chemical structure. Common examples include the use of Fourier-Transform Infrared spectroscopy (FTIR) to determine the structures of proteins and polysaccharides [1–3] and the use of Nuclear Magnetic Resonance (NMR) to determine the structure of polysaccharides in solution [4, 5]. Other highly specific examples include the use of Mass Spectrometry (MS), in combination with other preparatory techniques, for proteomics [6–8]. In some cases, a combination of these spectroscopic techniques may also be used to understand the chemical structure [9]. The aim of these techniques has been to lay the foundation that establishes the biopolymer's monomer composition, the functional groups, and to identify similarities or differences compared to other biopolymers.

Despite their versatility, spectroscopic techniques cannot provide direct information on the properties of a material or clear insights on a material's structure–property relationships. They only provide considerable insight into the chemical structure of the material. Obviously, an understanding of the chemical structure alone is not sufficient to suitably extract, process, and utilise various biopolymers. Biopolymers are typically extracted and separated as a concentrated system (>10 kg/m^3, often as high as 100 kg/m^3) using techniques such as centrifugation, sedimentation, and filtration together with additional downstream purification steps [10–12]. It is worth noting that these concentrations are much higher than the (highly) dilute regime where polymer systems are typically studied. Thus, a close understanding of the rheological properties of the system is required. Similarly, as highlighted in Chapter 1, the typical applications of biopolymers in the biomedical, food, agriculture, and building industries look to process them into hydrogels [13], foams [14], coatings [15], and composites [16, 17]. In these cases, a good understanding of the structure-property relationships, relating to rheology, which can respond to a very wide range of length scales (0.1-100 μm), is generally considered to be relevant as the basis to transform the same concentrated biopolymer system into a variety of materials. In view of the above, there is clearly a need for the actual determination of the rheological properties of complex (bio)polymer-based systems. This can be used directly in the optimisation of the extraction, processing, and application of these systems. In addition, rheological information has an extremely high sensitivity to minor interactions that are nearly impossible to find using FT-IR or NMR. For instance, the viscosity of materials can span at least 16 orders of magnitude [18, 19]. Thus, subtle changes in the property of materials are immediately apparent.

Given that the sensitivities and ability of rheometric techniques to provide high resolution information across multiple length scales remains well established [20], a close empirical assessment of the rheological parameters of concentrated biopolymer systems is needed. One such method is the evaluation of a biopolymer's viscosity as a function of concentration. This may in turn be used to describe the dynamics of a biopolymer system. Certainly, this approach has been used to describe both

the dynamics of uncharged synthetic polymers in solution [20] and synthetic polyelectrolytes in solution [21]. However, the attempt to describe the viscosity of biopolymer systems, and thus their associated dynamics over a given concentration range, remains under development [22, 23]. Amongst these, Sayko et al. suggest that it is possible to establish a dependence between the viscosity of concentrated biopolymer solutions and the weight-averaged molar mass (in place of concentration) [22]. This is carried out to isolate different relaxation regimes in the resulting curves (Rouse regime vs. entangled regime), whose respective slopes may be explained using prevalent scaling arguments for (bio)polymers in solution. However, it is worth highlighting that the persistence length (and thus the coil size) is strongly influenced by screening effects in the case of biopolymer systems [24] (See Chapter 2). Thus, the weight-averaged molar mass becomes an improper standard for mapping changes to viscosity. Based on a study conducted by the authors of this paper [24], the intrinsic viscosity may be used in its place as it is possible to capture changes to the coil size in this way. Moreover, the intrinsic viscosity may be used as an internal standard in cases where the complex chemical structure of the biopolymer system remains unestablished. This remains consistent with the second approach highlighted by Pathak et al., where the determination of the exact hydrodynamic conformation of antibody systems in solution remains highly elusive [23]. This method allows for the fitting of power series expansion curves that are similar to the Huggins equation [20]. In general, however, both approaches cover a very limited concentration range and remain specific to a particular subset of biopolymer systems.

Covering changes to the viscosity to such a limited extent is not particularly useful in describing the viscous properties of a wide variety of biopolymer systems. As such, it is important to cover the adverse shear thinning effects that are prevalent in the working concentration range of these systems [25]. Equally there is a need to cover the effects of "soft" charge-mediated interactions resulting from changes in pH, conductivity, and temperature, as well as changes to the viscosity due to a biopolymer's chemical structure. Thus, a strategy to characterise concentrated biopolymer systems using the consistency index from the Herschel–Bulkley model and to link the obtained value to the biopolymer's concentration by changing conditions such as pH, ionic strength, temperature, branching, and molar mass is proposed below. The approach highlighted covers both methods, i.e., power series expansions motivated using the Huggins equation and power laws motivated by scaling arguments. The aim of providing such a framework is to explain the properties of both known biopolymer systems that are frequently used in practice and novel biopolymer systems of which the chemical structure is unknown. Thus, the framework permits the rapid characterisation of a wide variety of biopolymer systems for practical scenarios pertaining to their extraction, processing, and application.

3.2. THE HERSCHEL-BULKLEY APPROACH

Upon attempting to determine the viscosity at elevated concentrations, it is observed that concentrated polymer systems seldom behave as Newtonian fluids and often exhibit shear-thinning behaviour [25]. It is also frequently found that the solid-like

gel structures resulting from the physical interpenetration of coils (in addition to the existing non-covalent interactions within biopolymers) themselves leads to the development of yield stresses and thixotropy [25]. Thus, polymers in the concentrated regime often exhibit pseudo plastic behaviour. Conventionally, the viscosity of polymer solutions is determined using zero-shear viscosity measurements [26, 27]. However, the solid-like structures of a yield stressing fluid often have elastic contributions at low shear stresses (or at low shear rates). This then limits the ability to experimentally obtain the expected initial plateau in the viscosity of a shear thinning fluid. What is proposed is to characterise polymeric systems over a very wide range of compositions using the Herschel-Bulkley model, which can describe many types of complex systems within the same framework [25]:

$$\sigma = \sigma_0 + K\dot{\gamma}^n \tag{3.1}$$

Here, σ represents the applied or observed shear stress, σ_0 represents the yield stress depicted by the fluid, and $\dot{\gamma}$ represents the observed or applied shear rate, K represents the consistency index, and n represents the power law index. It is worth noting that in the equation above, the units of K are arbitrarily defined based on the value of n. Thus, the Herschel-Bulkley equation may be suitably rewritten to restore dimensional consistency for K (in stress units) irrespective of the value of n:

$$\sigma = \sigma_0 + K\left(\frac{\dot{\gamma}}{1s^{-1}}\right)^n \tag{3.2}$$

As the Herschel-Bulkley model by itself holds no theoretical premise, it is worth discussing how it may be interpreted within this study. In cases where the value of the yield stress drops to zero and the value of the power law index is unity, Equation 3.2 reduces to Newton's law of viscosity, with the consistency index term representing the viscosity of the Newtonian fluid. In the case of a yield stress and a power law index not equal to 1, the consistency index represents the dissipative contribution to the stress at 1 s^{-1} shear rate. It is thus proposed that the consistency index might be used in place of viscosity to establish global trends in the behaviour of biopolymeric systems up to high concentrations. Thus, similar to the Huggins equation [20, 23], it is possible to estimate the consistency index of a concentrated biopolymer system using a power series expansion:

$$K = K_s\left(1 + [\eta]c + a_2\left([\eta]c\right)^2 + a_3\left([\eta]c\right)^3 + ...\right) \tag{3.3}$$

where $K_s = (\eta_s \text{ x } 1 \text{ s}^{-1})$ is the stress developed by the solvent at 1 s^{-1} shear rate (η_s= solvent viscosity). This may be suitably rearranged to yield a non-dimensional (universal) equation in terms of the "relative consistency index" (K/K_s) and "overlap factor" term ($[\eta]c$) [20, 23]:

$$\frac{K}{K_s} = 1 + [\eta]c + a_2\left([\eta]c\right)^2 + a_3\left([\eta]c\right)^3 + ... \tag{3.4}$$

Equally, as is typical from scaling approaches [20], it is possible to represent the relative consistency index as a power law function with respect to the overlap factor (for $[\eta]c > 1$):

$$\frac{K}{K_s} \propto \left([\eta]c\right)^{\alpha} \tag{3.5}$$

Note that the relative consistency index is the analog of the relative viscosity, and, indeed, at zero concentration, there is no distinction between K_s and η_s (solvent viscosity). The overlap factor represents the general idea that the change in consistency index should be scaled with respect to the space filling concentration of the macromolecular objects in the system. Even at concentrations up to 100 kg/m^3, these systems will frequently have a low solid content so that the molecules (or macromolecular objects) can indeed overlap and occupy the same volume. Thus, $(1/[\eta])$ is interpreted to be the value for the transition from a dilute to a semi-dilute system.

3.3. MATERIALS AND METHODS

3.3.1. MATERIALS

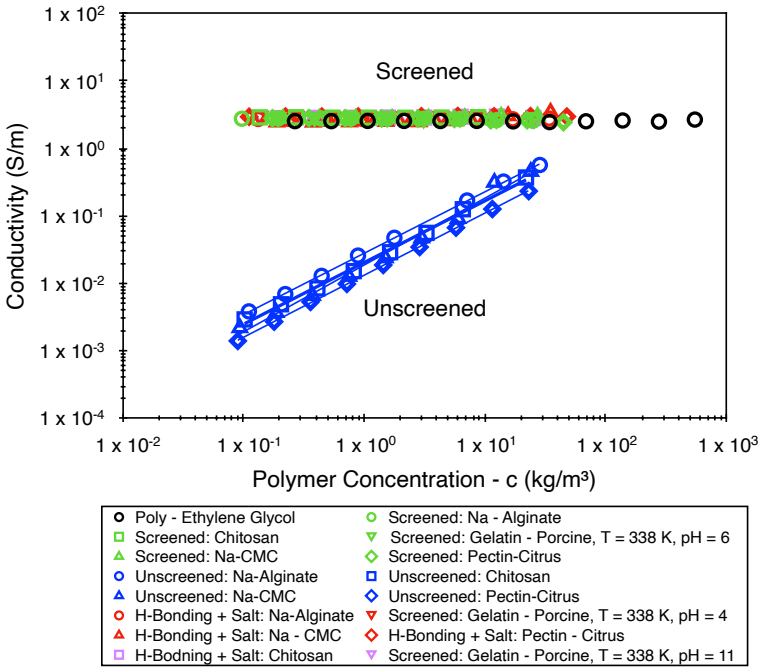

Figure 3.1: Conductivity of the samples tested (including those reported in Chapter 2 [24]). Guides to the eye are also provided for the "Unscreened" samples to highlight the differences in the values of their conductivity and their (somewhat) linear dependence on concentration.

All polymers used in this study were procured from Sigma-Aldrich and are

Table 3.1: List of polymers and their salient properties: type of functionalisation, architecture, and molar mass. Note: Molar mass (or range) is reported wherever it is provided by manufacturer.

Polymer Name	**Salient Properties**
Poly-Ethylene Glycol (PEG), CAS Number: 25322-68-3	End functionalisation with hydroxyl group, Avg. M_n = 20 kg/mol.
Sodium Alginate (Na-Alginate), CAS Number: 9005-38-3	Polyanion: Carboxyl group, High mannuronic acid content. Linear copolymer
Chitosan, CAS Number: 9012-76-4	Polycation: Amine group, Linear homopolymer, M_w ~ 50 to 190 kg/mol.
Sodium Carboxy Methyl Cellulose (Na-CMC), CAS Number: 9004-32-4	Polyanion: Carboxyl group, Degree of substitution = 0.9, Linearly substituted homopolymer, M_w ~ 250 kg/mol.
Pectin from Citrus Peels (Pectin-Citrus), CAS Number: 9000-69-5	Polyanion: Carboxyl group, Galacturonic acid ≥ 74.0%, Degree of methylation ≥ 6.7%, Branched heteropolymer.
Gelatin from Porcine Skin (Porcine-Gelatin), CAS Number: 9000-70-8	Polyampholyte: Carboxyl and amine group, Linear–collagen derivative.

tabulated in Table 3.1. The authors report (see Chapter 2) [24] that the specific choice of biopolymers offers comparison between linear polyanionic (Na-Alginate), polycationic (chitosan), and polyampholytic (porcine-gelatin) biopolymers. Equally, it is possible to compare biopolymers with differences in their architecture (Na-Alginate, Na-CMC, and pectin-citrus) and the quoted molar mass. Poly-ethylene glycol in particular was selected, for the sake of comparison, by virtue of being a synthetic water-soluble polymer.

All biopolymer systems were prepared by stirring the desired concentrations in deionized water for 24 h (86,400 s) in a sealed conical flask at 293 K. Increases to the conductivity were achieved by adding 0.2-0.3 M of NaCl to a fraction of the dissolved systems. Equally, hydrogen bonding was introduced by adjusting the pH using 1M HCl and 1M NaOH solutions. The 1M HCl and 1M NaOH solutions were also used to adjust the pH following dilution from higher concentrations. Figure 3.1

shows the conductivity of the samples (also those reported in Chapter 2 [24] - see Supplementary Material Subsection 3.7.1 for details about the pH of samples). As reported in Chapter 2 [24], the polymer concentrations being represented on the x-axis of all figures are believed to be within an error margin of 11% or 0.0453 decades.

3.3.2. METHODS

The consistency index was obtained for the concentrated biopolymer systems (samples not reported in Chapter 2 [24]) using a stress-controlled TA Instruments Discovery Hybrid Rheometer–3 (DHR-3). The samples were tested using a steel cone on plate setup with the use of a solvent trap. The smooth steel cone had a diameter of 40 mm and a cone angle of 2°, 0 min, and 50 s (0.035 rad). The truncation gap was maintained at 60 µm over the course of the experiment. All tests were performed at a temperature of 298 K.

The tests included performing a set of four linearly decreasing stress-controlled flow ramps between prescribed limits over a period of 60 s. The lower limit of these ramps was always prescribed to a zero-stress value. The first ramp was performed as a conditioning ramp to erase the sample history. The subsequent ramps were performed with rest times of 10 s, 100 s, and 1000 s to validate that the protocol yields reproducible results. The average consistency index from the three measurements was obtained along with a standard deviation by fitting the Herschel-Bulkley parameters to the three ramps with intermittent rest times. The fitting was carried out using the scipy.optimize.curve_fit() function on Python. The undesired features of the flow ramp curve such as initial inertial effects and the elastic recovery region of the flow ramp at low shear rates were removed before the fitting procedure. The reader is asked to refer to Supplementary Material Subsection 3.7.2 for more information about the Herschel-Bulkley curve fitting methodology.

In the case of some samples that presented low consistency index values (typically 10–100 mPa), it could not be ascertained if the cone on plate setup yielded a flow ramp curve with a linear Newtonian slope. This was because such samples produced high shear rates at low stress values, thereby making them difficult to test using the cone on plate setup. In such cases, the concentric cylinder setup was used to obtain a set of data points at five discrete stress values. The test was performed using a steel cup of diameter 30.36 mm and a steel DIN bob rotor with a diameter of 28.00 mm and a height of 42.07 mm. The DIN bob was maintained at a height of 5917.1 μm from the bottom surface of the cup. All tests were performed at a temperature of 298 K. The Herschel–Bulkley parameters were again fitted to these five data points to obtain the consistency index value along with a standard deviation.

3.4. RESULTS

Figures 3.2 to 3.5 represent the obtained consistency index plotted against the polymer concentration. The vertical error bars are indicative of the two-sigma (95%)

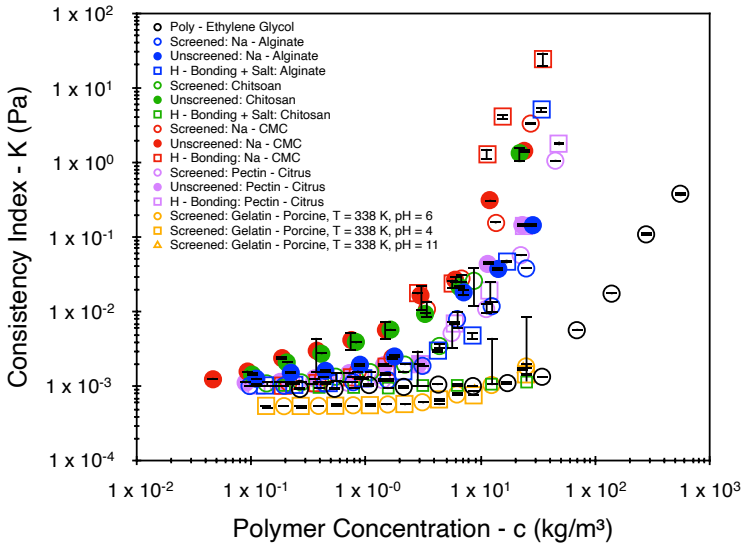

Figure 3.2: Consistency index as a function of polymer concentration for all biopolymer systems. The vertical error bars represent the two-sigma distribution (95% confidence interval).

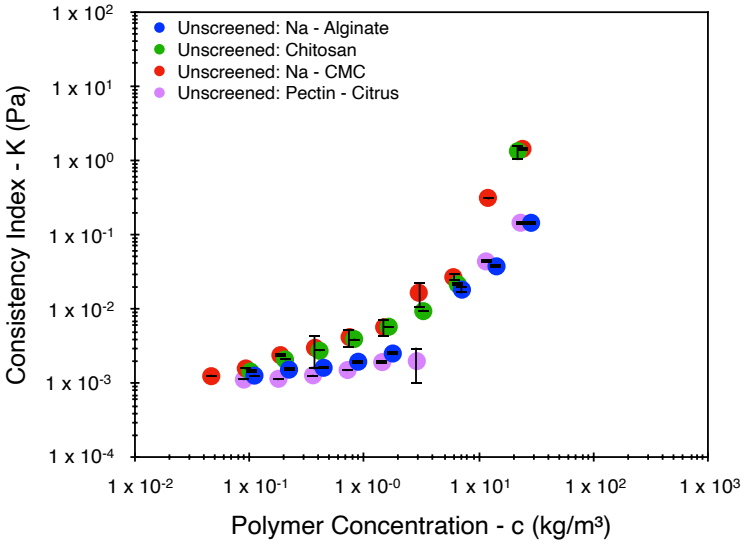

Figure 3.3: Consistency index as a function of polymer concentration for unscreened biopolymer systems. The vertical error bars represent the two-sigma distribution (95% confidence interval).

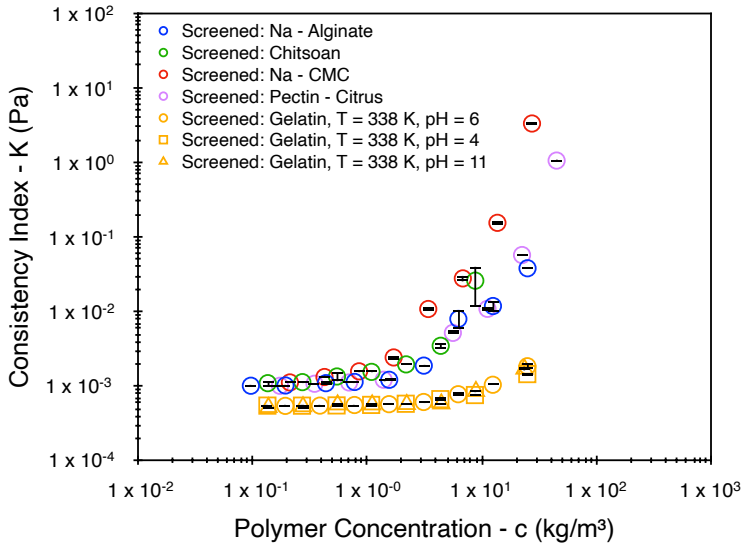

Figure 3.4: Consistency index as a function of polymer concentration for screened biopolymer systems. The vertical error bars represent the two-sigma distribution (95% confidence interval).

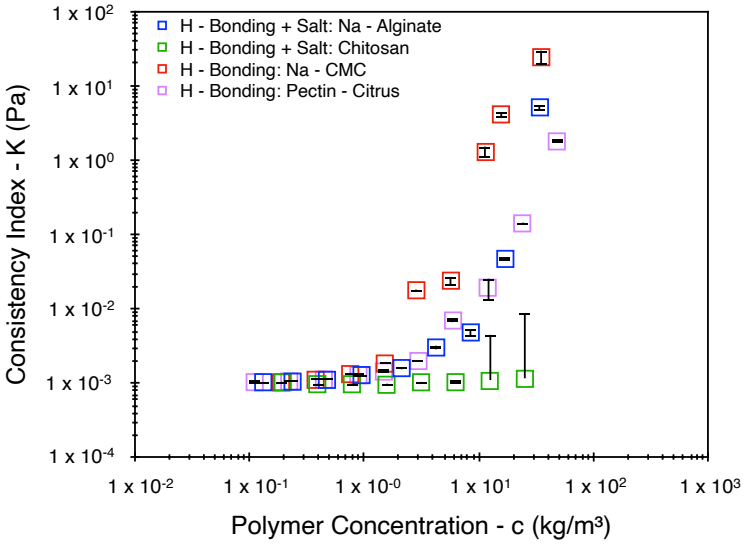

Figure 3.5: Consistency index as a function of polymer concentration for hydrogen-bonded systems. The vertical error bars represent the two-sigma distribution (95% confidence interval).

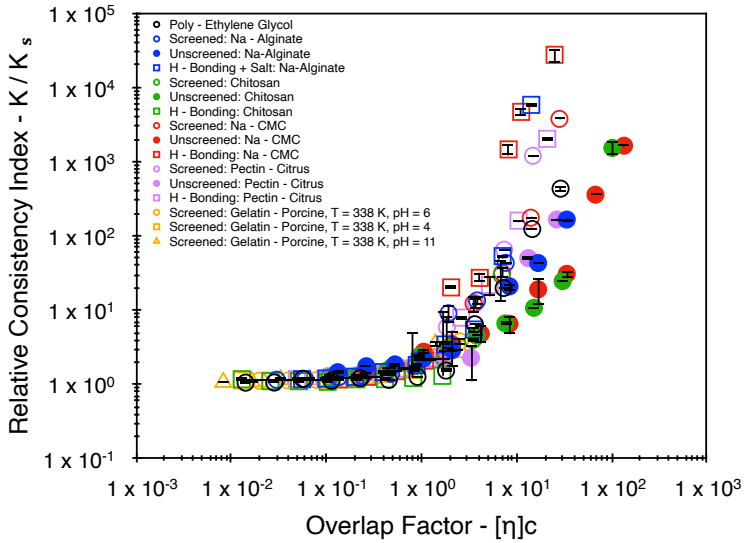

Figure 3.6: The relative consistency index vs. overlap factor for all systems. The vertical error bars represent the two-sigma distribution (95% confidence interval).

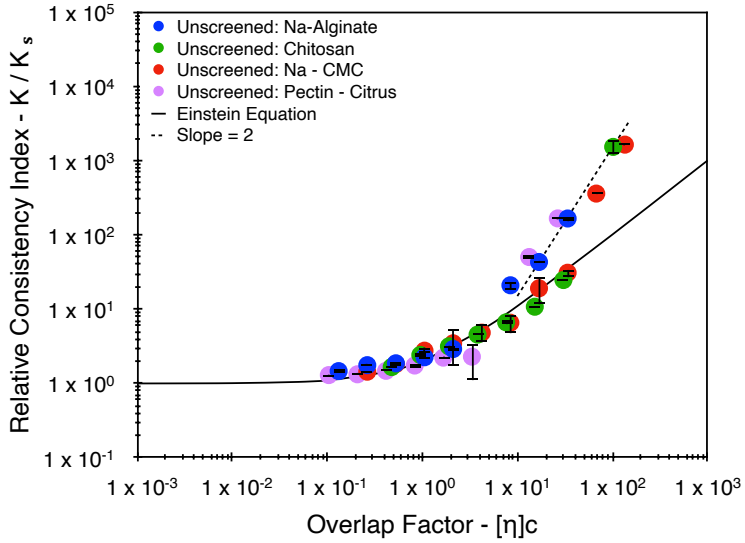

Figure 3.7: The relative consistency index vs. overlap factor for unscreened systems. The vertical error bars represent the two-sigma distribution (95% confidence interval).

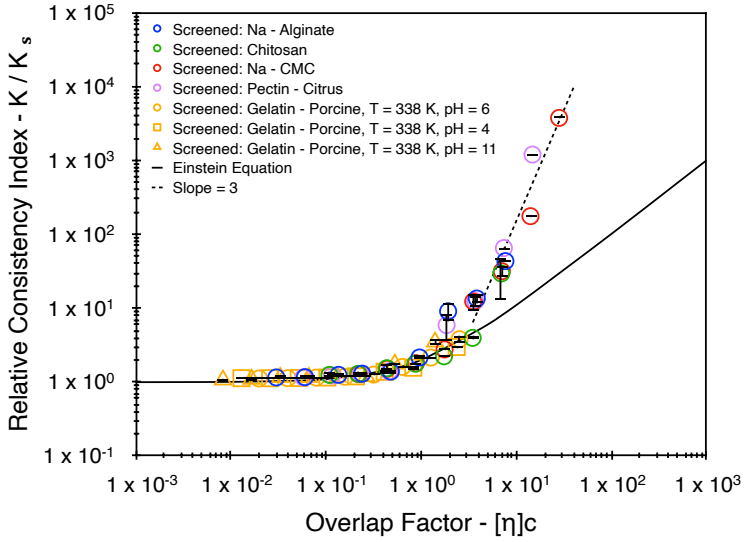

Figure 3.8: The relative consistency index vs. overlap factor for screened systems. The vertical error bars represent the two-sigma distribution (95% confidence interval).

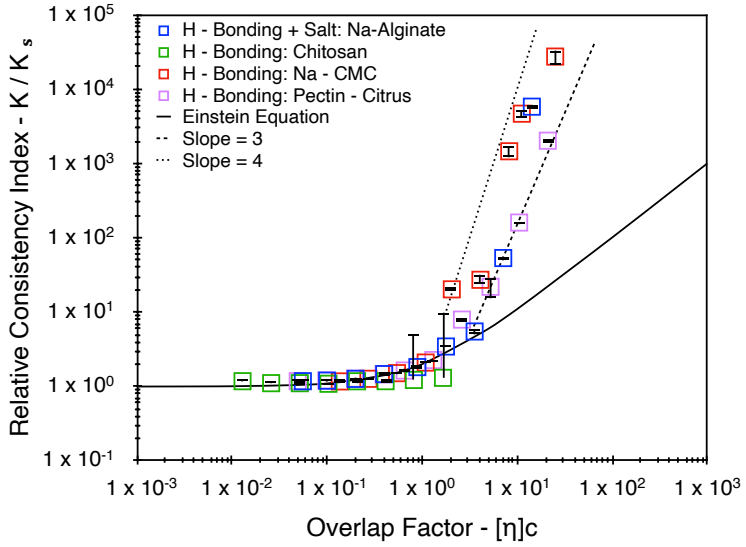

Figure 3.9: The relative consistency index vs. overlap factor for hydrogen-bonded systems. The vertical error bars represent the two-sigma distribution (95% confidence interval).

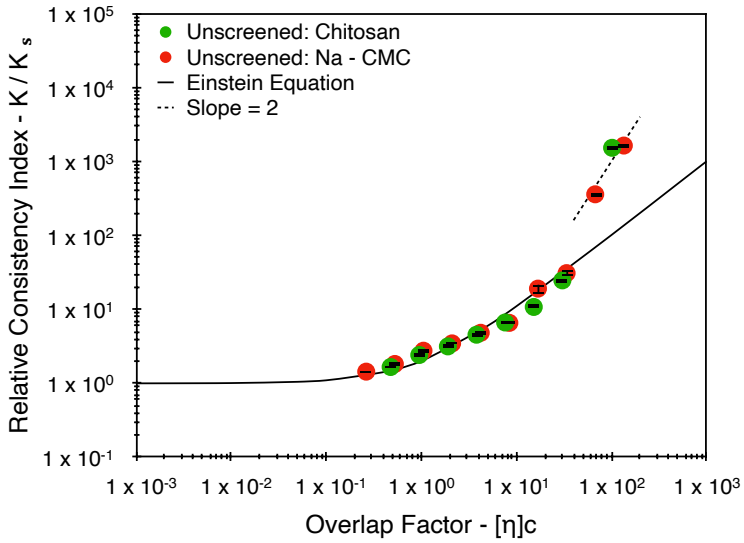

Figure 3.10: The relative consistency index vs. overlap factor for the unscreened chitosan and Na-CMC systems to highlight their delayed departure from the Einstein equation $\left([\eta]c > 10\right)$. The vertical error bars represent the two-sigma distribution (95% confidence interval).

Table 3.2: Experimentally obtained values for the intrinsic viscosity. (S.D. = Standard Deviation)

Biopolymer System	$[\eta]$ **(m^3/kg)** $\pm$ **S.D.**
Poly-Ethylene Glycol	0.053 $\pm$ 0.007
Screened: Na-Alginate	0.308 $\pm$ 0.065
Screened: Chitosan	0.795 $\pm$ 0.100
Screened: Gelatin-Porcine, T = 338 K, pH = 6	0.102 $\pm$ 0.024
Screened: Na-CMC	1.034 $\pm$ 0.037
Screened: Pectin-Citrus	0.332 $\pm$ 0.064
Unscreened: Na-Alginate	1.183 $\pm$ 0.157
Unscreened: Chitosan	4.636 $\pm$ 0.379
Unscreened: Na-CMC	5.624 $\pm$ 0.626
Unscreened: Pectin-Citrus	1.152 $\pm$ 0.175
H-Bonding + Salt: Na-Alginate	0.420 $\pm$ 0.042
Screened: Gelatin-Porcine, T = 338 K, pH = 4	0.095 $\pm$ 0.017
H-Bonding + Salt: Na-CMC	0.719 $\pm$ 0.016
H-Bonding + Salt: Pectin-Citrus	0.440 $\pm$ 0.027
H-Bonding + Salt: Chitosan	0.066 $\pm$ 0.027
Screened: Gelatin-Porcine, T = 338 K, pH = 11	0.060 $\pm$ 0.017

confidence interval. This interval is small in most cases. The cases that present with the largest errors are the ones evaluated at discrete stress values using the concentric cylinder setup. Thus, the error in estimating the consistency index with a greater precision is attributed to the fitting of the nonlinear Herschel-Bulkley model to a limited set of data points. A deviation from a linear set of trends is presented by almost all data sets in Figures 3.2 to 3.5, with the only exception being chitosan at elevated pH conditions with added salts (green unfilled squares - Figure 3.5). However, the solvent's viscosity is also impacted by the salinity and temperature at which the system was tested, thereby shifting data sets vertically. Similarly, all data sets are shifted horizontally by virtue of changes to the intrinsic viscosity. To account for this, it is important to represent the results of Figures 3.2 to 3.5 in terms of the relative consistency index and the overlap factor. The rescaled data sets are presented in Figures 3.6 to 3.10. The rescaling was possible due to the intrinsic viscosity calculations that were made at a low polymer concentration. Most of the intrinsic viscosity values are presented in Chapter 2 [24]. However, to aid interpretability, the entire list of values is report in Table 3.2 (conversion to the frequently used dL/g may be obtained upon multiplying all values by 10).

As anticipated, the data sets start showing deviations from the Einstein equation around the overlap factor value of $[\eta]c = 1$, except for the unscreened CMC and chitosan systems (green filled circles and red filled circles, respectively), where deviations were observed when $[\eta]c > 10$ (See Figure 3.10). Also, when presented in this fashion, the underlying similarities in the data sets become evident. To begin with, it is easy to describe the underlying differences in the various biopolymer systems in their deprotonated state (circles - filled and unfilled). Irrespective of the type of polyelectrolyte under consideration (polyanions or polycations), it appears that once the charged interactions are screened by increasing the ionic strength in the system, the relative consistency index may be described using a third-order power series expansion, or a power law curve with an α value around 3 (2.6 to 3.4 - Figure 3.8). However, when the charged interactions remain unscreened, the relative consistency index may be described using a second-order power series expansion, or a power law curve with an α value around 2 (1.7 to 2.3 - Figure 3.7).

In cases where hydrogen bonding was introduced, the third-order trends continue to persist in the case of the polyanions (Figure 3.9), with the change in the degree of association being reflected only in the value of the intrinsic viscosity. In this case, α values from 3 to 4 offer reasonable power law fits. However, a consistent rise or fall is not reflected in the value of intrinsic viscosity. In the case of alginate, this value rises roughly by a factor of 1.4; however, in the case of CMC, this value falls roughly by a factor of 1.4 (Table 3.2). Expectedly, the introduction of associative interactions within the coils and their associated changes in the coil dynamics are exclusive to the polymer system under consideration. This point is further highlighted upon comparing the results for chitosan with the results of the polyanions. When the pH is raised for chitosan, the intrinsic viscosity value drops roughly by a factor of 12 to suggest a strong association within the coils.

3.5. DISCUSSION

3.5.1. EXPLORING THE THEORETICAL PREMISE

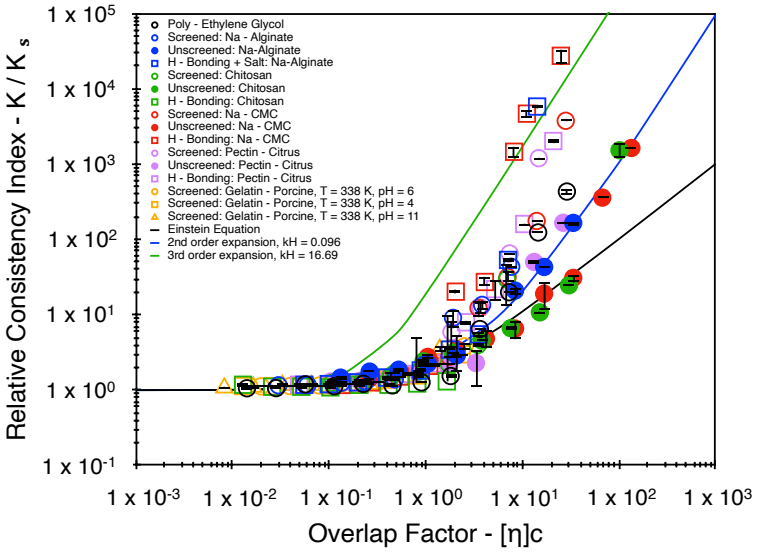

Figure 3.11: Trends in the relative consistency index explained using the Huggins equation. Note that the data points are carried over from Figure 3.6.

Upon examining the trends in Figures 3.6 to 3.10, it is noticeable that they follow from a logical interpretation of screening charged interactions. When the charges on a polymer chain remain unscreened and when $[\eta]c > 1$, a charged polymer chain is likely to experience repulsions from neighbouring like charges by virtue of a drop in the correlation length. Thus, the overlapping coils are likely to take up a collapsed conformation to mitigate interactions with neighbouring chains. In some cases, such as CMC and chitosan, these repulsive interactions may be expected to dominate up to $[\eta]c \approx 10$, thereby leading to a delayed onset for the deviation from the Einstein equation. However, once the polymer-polymer interactions are screened with the addition of salts, the charged sites of the coils are freer to overlap, leading to a sharper increase in the viscous dissipation term (the consistency index).

This is analogous to solvent quality-mediated interactions in uncharged polymers and their influence on the second-order virial coefficient term [20]. In the case of synthetic polymers that are in a good (athermal) solvent, the excluded volume interactions are expected to dominate, thereby leading to a large second-order virial coefficient term. However, as the system approaches the theta condition, the excluded volume approaches zero, thereby plausibly leading to a domination of the three-body interaction term at higher concentrations (the third-order coefficient). Under theta conditions, the polymer-polymer interactions are imagined to be negligible (the second-order coefficient). Pathak et al. [23] also report a more in-depth analysis of

the Huggins coefficient term and its potentially predictable correlation to the second virial coefficient term. However, it is reported that a direct correlation could not be found to link the terms together. In part, this shortcoming was also attributed to the failure of existing physical models for polymers. In contrast, Sayko et al. [22] managed to link the excluded volume interaction term(s) and changes to the ionic strength of the system and suggested that screening can indeed be used to minimise the excluded volume interactions.

In a similar light, previous literature sources suggest that the power series expansion may be limited to include only a second-order correction factor at elevated polymer concentrations and thus recommend to only use the Huggins coefficient term (k_H) as a descriptive term to describe the polymer-solvent and polymer-polymer interactions [28, 29]. Among these, Lewandowska et al. suggest comparatively lower k_H values for polymers in good solvents and higher k_H values for polymers in theta solvents or polymer coils that are associated via hydrogen bonding. Upon making a similar attempt to restrict the fit to only a second-order power series expansion, a similar increase in the value of k_H is noticeable. However, large deviations are observed between the fit and the experimental data (Figure 3.11). This clearly suggests the necessity for (at least) a third-order term in the power series expansion to account for the contribution of the plausible three body interactions.

Unlike the power series expansions, a strong theoretical justification is not provided here for the found power law indices. As suggested in some sources [26, 27], the precise values of the power law indices are highly specific to the type of network structure and the strength of the entangled junction points at elevated concentrations, as these would dictate the ease of reptation and the time scales for relaxation. Indeed in the case of the PEG system, it is found that the results may be suitably represented using a power index between 2 and 3. Given that the underlying differences in the chemical structure and branching between different polymer systems is clearly identifiable, the choice of power law indices may not be appropriate for all systems described here, but only for linear systems that are best described by a fractional power law dependence curve. It is worth highlighting, however, that these may not be easily arrived at for all systems, as the fractional power law index has been further developed only relatively recently for linear systems [30].

Thus, it is recognisable that there are still some theoretical objections to both approaches, i.e., power series expansions and scaling arguments. However, by trying to adopt both approaches, an attempt is made to highlight that there is a consistent set of experimentally observable trends that are still highly relevant for the extraction, processing, and utilisation of biopolymers in practical situations. At the very least, the approach of using the overlap factor term has also facilitated the explicit highlighting of the changes to the consistency index value due to screening effects in concentrated systems. Indeed, the hope is that, in due course, further clarity might be obtained by analysing a wide range of polymeric materials using the approach

described here.

3.5.2. YIELD STRESS AND POWER LAW INDICES

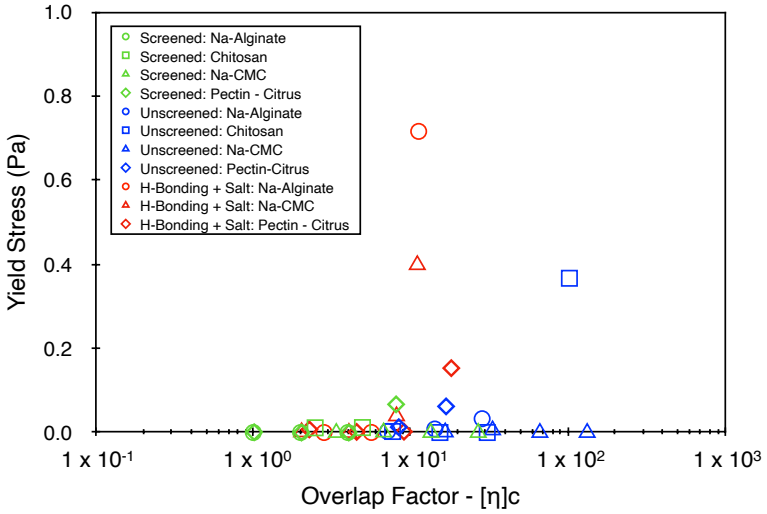

Figure 3.12: Yield stress from the Herschel-Bulkley fitting as a function of the overlap factor.

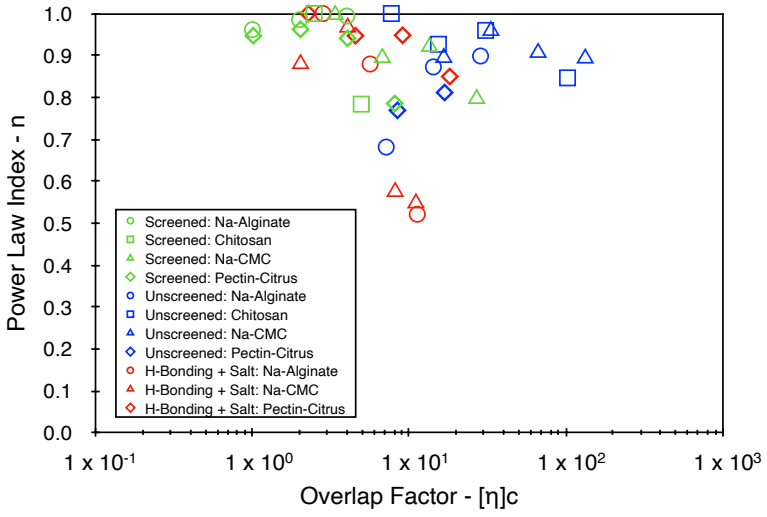

Figure 3.13: Power indices from the Herschel-Bulkley fitting as a function of the overlap factor.

The success in elucidating trends using the consistency index suggests that the approach may be extended to include the other two Herschel-Bulkley parameters. Figure 3.12 and Figure 3.13 represent the yield stress and the power law index values, respectively, for a select set of data points from the Herschel-Bulkley fitting. It is clear from Figure 3.12 that there is no consistent set of trends in the yield stress with respect to the concentration, with most samples exhibiting large variations in its value. Upon comparing the results of Figure 3.12 with those of Figure 3.13, the samples that present the largest yield stress values also typically present the lowest flow indices, suggesting a high degree of physical interaction between the polymer coils. However, the origin of these interactions is distinct in different systems. For example, in the case of the hydrogen-bonded alginate samples (red circles), the system enters an associated state with its macro-state being a granular fluid with potential non-covalent interactions between the soft (easily deformable) suspended particles. In contrast, the physical interactions in the unscreened and deprotonated alginate samples (blue circles) potentially correspond only to the entanglement of polymer coils (at relatively high concentrations compared to the hydrogen-bonded systems), with the bulk fluid being macromolecularly dissolved. Thus, the yield stress appears to be much more sensitive to an entire range of dynamic physical interactions that can persist within the concentrated biopolymer systems [31, 32]. The approach taken here is to explore the analogies (if any) between the dissipative part of the flow behaviour of a wide range of polymer systems. However, the yield stress also presents itself as an important physical property of concentrated biopolymer systems and deserves rigorous assessment separately (see Chapter 5).

3.6. CONCLUSIONS

A framework is provided to characterise biopolymer systems up to 100 times the overlap concentration and up to 100,000 times the solvent viscosity, using a set of experimentally observable trends for the Herschel-Bulkley consistency index. The range of values expressed here are significantly larger than previously reported values and should cover concentrations typically encountered in practice. In some cases, the observed trends agree with what, from theoretical arguments, should be found for uncharged, synthetic-linear polymer chains. The analysis is performed using either a generalised power series expansion (inspired by the Huggins equation) or a power law (scaling arguments). However, the proposed method also works for polymer systems that involve branching and exhibit dynamic cross-linking and the coil-to-rod transition type of phenomena (related to screening and solvent quality). Thus, there is sufficient scope to develop the theoretical arguments in support of the observed trends for complex biopolymer systems, as these may be used further to highlight the dynamics of biopolymer chains in solution. Regardless, this method provides the rapid determination of universal experimental trends, particularly at higher concentrations, and is highly useful for the efficient formulation of dedicated biopolymer products, as they invariably rely on good control over the rheology.

3.7. DATA AND SUPPLEMENTARY MATERIAL

The data from the rheology measurements is publicly accessible using the following link: https://doi.org/10.4121/f1ab8cce-67ec-4a8d-8f3b-4471db5d372e.

3.7.1. PH OF SAMPLES

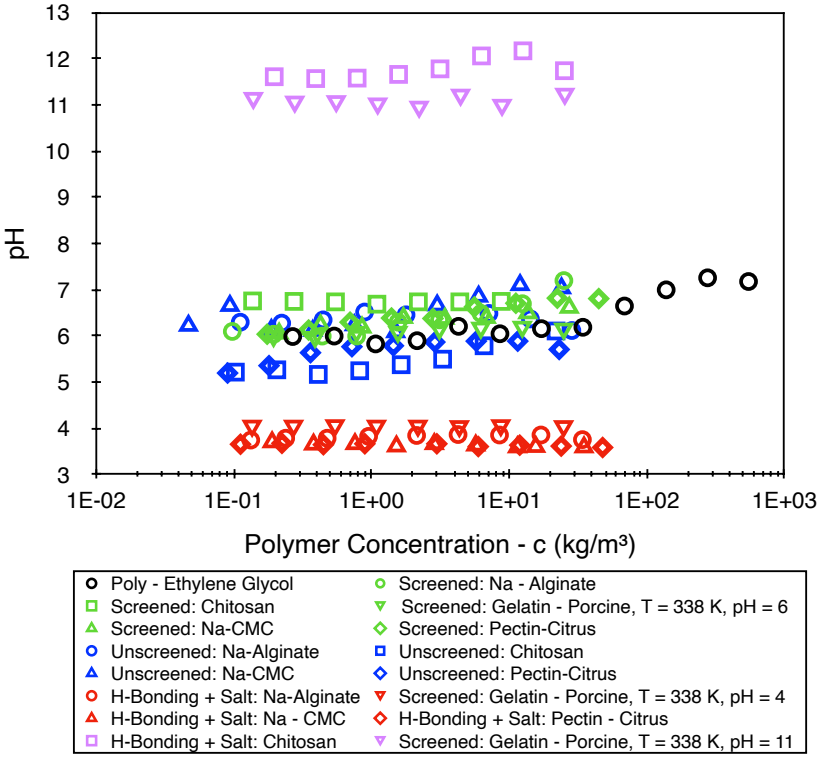

Figure 3.14: This figure shows the pH of all the samples that were tested.

3.7.2. FITTING THE HERSCHEL-BULKLEY MODEL

When performing a linear flow ramp experiment, it is possible to carry out both, increasing flow ramps (ramp up) as well as decreasing flow ramps (ramp down). However, the ramp down was particularly chosen to overcome the stress overshoot that typically results upon start-up flows in complex fluids (Figure 3.15). This also guaranteed clearly distinguishable features such as the yield stress (intercept made with the y-axis) whilst preserving the shear thinning behaviour (shape of the curve).

As mentioned in the main text, multiple ramps were performed with intermediate rest times of 10, 100 and 1000 seconds to validate that our protocol yields

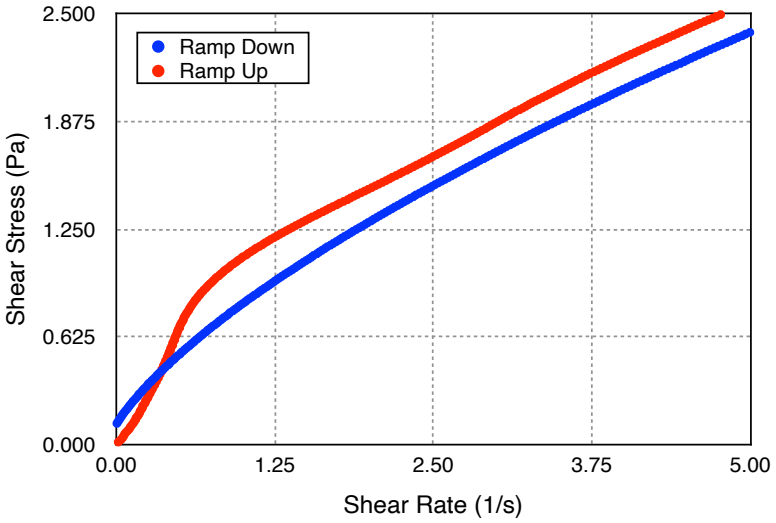

Figure 3.15: This figure shows the linear flow ramp curves performed for the same sodium alginate sample (pH = 3.72, polymer concentration = 2.87 g/dL, no added salts).

reproducibility in the results to a great extent. Figure 3.16 further highlights this point and additionally confirms that the uncertainty associated with fitting the Herschel-Bulkley parameters is negligible.

Given the non-linear nature of the Herschel-Bulkley model, the curve_fit() function from the SciPy library (Python programming language) was used. This function makes use of a non-linear least squares method to fit the chosen model to the data. Additionally, the function also provides the ability to conveniently change the initial guesses for the parameters of interest, the bounds of these parameters and returns the covariance matrix (Figure 3.17). As the parameters of interest in the Herschel-Bulkley model are the yield stress, the consistency index and the power law index, the resulting covariance matrix is a 3x3 matrix. The first row and column correspond to the yield stress covariance terms, the second row and column correspond to the consistency index covariance terms and the third row and column correspond to the power law index covariance terms respectively. The curve_fit() function was also used subsequently to fit the intrinsic viscosity values and the coefficient values for the power series expansions. Additional documentation about the function and its implementation within a Python environment is available on the following webpage: https://docs.scipy.org/doc/scipy/reference/generated/scipy.optimize.curve_fit.html.

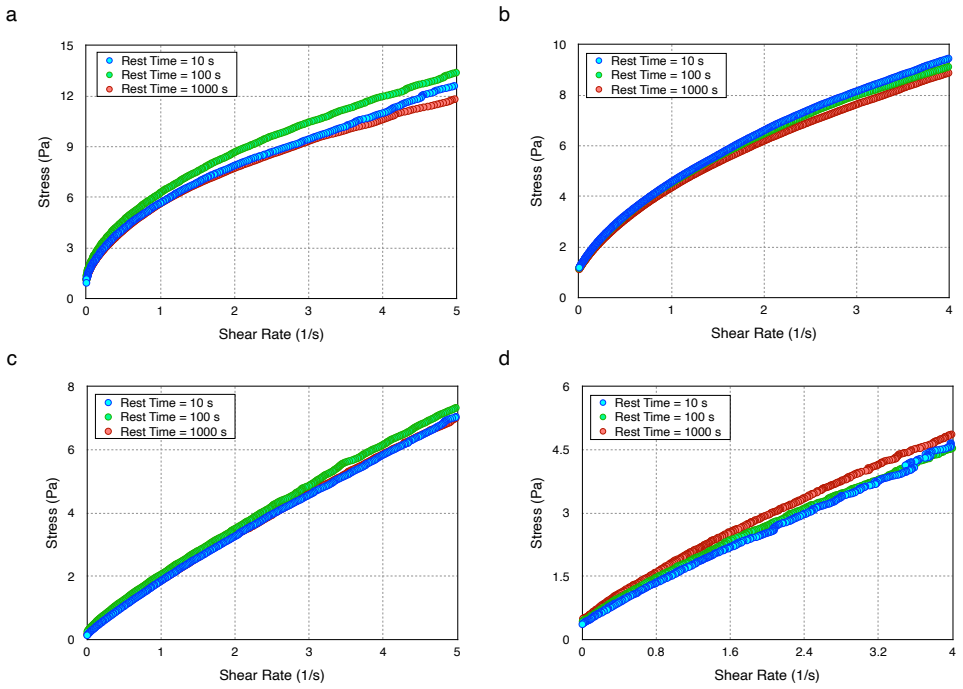

Figure 3.16: This figure shows the linear flow ramp down curves performed at different rest times for the following biopolymer systems: (a) sodium alginate - H-bonding + screening, polymer conc. = 3.41 g/dL, (b) sodium carboxy methyl cellulose - H-bonding + screening, polymer conc. = 1.56 g/dL, (c) citrus pectin - H-bonding + screening, polymer conc. = 4.78 g/dL, and (d) chitosan - Unscreened, polymer conc. = 2.19 g/dL.

```
[[ 7.22524313e-07 -3.98967735e-07  2.80410873e-05]
 [-3.98967735e-07  2.62383645e-07 -1.92955121e-05]
 [ 2.80410873e-05 -1.92955121e-05  1.44253646e-03]]
```

Figure 3.17: This figure represents the typical covariance matrix that is obtained using the scipy.optimize.curve_fit() function. The small values represented here are indicative of the high-quality fits that are possible using this method. The parameters are respectively: yield stress, consistency index, and the power law index.

REFERENCES

[1] B. Shivu, S. Seshadri, J. Li, K. Oberg, V. Uversky, and A. Fink. "Distinct β-sheet structure in protein aggregates determined by ATR–FTIR spectroscopy". In: *Biochemistry* 52 (2013), pp. 5176–5183. DOI: https://doi.org/10.1021/bi400625v.

[2] E. Gómez-Ordóñez and P. Rupérez. "FTIR-ATR spectroscopy as a tool for polysaccharide identification in edible brown and red seaweeds". In: *Food Hydrocolloids* 25 (2011), pp. 1514–1520. DOI: https://doi.org/10.1016/j.foodhyd.2011.02.009.

[3] M. Jackson and H. Mantsch. "The use and misuse of FTIR spectroscopy in the determination of protein structure." In: *Critical Reviews in Biochemistry and Molecular Biology* 30 (1995), pp. 95–120. DOI: https://doi.org/10.3109/10409239509085140.

[4] H. Cheng and T. Neiss. "Solution NMR spectroscopy of food polysaccharides". In: *Polymer Reviews* 52 (2012), pp. 81–114. DOI: https://doi.org/10.1080/15583724.2012.668154.

[5] T. Seviour, L. Lambert, M. Pijuan, and Z. Yuan. "Structural determination of a key exopolysaccharide in mixed culture aerobic sludge granules using NMR spectroscopy". In: *Environmental Science & Technology* 44 (2010), pp. 8964–8970. DOI: https://doi.org/10.1021/es102658s.

[6] S. Patterson and R. Aebersold. "Proteomics: The first decade and beyond". In: *Nature Genetics* 33 (2003), pp. 311–323. DOI: https://doi.org/10.1038/ng1106.

[7] S. Beranova-Giorgianni. "Proteome analysis by two-dimensional gel electrophoresis and mass spectrometry: Strengths and limitations". In: *TrAC Trends in Analytical Chemistry* 22 (2003), pp. 273–281. DOI: https://doi.org/10.1016/S0165-9936(03)00508-9.

[8] M. Tyers and M. Mann. "From genomics to proteomics". In: *Nature* 422 (2003), pp. 193–197. DOI: https://doi.org/10.1038/nature01510.

[9] G. Lawrie, I. Keen, B. Drew, A. Chandler-Temple, L. Rintoul, P. Fredericks, and L. Grondahl. "Interactions between alginate and chitosan biopolymers characterized using FTIR and XPS". In: *Biomacromolecules* 8 (2007), pp. 2533–2541. DOI: https://doi.org/10.1021/bm070014y.

[10] V. Kontogiorgos. *Pectin: Technological and Physiological Properties*. Cham, Switzerland: Springer International, 2020.

[11] T. Seviour, N. Derlon, M. Dueholm, H.-C. Flemming, E. Girbal-Neuhauser, H. Horn, S. Kjelleberg, M. van Loosdrecht, T. Lotti, and M. Malpei. "Extracellular polymeric substances of biofilms: Suffering from an identity crisis". In: *Water Research* 151 (2019), pp. 1–7. DOI: https://doi.org/10.1016/j.watres.2018.11.020.

[12] J. O'Mahony and P. Fox. "Milk Proteins: Introduction and Historical aspects". In: *Advanced Dairy Chemistry: Volume 1A: Proteins: Basic Aspects*. New York, NY, USA: Springer, 2013, pp. 43–85.

[13] S. Van Vlierberghe, P. Dubruel, and E. Schacht. "Biopolymer-based hydrogels as scaffolds for tissue engineering applications: A review". In: *Biomacromolecules* 12 (2011), pp. 1387–1408. DOI: https://doi.org/10.1021/bm200083n.

[14] S. Zhao, W. Malfait, N. Guerrero-Alburquerque, and G. Koebel M.M.; Nyström. "Biopolymer aerogels and foams: Chemistry, properties, and applications". In: *Angewandte Chemie International Edition* 57 (2018), pp. 7580–7608. DOI: https://doi.org/10.1002/anie.201709014.

[15] T. Xu, C. Ma, Z. Aytac, X. Hu, K. Ng, J. White, and P. Demokritou. "Enhancing agrichemical delivery and seedling development with biodegradable, tunable, biopolymer-based nanofiber seed coatings". In: *ACS Sustainable Chemistry & Engineering* 8 (2020), pp. 9537–9548. DOI: https://doi.org/10.1021/acssuschemeng.0c02696.

[16] J. Zlopasa, B. Norder, E. Koenders, and S. Picken. "Origin of highly ordered sodium alginate/montmorillonite bionanocomposites". In: *Macromolecules* 48 (2015), pp. 1204–1209. DOI: https://doi.org/10.1021/ma502147m.

[17] P. Kanmani and J.-W. Rhim. "Properties and characterization of bionanocomposite films prepared with various biopolymers and ZnO nanoparticles". In: *Carbohydrate Polymers* 106 (2014), pp. 190–199. DOI: https://doi.org/10.1016/j.carbpol.2014.02.007.

[18] G. Fulcher. "Analysis of recent measurements of the viscosity of glasses". In: *Journal of the American Ceramic Society* 8 (1925), pp. 339–355. DOI: https://doi.org/10.1111/j.1151-2916.1925.tb16731.x.

[19] L. Korson, W. Drost-Hansen, and F. Millero. "Viscosity of water at various temperatures". In: *The Journal of Physical Chemistry* 73 (1969), pp. 34–39. DOI: https://doi.org/10.1021/j100721a006.

[20] M. Rubinstein and R. Colby. *Polymer Physics*. Oxford, UK: Oxford University Press, 2003.

[21] M. Rubinstein, R. Colby, and A. Dobrynin. "Dynamics of semidilute polyelectrolyte solutions". In: *Physical Review Letters* 73 (1994), p. 2776. DOI: https://doi.org/10.1103/PhysRevLett.73.2776.

[22] R. Sayko, M. Jacobs, and A. Dobrynin. "Quantifying properties of polysaccharide solutions". In: *ACS Polymers Au* 1 (2021), pp. 196–205. DOI: https://doi.org/10.1021/acspolymersau.1c00028.

[23] J. Pathak, S. Nugent, M. Bender, C. Roberts, R. Curtis, and J. Douglas. "Comparison of Huggins coefficients and osmotic second virial coefficients of buffered solutions of monoclonal antibodies". In: *Polymers* 13 (2021), p. 601. DOI: https://doi.org/10.3390/polym13040601.

[24] A. Raja, P. Wilfert, and S. Picken. “Charge mediated changes to the intrinsic viscosity of biopolymer systems”. In: *Polymers* 16 (2024), p. 2894. DOI: https://doi.org/10.3390/polym16202894.

[25] T. Osswald and N. Rudolph. *Polymer Rheology: Fundamentals and Applications*. Munich, Germany: Carl Hanser Verlag GmbH, 2015.

[26] J. Sprakel, J. van der Gucht, M. Stuart, and N. Besseling. “Brownian particles in transient polymer networks”. In: *Physical Review E* 77 (2008), p. 061502. DOI: https://doi.org/10.1103/PhysRevE.77.061502.

[27] J. Van der Gucht, W. Besseling N.; Knoben, L. Bouteiller, and M. Stuart. “Brownian particles in supramolecular polymer solutions”. In: *Physical Review E* 67 (2003), p. 051106. DOI: https://doi.org/10.1103/PhysRevE.67.051106.

[28] J. Bicerano, J. Douglas, and D. Brune. “Model for the viscosity of particle dispersions”. In: *Journal of Macromolecular Science, Part C* 39 (1999), pp. 561–642. DOI: https://doi.org/10.1081/MC-100101428.

[29] K. Lewandowska, D. Staszewska, and M. Bohdanecký. “The Huggins viscosity coefficient of aqueous solution of poly (vinyl alcohol)”. In: *European Polymer Journal* 37 (2001), pp. 25–32. DOI: https://doi.org/10.1016/S0014-3057(00)00074-4.

[30] A. Likhtman and T. McLeish. “Quantitative theory for linear dynamics of linear entangled polymers”. In: *Macromolecules* 35 (2002), pp. 6332–6343. DOI: https://doi.org/10.1021/ma0200219.

[31] K. te Nijenhuis. “On the nature of crosslinks in thermoreversible gels”. In: *Polymers Bulletin* 58 (2007), pp. 27–42. DOI: https://doi.org/10.1007/s00289-006-0610-7.

[32] P.-G. De Gennes. *Scaling Concepts in Polymer Physics*. Ithaca, NY, USA: Cornell University Press, 1979.

4

PROPERTIES OF EXTRACELLULAR MACROMOLECULE-CATION COMPLEXES

In light of the growing demand for biopolymers, Extracellular Polymeric Substances (EPS) are considered as relevant bioresources that can be suitably recovered from wastewater treatment processes. However, very little effort is focussed on assessing the composition of the inorganic fractions within EPS, as well as their overarching influence on the overall physico-chemical properties. Therefore, this study assesses variations in the composition of these inorganic fractions and their specific impact on extraction, processing and application of EPS. As noted here, up to 18% w/w of the solid mass of EPS extracted from a full scale Aerobic Granular Sludge (AGS) installation, is inorganic and is predominantly made up metals such as Na, Mg, Al, K, Ca, and Fe. Using a number of purification steps, followed by the selective readdiction of these metallic cations, a 2.8 increase to properties such as the yield stress and viscosity, and up to a 3.0 fold increase to coil size, respectively, were also noted. Additionally, it is revealed that other wastewater treatment such steps, such as the utilization of iron alongside the initial AGS treatment (for phosphorus removal), further leads to the accumulation of inorganic forms of phosphorus within EPS, which potentially improves its flame retardant capabilities. Thus, specific modifications to the existing extraction protocol of EPS, as well as downstream processing steps that can modify the rheological behaviour of EPS, using the cations listed above, are discussed in sufficient detail. This knowledge can be leveraged further to tailor the properties of EPS for different applications.

At the time of finalising this thesis, this chapter is submitted to *Bioresource Technology* for publication as: A. Raja, P.K. Wilfert, and S.J. Picken, "Investigating the Properties of Extracellular Polymeric – Cation Complexes from Aerobic Granular Sludge".

4.1. INTRODUCTION

Recent projections for polymer waste generation clearly suggest the growing demand for sustainable alternatives across a wide number of industries [1]. Thus, the need to identify and produce critically vetted alternatives remains highly relevant. Amongst these, extracellular polymeric substances (EPS) have already been identified as attractive alternatives, with the most ubiquitous examples being exopolysaccharides such as cellulose [2]. Additionally, recent advances made using aerobic granular sludge (AGS) technology have also identified EPS extracted from wastewater as being another appealing alternative [3, 4]. EPS extracted from AGS (and potentially other wastewater treatment processes) is useful as it can be extracted from a low value source (i.e. wastewater), can be produced at relatively high yields, and may be suitably applied in different industries due to its ability to form hydrogels and flame retardant composite materials [3, 5]. Particularly, in one study [3], the potential for EPS from AGS to behave similar to alginate was identified. It was also identified that the extracted EPS could have up to 30 % w/w ash content (with respect to total solids). A detailed set of follow up studies conducted by Felz and coworkers [6, 7] highlights that the ability of EPS to crosslink with cations, as well as the corresponding elastic properties of the resulting hydrogels, are different when compared to alginate. Specifically, they [6] hypothesise that several cations may contribute towards the structural stability of EPS.

Thus, the goal of this study is to assess how specific cations can impact the physico-chemical properties of EPS from AGS, and thereby govern its extraction, processing and application. For instance, cations impact the yield of the polymeric substances recovered from AGS. Based on a recent study conducted on EPS from multiple full scale AGS installations, there are certainly notable differences (up to a factor of 3 for iron) in the concentration of cationic species, depending on the source of extraction [8]. As the predominantly negatively charged EPS is likely to interact / crosslink with cationic species, notable differences in the concentration of these cationic fractions can also lead to variability in the hydrogel forming characteristics of EPS, and resulting rheological properties such as the moduli and viscosity [6]. The (in)ability of EPS to readily bind with specific cations can also impact the ability of EPS to function as a biobased adsorbing agent for agricultural purposes [8]. Alternatively, the presence of cations within EPS may be instrumental in the accumulation of other species such as phosphorus, which in turn is useful in enhancing its flame-retardant characteristics [5, 9].

Upon conducting a review of existing literature, it was possible to arrive at a list of cations that display the greatest likelihood to interact with both the (granular) sludge, as well as EPS. For instance, EPS extracted from a freshwater source is likely to have a difference in the concentration of sodium (Na^+) when compared to EPS extracted from a source with saltwater intrusion. Differences in the concentration of Na^+ can induce a screening of the charged sites within the sludge as well as EPS. The extraction of EPS is facilitated by the successful dissolution of the macromolecular fractions under alkaline conditions [3]. In commercial settings, this is facilitated by

the addition of potassium hydroxide (KOH) [10]. Thus, K^+ can also be expected to influence the charge mediated screening within the EPS. Further, some cations are known to facilitate other wastewater treatment processes. It remains well established that cations such as magnesium (Mg^{2+}) and calcium (Ca^{2+}) can form crosslinks within the sludge during wastewater treatment [11]. The presence of either cation has also been shown to crosslink successfully with EPS [6, 12, 13] . Therefore, changes to the concentration of Mg^{2+} and Ca^{2+}, and the hardness of water depending on the location of the influent, is also bound to influence the structural stability and macromolecular conformation of EPS. Equally, the primary purpose of wastewater treatment is not to extract EPS, but is rather to remove (or reduce) undesirable chemical species such as phosphorus (P) [14]. These P compounds are typically removed by dosing the wastewater using aluminium (Al^{3+}) or iron (Fe^{2+} and Fe^{3+}) [15]. Expectedly, the levels of Mg^{2+}, Al^{3+}, Ca^{2+}, Fe^{2+} and Fe^{3+} are different across multiple treatment plants and is partly dependent on (empirically) established practices. It is also worth noting that Felz and coworkers report (in supplementary text) , that over 90% of the total inorganic mass identified in AGS is attributable to the 7 cations listed above [6].

For this reason, the specific impact to the physico-chemical properties, by the above mentioned 7 cations, on purified / unpurified EPS is presented below. First, the purification of EPS was carried out to reduce the existing cationic (and inorganic) components. The reductions achieved are reported in terms of changes to the elemental and inorganic composition. Once purified, cations were (re)introduced and the subsequent changes to the pH, conductivity and solubility were recorded. Rheology was used to quantify changes to macromolecular size, viscosity and yield stress (analogous to gel strength). Finally, the role of individual cations is categorically discussed and summarised, so that this information may be suitably leveraged to extract, process and optimise EPS for specific applications.

4.2. MATERIALS AND METHODS

4.2.1. SOURCE OF EPS

The EPS was extracted from the municipal wastewater treatment plant (WWTP) in Utrecht, The Netherlands, using AGS. The pilot scale batch extraction facility was fed with (blended) excess sludge with a total solids content of 3-4 % w/w. As reported [8], the extracted EPS had approximately 3 times higher iron content compared to other sources in the Netherlands. This is due to the biological phosphate removal aided by the addition of iron salts during treatment.

The extraction process was similar to the alkaline dissolution - acid precipitation protocol established earlier [3]. The base used was KOH and the acid used was HCl. A more detailed overview of the extraction is available in Supplementary Material Subsection 4.6.1. The EPS was sampled as an acidic gel product and stored in a cold storage facility (277 K) from July 2022. Although the stored EPS was utilised for a prolonged duration (up to June 2024), the gel's rheological properties were frequently

tested (see subsection 4.2.5). Only minimal deviations were observed suggesting that no gross degradation occurred within the sample. Thus, the sample was deemed sufficiently representative for the subsequent analytical steps.

4.2.2. SAMPLE PURIFICATION

The purification of EPS was carried out using either dialysis or washing. The adoption of either purification strategy simultaneously established the efficiency with which available cations and low molar mass components may be removed using two relatively simple purification routes.

DIALYSIS

An acid EPS sample, with a recorded pH and conductivity of 2.81 and 0.82 S/m respectively, was used for dialysis at room temperature (293 K and 50% RH). The dialysis protocol is summarised in Table 4.1. Approximately 90 mL (90 cm^3) of the sample after Step 2, Table 4.1 was transferred into a Thermo Fischer Scientific SnakeSkin™ tubing with a rated MWCO of 3.5 K. The dialysed sample following Step 3, Table 4.1 shall be henceforth called "Dialysed - Blank" or "Blank".

Table 4.1: The dialysis protocol for the EPS sample.

Step	**Remarks**
Step 1: Alkaline dissolution of acid gel suspension	Dissolution through dropwise addition of 5M NaOH solution. pH and conductivity are recorded. Final pH is typically between 10 and 11.
Step 2: Screening of charged interactions	Adding 0.2 M of KCl to remove undesired low molar mass substances. pH and conductivity are recorded. Final conductivity is typically around 3 S/m.
Step 3: Dialysis for 48 hours	Rated MWCO: 3.5 K. pH and conductivity are recorded.

WASHING

The untreated acid EPS (henceforth "Untreated") was utilised further for acid washing. Two distinct washing protocols were adopted to mimic the effect of screening during dialysis: one with no added KCl (henceforth "Washed - No Added KCl") and one with added KCl (henceforth "Washed - Added KCl"). These protocols are summarised in Tables 4.2 and 4.3 respectively. All washing steps were carried out using a washing solution that was at the same pH (± 0.1) as the samples.

Table 4.2: The washing steps for the "Washed - No Added KCl" sample.

Step	Remarks
Step 0: Measure pH and Conductivity	"Untreated" Sample
Step 1: Dilution by washing solution	Solution = HCl, Dilution Factor = 2
Step 2: Centrifugation	3880 g, 600 s, 298 K
Step 3: Decanting	Photographs were taken. Supernatant decanted and precipitate retained. Steps 1-3 repeated a total of 4 times.
Step 4: Measure pH and Conductivity	pH = 2.83, Conductivity = 0.10 S/m

Table 4.3: The washing steps for the "Washed - Added KCl" sample.

Step	Remarks
Step 0: Measure pH and Conductivity	"Untreated" Sample
Step 1: Dilution by washing solution	Solution = HCl + 0.2M KCl, Dilution Factor = 2
Step 2: Centrifugation	3880 g, 600 s, 298 K
Step 3: Decanting	Photographs were taken. Supernatant decanted and precipitate retained. Steps 1-3 repeated a total of 4 times.
Step 4: Measure pH and Conductivity	pH = 2.77, Conductivity = 1.98 S/m
Step 5: Dilution by washing solution	Solution = HCl, Dilution Factor = 16
Step 6: Centrifugation	3880 g, 600 s, 298 K
Step 7: Decanting	Photographs were taken. Supernatant decanted and precipitate retained.
Step 8: Measure pH and Conductivity	pH = 2.83, Conductivity = 0.19 S/m

4.2.3. COMPOSITIONAL ANALYSIS

The composition analysis was carried out using a combination of Thermogravimetric Analysis (TGA), Inductively Coupled Plasma - Optical Emission Spectrometry (ICP-OES), Phosphorus - Nuclear Magnetic Resonance (^{31}P-NMR), and Scanning

Electron Microscopy (SEM).

TGA

The total dried solids (TS) and volatile solids (VS) of the "Untreated", "Dialysed - Blank", "Washed - No Added KCl", and "Washed - Added KCl" samples were evaluated using a Perkin Elmer TGA 8000 device, equipped with ceramic crucibles (Perkin Elmer - part no. N5370464). The furnace was purged with air flowing at a rate of 40 mL/min (0.67 cm^3/s). A custom method was setup to estimate the TS and the VS (see Figure 4.1). The initial average mass of the sample was recorded between (0 - 60) s at 298 K (1st plateau). To calculate the TS and VS, the average mass of the samples was recorded between (1500 - 1800) s at 378 K (2nd plateau), and from 4200 s until the end of the method at 823 K (3rd plateau) respectively.

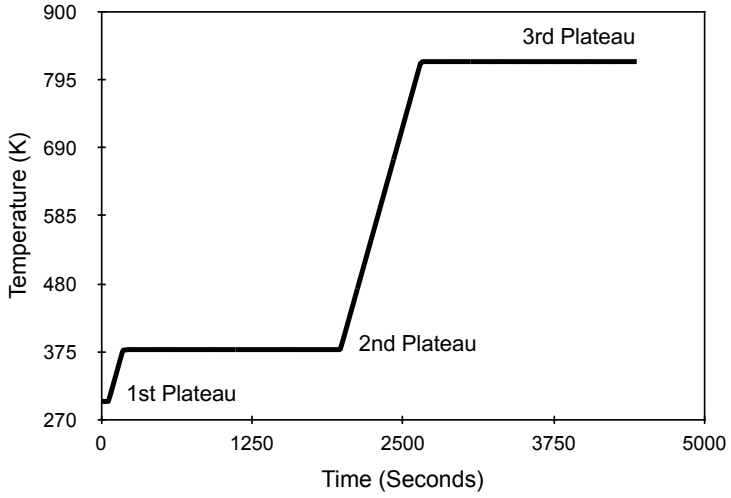

Figure 4.1: The thermogravimetric analysis method file used to estimate the total dried solids (TS) and volatile solids (VS) across the various EPS. The plateaus represent the isotherms at 298 K (1st plateau), 378 K (2nd plateau) and 823 K (3rd plateau).

ICP-OES

The inorganic elemental composition of the "Untreated", "Dialysed - Blank", "Washed - No Added KCl" and "Washed - Added KCl" samples was measured according to the method outlined by Bahgat et al. (after microwave digestion), using a Perkin Elmer Optima 5300 DV device, equipped with an OES detector and a Perkin Elmer ESI-SC-4 DX fast autosampler [10]. All measurements were carried out in duplicate. The average concentration (in % w/w) was measured for a total of 33 analytes (see Supplementary Material Subsection 4.6.2) and these values were further used

to calculate the elemental composition of the non-volatile solids, as well as the concentration of the individual analytes in relation to the TS (in % w/w).

^{31}P-NMR

Table 4.4: The pH of EPS and sodium adenosine diphosphate (Na-ADP) samples used for ^{31}P-NMR analysis.

Sample Name	pH
"Washed - No Added KCl"	9.18
"Washed - Added KCl"	9.32
Na-ADP	9.32

Based on the results obtained from the ICP-OES measurements, the "Washed - No Added KCl" and "Washed - Added KCl" samples were selected for liquid state ^{31}P-NMR analysis, along with sodium - adenosine diphosphate (Na-ADP) from Sigma-Aldrich (95% purity - Zwijndrecht, The Netherlands). The Na-ADP measurements were used to verify that P-P coupled signals could be measured using the setup. Additionally, to ensure that all peaks were discernible around 0 ppm, the use of an internal standard was foregone. Thus, Na-ADP also served as a reference sample to label peaks that were observed from the washed EPS samples.

The sample preparation for NMR-analysis is based on the existing single step preparation protocols for soil samples and EPS [16, 17]. Both washed EPS samples were freeze dried at 193 K and 100 Pa to remove moisture from the sample. Subsequently, 0.1 g of each EPS sample, as well as the Na - ADP, was dissolved using 3.5 cm^3 (or mL) of 0.10 M EDTA - 0.38 M NaOH solution. Further, 0.5 cm^3 of D_2O was added to the EPS samples (for magnetic locking), to bring their total volume up to 4 cm^3. For the Na-ADP sample, 1 M NaOH solution was used to adjust the pH. Following this, 3.5 cm^3 of this sample was mixed with 0.5 cm^3 of D_2O to bring the total volume up to 4 cm^3. The pH of all samples was recorded prior to measurement, and is reported in Table 4.4. The pH value was intentionally maintained around 9.2 to mitigate the risk of sample degradation at elevated pH conditions. As all samples are within 0.2 decades on the pH scale, no relevant shift was expected in the NMR peaks. All samples were refrigerated for approximately 1 week (~ 604,800 s) at 277 K prior to measurement.

All ^{31}P-NMR measurements were carried out using a Bruker Avance 600 MHz spectrometer, a 10 mm probe, an operation frequency of 242.94 MHz, and a pulse with of 30° (0.524 rad). The spectra for EPS samples were acquired using an acquisition time of 0.80 s, a relaxation delay of 50 s, and 1500 scans. By contrast, the spectrum of the Na-ADP sample was acquired using an acquisition time of 0.3408 s, a relaxation delay of 2 s, and 32 scans. Finally, all spectra were imported into MestReNova (version 15.0.1) to carry out the peak integration of desired peaks.

SEM

Based on the results obtained from the ^{31}P-NMR analysis, a new "Washed - No Added KCl" sample was prepared for assessment using SEM. Further, a droplet of the EPS sample was dried on the surface of a glass slide with the help of a vacuum oven (313 K, 24 hours). The observations were carried out using a JEOL JSM-IT700HR microscope. Multiple scans were performed using a voltage of 15.0 kV and a back-scattered electron detector to highlight density differences within the sample.

4.2.4. SALT ADDITION

Table 4.5: The salts that were added to the various fractions of the EPS post dialysis.

Salt (0.1M)	Nominal Valence
NaCl	1+
KCl	1+
$MgCl_2 \cdot 6H_2O$	2+
$CaCl_2$	2+
$FeCl_2 \cdot 4H_2O$	2+
$Al(NO_3)_3 \cdot 9H_2O$	3+
$FeCl_3$	3+

Upon dialysis, a concentration series lower than 1.5 kg/m^3 (1.5 mg/mL) was prepared by diluting the "Dialysed - Blank" sample using an NaOH solution that was at roughly the same pH (± 0.1) as the samples. Following this, each one of the diluted samples in the series were split into 8 equal parts and 0.1 M of a desired salt was added to 7 of them, with 1/8 parts being reserved as the "Dialysed - Blank" sample. The salts that were added to each one of the 7 parts is documented in Table 4.5. The pH and conductivity of the resulting samples were recorded, and the most concentrated samples were photographed before and after centrifugation (3880 g, 298 K, 600 s). All samples were then refrigerated at 277 K until they could be tested further for their rheological properties.

4.2.5. RHEOLOGY

Rheology was used to calculate both, the intrinsic viscosity of the dialysed samples, as well as the flow characteristics of the washed samples. The intrinsic viscosity allowed for the quantification of the macromolecular size of the dialysed systems, including cationic complexes if present [18]:

$$\frac{\eta}{\eta_s} = 1 + [\eta]c \tag{4.1}$$

Here η represents the solution viscosity, η_s represents the solvent viscosity, c represents the mass concentration and $[\eta]$ represents the intrinsic viscosity

(inverse units of mass concentration). Equally, the Herschel-Bulkley parameters were measured for the acidic EPS samples to cover changes to the flow characteristics:

$$\sigma = \sigma_0 + K\left(\frac{\dot{\gamma}}{1s^{-1}}\right)^n \tag{4.2}$$

Here σ represents the applied stress (in Pa), $\dot{\gamma}$ represents the measured shear rate (in 1/s), σ_0 represents the yield stress (in Pa), K represents the consistency index (in Pa) and n represents the flow index (no units). Collectively σ_0, K and n are termed as the Herschel-Bulkley parameters [19]. A detailed interpretation of the rheological parameters is not provided as this is readily available in the sources cited above (also see Chapters 2 and 3).

All rheological measurements were carried out at 298 K using a stress-controlled TA Instruments Discovery Hybrid Rheometer - 3. A smooth, stainless steel concentric cylinder setup was used to measure the intrinsic viscosity of the "Dialysed - Blank" sample and dialysed samples with 0.1 M of salt. The cup has a diameter of 30.36 mm, and the DIN bob has a diameter 28 mm and a height of 42.07 mm. The bob was maintained a height of 5917.1 μm from the bottom surface of the cup. To mitigate the risk of flow instabilities due to higher shear rates (> 100 s^{-1}), a stress value ≤ 0.1 Pa was used to measure the viscosity. Each sample was held at this constant stress value for a total period of 600 s to ensure a development of a constant viscosity value. The setup was also used to obtain the viscosity of de-ionised water (reference viscosity value for solvent).

The "Washed - No Added KCl", "Washed - Added KCl" and "Untreated" samples were prepared for rheology by diluting the three samples to a concentration of 0.35 kg/m^3 (35 mg/mL). The dilutions took place using an HCl solution with the same pH (± 0.1) as the samples. These sample were tested for their Herschel-Bulkley parameters using a sandblasted cone (40 mm, 0.035 rad) on plate setup to mitigate slip. The surface of the plate was roughened by attaching a small strip of 400 grit sandpaper. A set of four linearly decreasing stress-controlled flow ramps (ramp time = 60 s, final value = 0 Pa) were performed on each sample. The first ramp was used as a conditioning ramp to erase the sample history. The subsequent ramps were performed with a randomised sequence of intermediate rest times of 10 s, 100 s and 1000 s. The Herschel-Bulkley parameters were obtained using the scipy.optimize.curve_fit() function in Python. Data points corresponding to initial inertial effects and elastic recovery at low shear rates were removed before the fitting procedure.

4.3. RESULTS

4.3.1. SAMPLE PURIFICATION

From Figure 4.2, it is clear that dialysis led to the considerable leaching of undesirable non-polymeric (lower molecular weight) organic substances. These (potentially humic) substances notably contribute towards the turbidity and colour

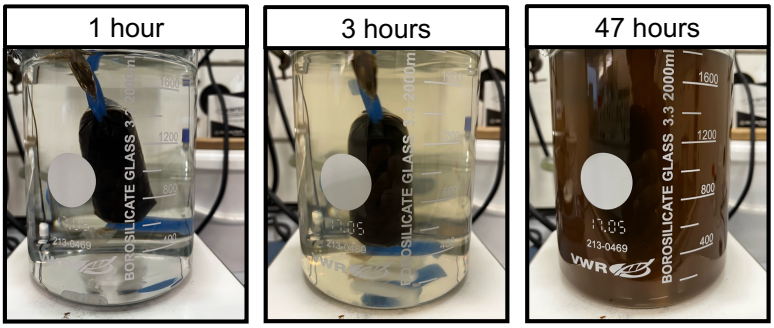

Figure 4.2: The leaching of non-polymeric organic substances from EPS (within the dialysis bag) and into the diluent. The photos were taken at different timesteps during dialysis (left to right) - 1 hour, 3 hours and 47 hours.

Table 4.6: The pH and conductivity of the EPS at different stages of the dialysis process.

Dialysis Step	pH	Conductivity (S/m)
Pre-Dialysis: 5M NaOH Addition	10.3	1.24
Pre-Dialysis: 0.2M KCl Addition	9.96	3.06
Post Dialysis	9.30	0.29

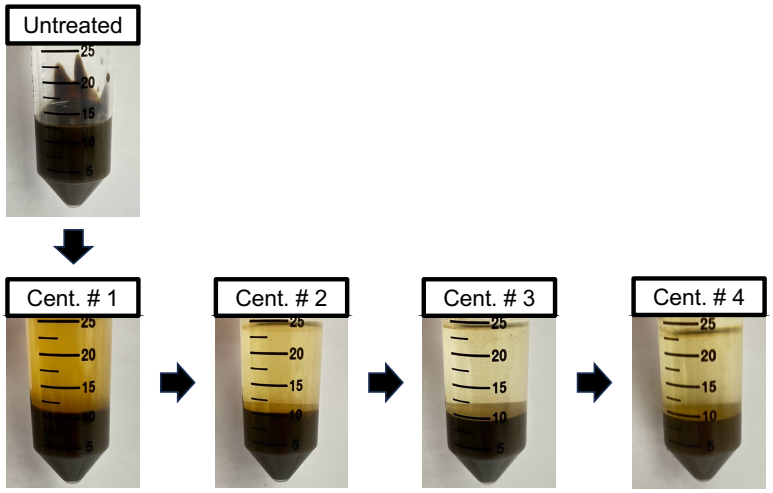

Figure 4.3: The "Washed - No Added KCl" sample before supernatant decanting was carried out. The label "Cent. #" highlights the centrifugation cycle in question. (See Table 4.2 - Steps 2 and 3). Note the reduction in the turbidity and colour of the supernatant after each centrifugation cycle.

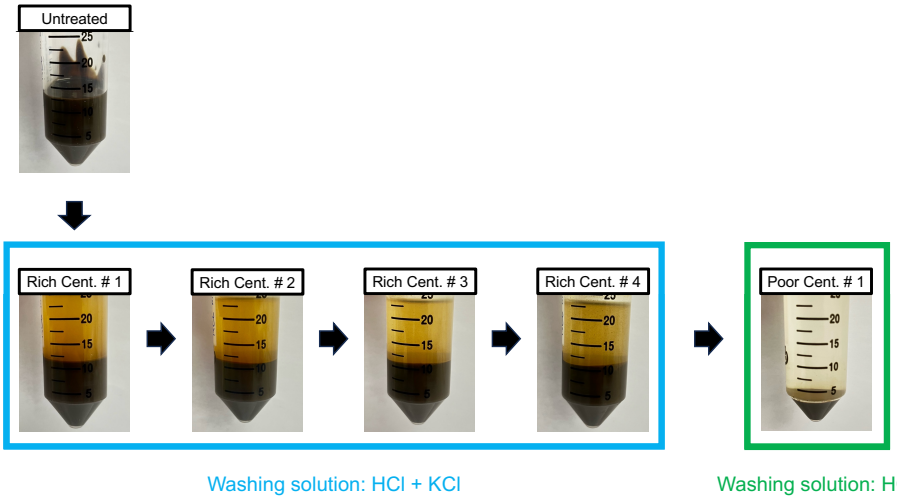

Figure 4.4: The "Washed - Added KCl" sample before the supernatant decanting was carried out. The label "Rich Cent. #" in combination with the blue frame highlights that KCl was present within the washing solution. The label "Poor Cent. #" in combination with the green frame highlights that KCl was absent within the washing solution. (See Table 4.3 - Steps 1, 2, 3, 5, 6 and 7). Note the retention in the turbidity and colour of the supernatant after each "Rich" centrifugation cycle.

Table 4.7: The pH and conductivity of the "Washed - No Added KCl" sample at different stages of washing.

Step Number (Table 4.2)	pH	Conductivity (S/m)
Step 0	2.81	0.82
Step 4	2.81	0.10

Table 4.8: The pH and conductivity of the "Washed - Added KCl" sample at different stages of washing.

Step Number (Table 4.3)	pH	Conductivity (S/m)
Step 0	2.81	0.82
Step 4	2.77	1.98
Step 8	2.83	0.19

of the EPS. Therefore, it appears that the attempt to screen charged interactions successfully contributes towards the removal of these undesirable, and probably charged, low molar mass organic substances during dialysis. The pH and conductivity from each stage of the dialysis procedure is reported in Table 4.6. The conductivity value of 0.29 S/m post dialysis confirms that the dialysis was successful in reducing

the salt content within EPS.

Figures 4.3 and 4.4 represent the photographs that were taken before each decanting step for the No Added KCl and Added KCl acidic washing protocols respectively. From these figures, it is clear that the addition of KCl is successful in retaining the colour and turbidity of the supernatant, and therefore successful in the removal of low molar mass (organic) substances. It is worth remarking that the removal of salts from the "Untreated" sample is not hindered due to the addition of KCl, as both washing protocols are successful in lowering the conductivity below 0.2 S/m (see Tables 4.7 and 4.8). These conductivity values are lower than the conductivity of the "Dialysed - Blank" sample at the end of dialysis and therefore suggest a somewhat lower free ion concentration in solution.

4.3.2. COMPOSITIONAL ANALYSIS

Table 4.9: The total dried solids (TS), volatile solids (VS), quantified non-volatile solids as a percentage of the TS (ICP / TS) and the unquantified non-volatile solids as a percentage of the TS (U / TS). Note that the summation of the last three columns yields 100 % w/w TS.

Sample	TS (% w/w)	VS (% w/w)	VS / TS (% w/w)	ICP / TS (% w/w)	U / TS (% w/w)
"Untreated"	7.06	5.80	82.16	11.40	6.44
"Dialysed - Blank"	4.39	3.38	76.92	14.83	8.25
"Washed - No Added KCl"	5.96	5.10	85.50	8.81	5.69
"Washed - Added KCl"	6.10	5.22	85.47	9.18	5.35

The results from the thermogravimetric analysis are summarised in Table 4.9. Both dialysis and washing led to an overall reduction in the TS of the sample, and was therefore successful in the removal of undesirable low molar mass substances. Dialysis has the greatest reduction to the TS (roughly 38 %) to suggest that it is better suited at the gross removal of these substances.

It is worth noting, that either purification strategy has a marginal impact on the VS / TS ratio within the EPS, and in the case of dialysis, there is in fact a reduction to the VS / TS ratio by roughly 5% w/w. By combining these results with the visual inferences gained from sample turbidity and colour, it appears that there is a considerable fraction of non-volatile substances (over 10% w/w of TS) bound to all forms of organic matter within EPS, irrespective of their molar mass.

The results from the ICP-OES analysis are also summarised in Table 4.9. In general, 25 / 33 analytes were found to be within their detectable concentration range for all 4 samples (see Supplementary Material Subsection 4.6.2 for the complete list). The relative amounts of the analytes measured using ICP-OES were summed up to calculate the ICP / TS values in Table 4.9. The remaining (uncertain) TS mass

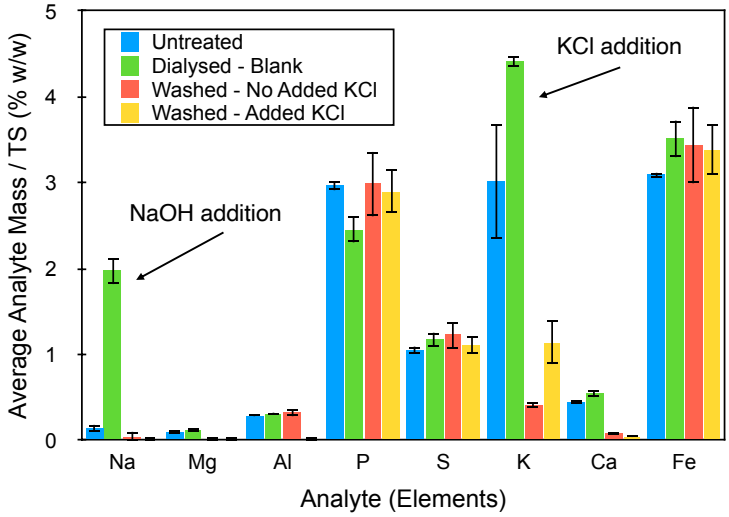

Figure 4.5: The relative amounts of analytes (as a percentage of the total solids - TS) from ion coupled plasma - optical emission spectroscopy (ICP-OES) analysis for the top 8 analytes in terms of their concentration. The error bars represent the two-sigma distribution (95% confidence interval). Note that the relative concentrations of P, S and Fe remain roughly the same for all 4 samples.

was used to calculate the U / TS values in Table 4.9, by subtracting the sum of VS / TS and ICP / TS from 100. In all cases, the U / TS values are less than 9% w/w. In part, this mass can be attributed to non-solubilised compounds such as silicates and oxides during ICP analysis. Further, a plot of the top 8 analytes in terms of their relative amounts is shown in Figure 4.5 for all 4 samples. The large spikes observed in the relative amounts of Na and K in the case of the "Dialysed - Blank" sample has been associated to the addition of NaOH and KCl during the dialysis process. In general, it appears that P, S and Fe remain invariant to the purification strategies that were adopted, and by themselves account up to 7% w/w of the TS mass. In the case of the washed samples, this means that P, S and Fe make up roughly half of the total non-volatile mass and in other cases, they consistently make up a large proportion of the non-volatile mass. Additionally, P:Fe are in a molar ratio of approximately 3:2 within all samples. Finally, the presence of iron oxides may also explain the orange hue noted during TGA (see Figure 4.6).

Figures 4.7, 4.8 and 4.9 represent the ^{31}P-NMR spectra for the Na-ADP , "Washed - No Added KCl" and "Washed - Added KCl" samples respectively. The coupled peaks of Na-ADP, with an (almost) equal integration area are observable in Figure 4.7. The smaller peaks observed in Figure 4.7 are suspected to correspond to the 5% impurities within this sample. The lack of coupled peaks in Figures 4.8 and 4.9,

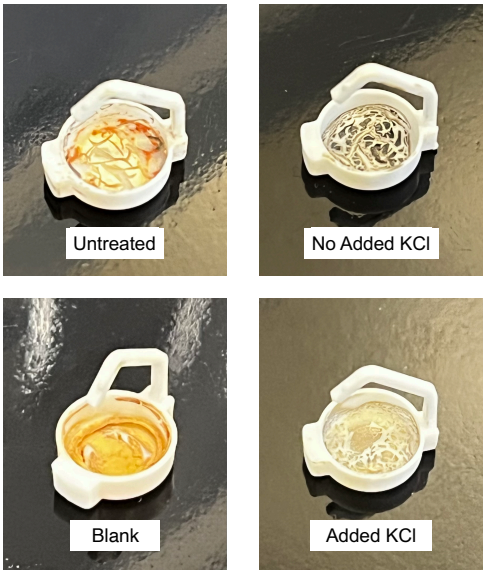

Figure 4.6: The crucibles following the thermogravimetric analysis (TGA). Note the orange hue in the case of the "Untreated" and "Blank" samples that suggest the presence of iron oxides within EPS.

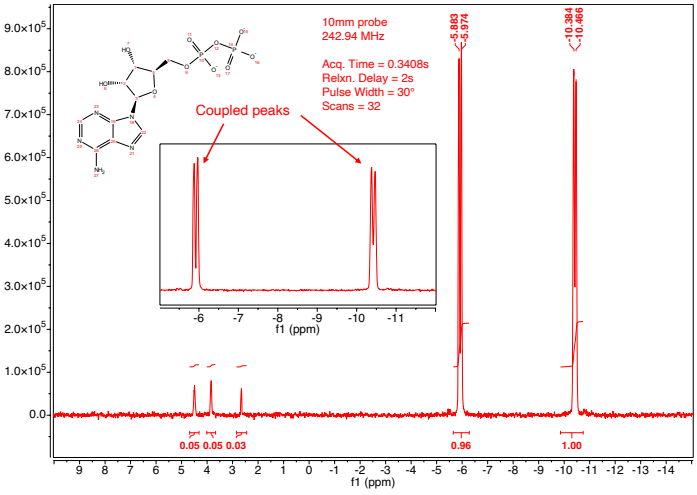

Figure 4.7: The ^{31}P-NMR spectrum for sodium adenosine diphosphate (Na-ADP). The inset represents the region from (-6) to (-11) ppm. Note the coupling between peaks corresponding to the phosphate groups.

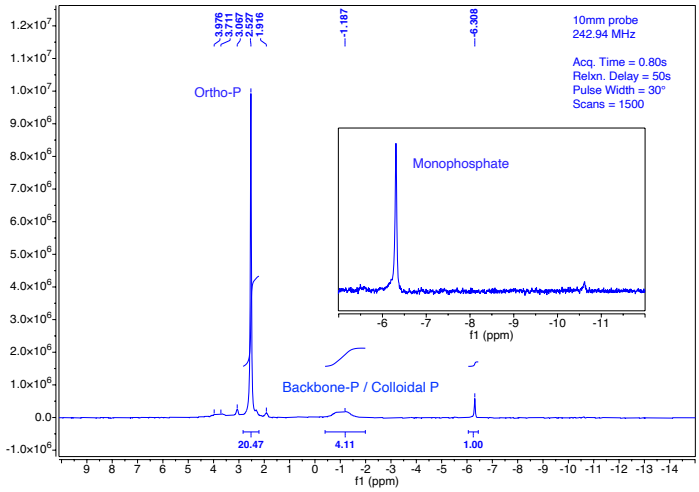

Figure 4.8: The ^{31}P-NMR spectrum for the "Washed - No Added KCl" sample. The inset represents the region from (-6) to (-11) ppm. Note the peak broadening around (-1) ppm and the integration areas corresponding to the major peaks in the spectrum.

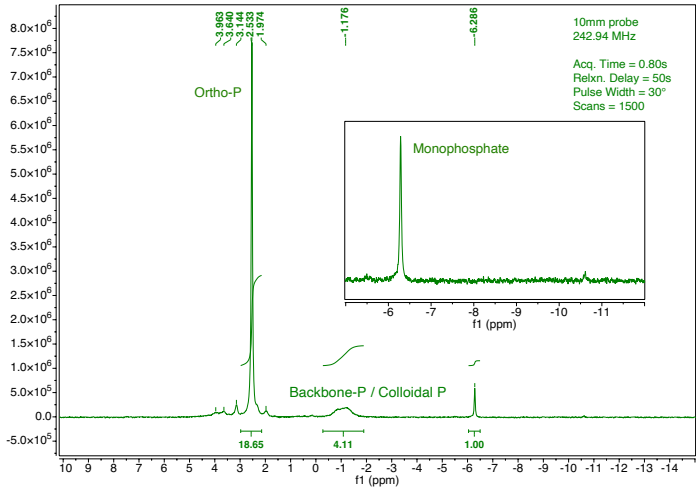

Figure 4.9: The ^{31}P-NMR spectrum for the "Washed - Added KCl" sample. The inset represents the region from (-6) to (-11) ppm. Note the peak broadening around (-1) ppm and the integration areas corresponding to the major peaks in the spectrum.

Figure 4.10: The typical scanned area observed using a scanning electron microscope and a back scattered electron detector for the "Washed - No Added KCl" sample. Note the high-density sports corresponding to both, large particles (> 1 μm) and small particles (< 1 μm).

along with the absence of a peak between (-10) and (-11) ppm (unlike Na-ADP) suggest that only monophosphate sugar groups are present within EPS. Additionally, peak broadening is also observable around (-1) ppm and is attributed to both P-groups attached to the backbone polymeric chains of EPS, or nano colloidal P particles. Finally, a sharp peak between 2 and 3 ppm is observed with a relatively large integration area (~ 18.6 to 20.5 times more than monophosphate groups). This has been attributed to the presence of monobasic orthophosphate groups in solution. Although it is acknowledged that neither purification protocol was adopted to selectively remove a particular P-species, the presence of dissolved (or sufficiently mobile) orthophosphate at such large quantitates comes as a surprise.

Figure 4.10 shows the electron microscopy image of the "Washed - No Added KCl" sample. The density differences within the dried EPS film are clearly discernible using the back scattered electron detector. Although most high-density spots correspond to micron sized particles within the sample, several sub-micron sized high-density spots are also distinguishable within the background, suggesting the presence of nanoparticles.

4.3.3. SALT ADDITION

Figure 4.11 shows the samples following the addition of salts. Although the "Blank", NaCl, KCl and $MgCl_2$ samples show no signs of precipitation before centrifugation, precipitation was observed across all samples following centrifugation. However, it is worth noting that the "Blank", NaCl and KCl samples did not precipitate completely, and that their supernatants still retained their turbidity after centrifugation. Unlike other samples with multivalent ions, the $MgCl_2$ sample showed no signs of precipitation before centrifugation, and precipitated completely after centrifugation to suggest the potential formation of a complex that is not prone to spontaneous precipitation.

The average pH and conductivities of the samples following the addition of salt is shown as a two-dimensional plot in Figure 4.12. Expectedly, a progressive increase in the conductivity, with valence, is observed for all samples. Particularly, the conductivity levels of trivalent salts ($Al(NO_3)_3$ and $FeCl_3$) are high enough to induce complete screening of charged moieties. Equally, a lowering of the pH was noted for all samples upon the addition of salt. Whilst changes to the pH was minimal in a few cases (< 1.5 for NaCl, KCl and $MgCl_2$), a larger change in its value was noted in all other cases. Specifically, for the $FeCl_2$, $FeCl_3$ and $Al(NO_3)_3$ samples, an exceptional swing to the pH was noted, with the pH falling below the expected pKa range of anionic functional groups (carboxylic and phosphate groups). This is where the gelling of EPS is typically noted upon acidification [3].

4.3.4. RHEOLOGY

Figure 4.13 shows the measured relative viscosity as a function of the EPS concentration for all dialysed samples. The intrinsic viscosities were obtained using Equation 4.1 and are reported in Table 4.10. In general, the intrinsic viscosity was estimated using 5 data points (see Figure 4.13). However, exceptions had to be made in the case of iron salts, with only 3 and 4 data points being used in the case of the Fe^{2+} and Fe^{3+} samples respectively, and are therefore expectably less accurate (see standard deviation values in Table 4.10). This was because a clear single value was not observed in the value of the viscosity for all concentrations, thereby suggesting precipitation within the concentric cylinder setup. Very minimal deviation is noted in the value of the intrinsic viscosity of the "Blank", Na^+ and K^+ data sets (~ 0.37 m^3/kg). By contrast, all other data sets present an increase in the value of the intrinsic viscosity to suggest the formation of a larger macromolecular complex. In particular, both the Ca^{2+} and the Al^{3+} data sets present intrinsic viscosity values greater than 1 m^3/kg, with the Ca^{2+} data set presenting the largest intrinsic viscosity of 1.14 m^3/kg to suggest a threefold increase in the size of the macromolecular complex (compared to the "Blank"). The dramatic increase to the intrinsic viscosity in these two cases is believed to occur due to a substantial increase to the chain length (chain extension), suggesting that cations interactions primarily act at the chain ends. Alternatively, the individual polymer coils could be randomly associating together in a "random walk" like fashion, where again the intrinsic viscosity will increase with the square root of the degree of association [18].

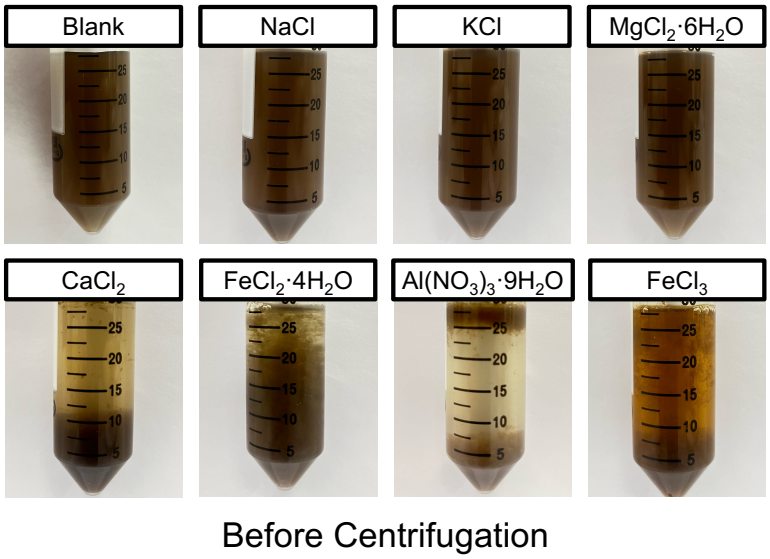

Figure 4.11: The dialysed samples that were photographed following the addition of salt, both before and after centrifugation (3880 g, 298 K, 600 s). The concentration of EPS within all the samples is 1.25 kg/m^3 (before the addition of salt).

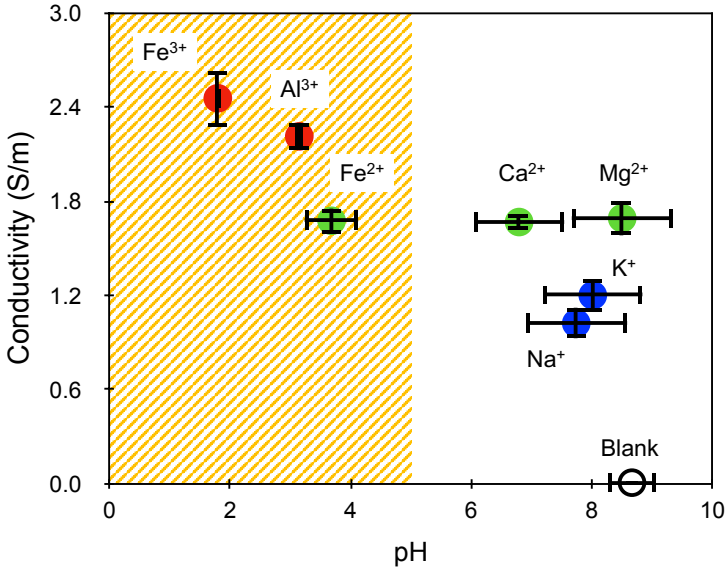

Figure 4.12: The average pH and conductivities of the dialysed samples following the addition of salt. The hatched region represents the pH range where an increase to the yield stress was observed to suggest the formation of hydrogen bonds (see Supplementary Material Subsection 4.6.3). Both, the horizontal and vertical error bars represent the two-sigma distribution (95% confidence interval).

Figure 4.14 shows the flow curves of the "Untreated", "Washed - No Added KCl" and "Washed - Added KCl" samples with different intermediate rest times. The values of the parameters from the Herschel-Bulkley curve fitting procedure are recorded in Table 4.11. It is clear that the adoption of either washing protocol is successful in increasing both the yield stress and consistency index, and in lowering the flow index of the washed EPS. Collectively, this may be viewed as an improvement in the viscoplastic flow properties with washing. The Herschel-Bulkley parameters in Table 4.11 appear to be independent of the washing protocol. However, these values are a result of the averaging across three measurements. A closer inspection of Figure 4.14 highlights the dependence of the flow behaviour on intermediate rest times. In general, a rest time of 1000 s is successful in increasing the slope of the flow curves for all samples. However, it appears that the "Washed - No Added KCl" sample displays the strongest dependence on rest times, with a distinguishable increase in the slope of the flow curves with increasing rest times. Although this time dependent behaviour may be labelled as thixotropic sample recovery by an intrepid rheologist, it is worthwhile to exercise some caution, as such time dependent recovery in the flow properties occur even after viscoelastic stress relaxation [20, 21]. As such, no

effort is made to categorise this transient response, and it is simply reported that only the No Added KCl washing protocol is successful in enticing this behaviour.

Table 4.10: The intrinsic viscosity ($[\eta]$) of the dialysed samples following the addition of salt. (S.D. = Standard Deviation)

Data Set	$[\eta]$ **(m^3/kg) ± S.D.**
"Blank"	0.38 ± 0.02
0.1M Na^+	0.38 ± 0.01
0.1M K^+	0.36 ± 0.03
0.1M Mg^{2+}	0.62 ± 0.05
0.1M Ca^{2+}	1.14 ± 0.12
0.1M Fe^{2+}	0.73 ± 0.08
0.1M Al^{3+}	1.08 ± 0.03
0.1M Fe^{3+}	0.63 ± 0.32

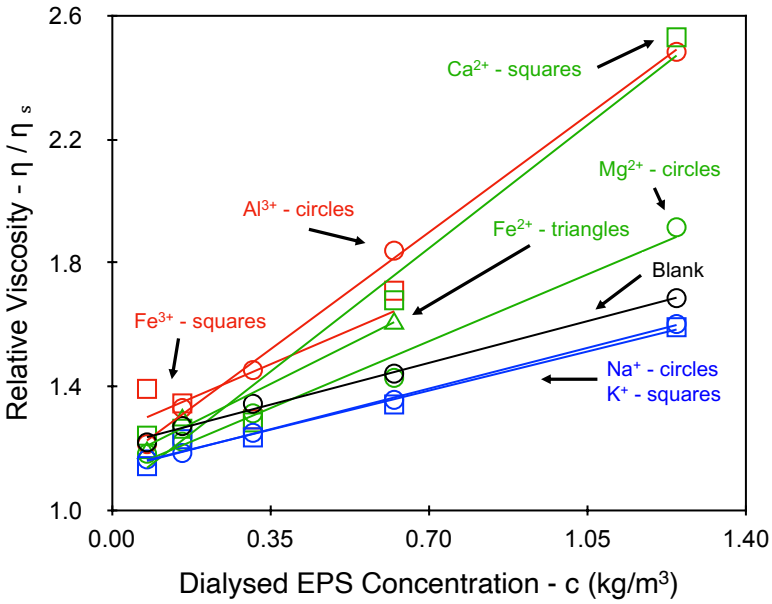

Figure 4.13: The relative viscosity as a function of the dialysed concentration of EPS (before the addition of salt). The straight lines act as a guide to the eye to represent the apparent slope made by each data set.

Table 4.11: The averaged Herschel – Bulkley parameters, i.e. the yield stress (σ_0), the consistency index (K) and the flow index (n). (S.D. = Standard Deviation)

Sample	σ_0 ± **S.D. (Pa)**	K ± **S.D. (Pa)**	n ± **S.D. (Pa)**
"Untreated"	1.298 ± 0.018	0.462 ± 0.009	0.457 ± 0.016
"Washed - No Added KCl"	3.068 ± 0.132	1.212 ± 0.101	0.364 ± 0.055
"Washed - Added KCl"	2.768 ± 0.279	1.309 ± 0.212	0.379 ± 0.036

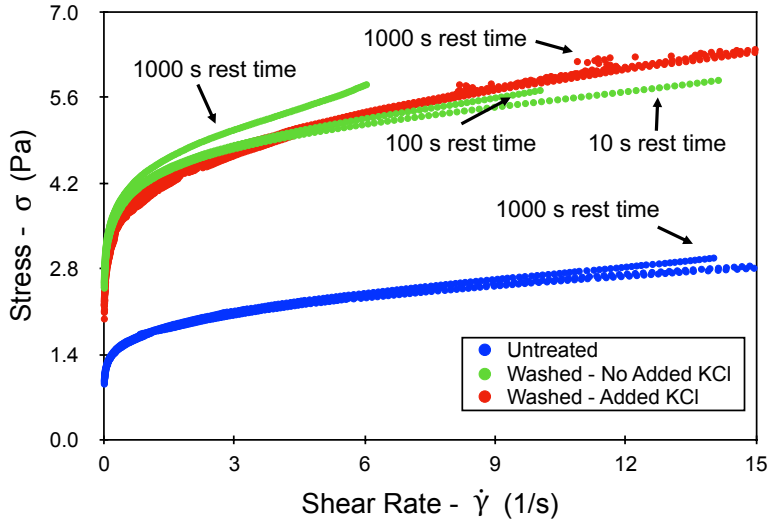

Figure 4.14: The flow curves of the "Untreated", "Washed - No Added KCl" and "Washed - Added KCl" samples after different intermediate rest times - 10 s, 100 s and 1000 s.

4.4. DISCUSSION

4.4.1. MONOVALENT CATIONS

As the EPS is extracted using an alkaline dissolution step (pH 9 to 11), followed by an acid precipitation step, approximately (10^{-5} - 10^{-3}) M of salt may be expected within EPS due to the neutralisation of the base. As highlighted earlier, in cases where the EPS is extracted from a saltwater environment, a further increase in the concentration of Na^+ may be expected. It is therefore important to evaluate the impact of these monovalent cations on the composition and properties.

In combination with ICP-OES results, it appears that despite minimal changes to the VS/TS ratio, acidic washing can still be used to control the levels of monovalent cations within EPS post extraction. Certainly, the removal of monovalent cations, along with other small organic molecules, is instrumental in improving the rheological properties such as yield stress and consistency index by at least a factor

of 2. Conversely, it is observed that variation in the concentration of Na^+ and K^+ up to 0.1 M has no major impact on the conformation of the dissolved macromolecule. It is believed that this is somewhat unprecedented for biopolymers, as changes to the salt concentration by 0.1 M is normally quite successful in changing the coil size of polysaccharides [22]. Additionally, the turbidity of the dissolved macromolecular solutions with added NaCl and KCl remains consistent with the "Dialysed - Blank" sample. Notable changes that were observed to the solubility over time, have also been attributed to the "folding" within the protein rich fractions of EPS [7]. Therefore, although variations in the levels of monovalent cations may be expected during the alkaline dissolution stage, they are not expected to impact the solubility of the EPS during extraction.

It is worth noting however, that the concentration of salt being described here is based on levels typically observed during EPS extraction [8]. In cases where sea water is directly used during extraction, molarities greater than 0.4 M may be anticipated for Na^+ [23]. Equally, it is recognised that variations in the amounts of KCl during washing may also lead to the selective removal of small organic molecules, and therefore influence the time dependent recovery of the viscoplastic flow properties. Although the latter point is covered to a limited extent, there definitely is a need to investigate the specific influence of these organic species on the rheological properties. However, this is beyond the scope of the current work.

4.4.2. Mg^{2+}, Ca^{2+} AND Al^{3+}

As stated earlier, the addition of both Mg^{2+} and Ca^{2+} has been noted to increase the dewatering ability of sludge, as well as gelling of wastewater EPS [6, 11]. This is because of the ability of either ion to form crosslinks between the anionic functional groups. Despite the ability of these cations to form crosslinks, it appears that their relative concentrations may be reduced via washing. As such, the washing was carried out in the acidic state, where the anionic groups within EPS remain protonated. Equally, the relative concentrations of both cations was low within the "Untreated" EPS (< 1% w/w of TS). However, once the pH is increased during dialysis, and the concentration of both cations is increased to 0.1 M, it is unsurprising that they were successful in precipitating EPS post dialysis and therefore, increase the intrinsic viscosity (Table 4.10).

In particular, the precipitation using Mg^{2+} warrants some attention. It is well established that the formation of complexes within wastewater biopolymers is a transient process [11]. This has been attributed to the availability of charged sites for the formation of cationic crosslinks in what may only be described as a multi-ingredient soup of competing chemical species. Upon taking a closer look at the dialysed samples with (added) Mg^{2+}, no changes to the solubility / precipitation are observed before centrifugation. It is thus recognised that the thermodynamically "meta-stable" floccular Mg^{2+} - EPS could be a result of such slow complex formation. This argument is further supported by the fact that the intrinsic viscosity of the dialysed sample with 0.1 M of Mg^{2+} is smaller than

the intrinsic viscosity of the sample with 0.1 M of Ca^{2+} to suggest an overall smaller macromolecule size (Table 4.10). Therefore, the ratio of Mg^{2+} to Ca^{2+} ions may be controlled in an effort to control the rheology and solubility of EPS complexes.

Much like the divalent ions, Al^{3+} too has the potential to form crosslinks with the anionic groups within EPS. Indeed, an increase in the intrinsic viscosity is also reported upon the addition of Al^{3+} ions (Table 4.10). However, a reduction in the pH is also observed due to the addition of 0.1 M of Al^{3+}. Once again, it is possible to protonate the anionic groups at these pH values (see Figure 4.12). Thus, multiple routes for cross-linking are present within this sample. This provides the opportunity to gel the EPS without the use of harsh inorganic acids such as HCl. As such, it is unclear if all 0.1 M of Al^{3+} participates in the cationic bridging. This is worth highlighting because the relative amount of Al remains invariant to purification, except in the case of the "Washed - Added KCl" sample, where a reduction in its concentration is noticeable. In this particular case, a change to the turbidity and colour of the supernatant is also reported (See Figure 4.4). Therefore, it is equally likely, that upon reaching a certain pH value, the remaining Al^{3+} complexes with the low molar mass organic matter and may therefore be susceptible to purification via washing.

4.4.3. Fe^{2+} AND Fe^{3+}

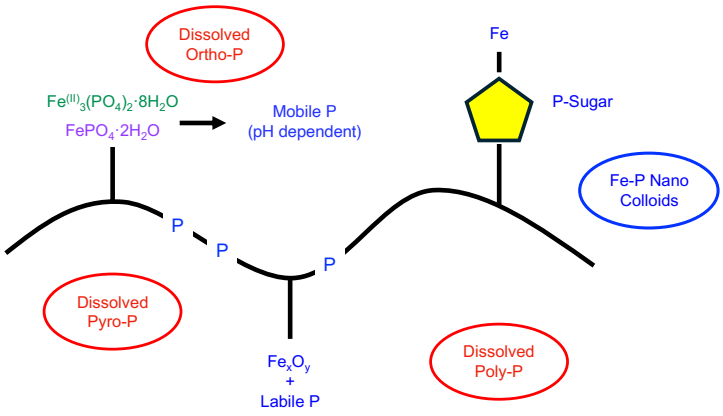

Figure 4.15: The expected Fe-P interactions within the polymeric fractions of EPS. The elliptical bubbles represent species that are presumably present in solution (or suspension). The species within the red ellipses represents P compounds that can be removed via dialysis or washing. The species in blue represent the compounds that are likely present within the sample despite dialysis or washing.

The ability of Fe to change the conformation of the macromolecular fractions within EPS is worth remarking. Much like Al^{3+}, the marked reduction to the

pH upon the addition of Fe^{2+} and Fe^{3+} can also result in the formation of hydrogen bonds. Equally, both ions can also complex with anionic sites within the polymeric fractions, thereby leading to the formation of bigger macromolecular complexes. It is worth noting that in both these cases, despite large uncertainties, it appears that both these ions are also successful in increasing the intrinsic viscosity when compared to the "Dialysed - Blank" sample (Figure 4.13 and Table 4.10).

As mentioned earlier, a relatively larger concentration of Fe was expected within the final EPS as a result of the upstream dosing. However, it comes as a surprise that large concentrations of P were recorded within the "Untreated" EPS sample [8]. Furthermore, both elements remain invariant to either route of purification, i.e. dialysis and washing. Although, a similar question may be posed for the presence of S within EPS, this is still attributable to the presence of sulphated glycans [24], as well as amino acid residues such as cysteine and methionine. Additionally, the relative concentration of S (compared to P and Fe) is approximately 3 times lower by mass. As such, it appears that both P and Fe are either strongly bound to each other in solution / suspension, or strongly bound to each other within polymeric fractions of EPS. To facilitate a discussion in this direction, the expected Fe-P interactions within EPS are mapped in Figure 4.15.

For the purposes of this discussion, the presence of P within the polymer backbone is excluded. Although these backbone species are likely to show up both in the ICP-OES and ^{31}P-NMR results, their presence within the backbone suggests that they are in their reduced state and therefore, incapable of complexing with Fe. Equally, the presence of dissolved P-ions or P-species may be overlooked as these can be removed via dialysis and washing. Thus, the discussion is limited to four species: Fe bound to phosphorylated sugars, Fe-P minerals such as vivianite and strengite, P adsorbed to iron oxide particles and Fe-P nano colloidal particles.

As highlighted earlier, the ICP-OES analysis suggests a molar ratio of 3:2 for P:Fe. This supports the hypothesis that 2 Fe^{3+} ions are bound to 3 monophosphate sugar groups within EPS (PO_4^{2-} at pH ~ 9.2). Upon performing the ^{31}P-NMR analysis, the absence of coupled P signals within the washed EPS supports the likelihood of Fe being bound to monophosphates. However, there appears to be 18.6 - 20.5 times more orthophosphates compared to the monophosphate sugar groups. Thus, although the presence of Fe bound to phosphorylated sugars cannot be excluded, it is unlikely that it is present in large concentrations within the EPS.

The presence of both vivianite and strengite in wastewater remains well established [15, 25]. Equally, these minerals have been shown to exhibit a pH-sensitive solubility. Whilst vivianite is soluble under low pH conditions [26], strengite is soluble under high pH conditions [27]. Thus, it is expected that the bulk of the vivianite is removed during the alkaline dissolution phase, where the dissolved EPS is separated from the undissolved substances. However, the successful removal of vivianite is limited by the separation efficiency of the solid-liquid separation technique employed and thus,

paves the way for it to end up within the acidic EPS (albeit in small concentrations). By contrast, strengite may only be removed using dialysis at elevated pH. Therefore, it is possible that either mineral ends up as an adsorbed product within acidic EPS, with the acidic conditions specifically facilitating the slow release of mobile P species such as orthophosphate from vivianite. Iron, however, is present as Fe^{2+} within vivianite, and Fe^{3+} within strengite. Therefore, the speciation of iron is controlled by the ratio of vivianite to strengite present within EPS. As such, no effort is made here to quantify the relative amounts of Fe ions using ICP-OES. Thus, there is sufficient scope to quantify the relative amounts of Fe^{2+} and Fe^{3+} in future work. It is worth acknowledging, that the presence of adsorbed minerals in EPS has not been reported in literature and, its presence in the final EPS is somewhat unprecedented. Expectedly, the presence of minerals such as vivianite and strengite would result in high density particles detectable by SEM. But the particles imaged using SEM do not have a symmetric crystalline structure to suggest the presence of minerals.

The strongest hypotheses are the presence of iron oxide micro and nano particles. Much like the minerals above, iron oxides exhibit a pH sensitive behaviour, with the selective adsorption and labile binding of P species under acidic pH conditions [28]. This also explains the somewhat lower P concentration within the "Dialysed - Blank" sample, as the P species desorb under alkaline conditions. The labile nature of the adsorption also explains how P may not re-enter the solution, making it somewhat impervious to washing. Similarly, iron oxides needn't have a characteristically crystalline shape, but could yet be present as high-density micron sized particles that can be observed using SEM. Another observation that supports the presence of iron oxide particles is the colour of the supernatant (see Figures 4.3, 4.4 and 4.11). Upon closely observing Figure 4.11, it is noticeable that the addition of Fe^{3+} ions resulted in the characteristic "rust" colour observed in the supernatant of the washed (acidic) EPS samples (Figures 4.3 and 4.4). The presence of iron oxides may be confirmed using other spectroscopic techniques [29], however, it is worth remarking that the interest in trying to characterise iron oxide particles within EPS is a highly selective exercise that is targeted at a very small fraction of the total solid mass.

Similarly, the use of iron oxide nano-particles, as well as nano-zero valent iron (NZVI) have been proposed for wastewater treatment in the recent years [30, 31]. Although the use of such nanoparticles is not prevalent in the extraction site in Utrecht, the potential for these particles to enter the wastewater, and eventually the sludge cannot be discounted [31]. Much like hydroxyapatite nanocrystalline particles [32, 33], Fe nanoparticles can favourably bind to P-species in solution to give rise to Fe-P nano colloidal particles. It is worth noting that the presence of such non-apatite inorganic particles (NAIP) within EPS has been confirmed in recent studies [9]. The presence of Fe-P nano colloidal particles is successful in explaining some of the other phenomena observed during analysis: invariance to purification strategies via dialysis or washing, the presence of broad peaks in the ^{31}P-NMR spectra and the presence of high-density sub-micron particles observed using SEM.

Overall, the downside to the presence of Fe in EPS is the potential (re)accumulation of P. Although P itself only makes up roughly 3% of the TS, it's presence within EPS is certainly unaccounted for during extraction, thereby increasing the total non-volatile mass. More importantly, based on the analytical procedure highlighted here, it is tedious to decipher the various forms in which P is present within EPS. Certainly, it is acknowledged that the presence of P in EPS need not be detrimental and can pave the way for interesting characteristics such as flame retardancy [9]. This example of Fe and P however, serves to reinforce the ideology that the properties of the extracted EPS are strongly influenced by the presence (or absence) of specific cations.

4.5. CONCLUSIONS

In general, it is worth highlighting that despite purification, at least roughly 14% and up to 23% of the total solid mass within EPS is attributable to the presence of non-volatile solids, with a considerable proportion of this mass being inorganic cations. Thus, it is questionable to label these extracellular substances as simply "polymeric" or "organic". Based on the observations reported here; the presence of cations is bound to influence the solubility through macromolecular complexation, also acting to modify the yield stress and viscosity.

Although the conformation of EPS coils in solution appear to be insensitive to changes in Na^+ and K^+ concentration, even minute changes to the VS/TS ratio, due to the removal of these monovalent cations by washing, is instrumental in improving the yield stress and the viscosity of acidic EPS.

It is also clear that controlling the ratio of Ca^{2+} to Mg^{2+} ions influences that rates and mechanisms of complexation, thereby impacting the intrinsic viscosity, resulting in hydrogel systems with tuneable mechanical properties. Additionally, Al^{3+} can be used to simultaneously increase the (intrinsic) viscosity, as well as to protonate the anionic EPS by reducing the pH. This provides the opportunity to gel the EPS without the use of harsh inorganic acids such as HCl.

Finally, there is still sufficient scope to study changes to the intrinsic viscosity of EPS due to the addition of Fe^{2+} and Fe^{3+}, and is therefore earmarked as a task for future publications. Fe is also instrumental in the accumulation of P species within EPS, and serves to reinforce the flame retardant characteristics of EPS.

Thus, a close assessment of the inorganic composition within EPS remains mandatory for both a qualitative, as well as a quantitative assessment of the solubility, gelling, rheological and flame retardant properties of EPS. In return, the understanding gained may be used to closely control the properties of EPS, thereby making them even more appealing as alternatives to conventional (bio)polymers.

4.6. DATA AND SUPPLEMENTARY MATERIAL

The data from the TGA, the ICP-OES, and the rheology measurements is publicly accessible using the following link: https://doi.org/10.4121/e7a18f71-e5c8-445d-9852-21119d43e215

4.6.1. EXTRACTION PROTOCOL FOR EPS

An overview of the protocol for pilot scale extractions developed by Bart Verkooijen (TU Delft) and Dr. Philipp K. Wilfert (co-promotor) is summarised in Table 4.12. For more details about the extraction protocol, the reader is asked to contact Philipp K. Wilfert (philipp.zantout-wilfert@th-luebeck.de).

4.6.2. CONCENTRATION OF ANALYTES FROM ICP-OES

Table 4.13 summarises both, the list of analytes the ICP-OES analysis, as well as their relative concentrations (in % w/w of TS).

4.6.3. YIELD STRESS VS. PH

Figure 4.16 depicts the dependence of yield stress on pH.

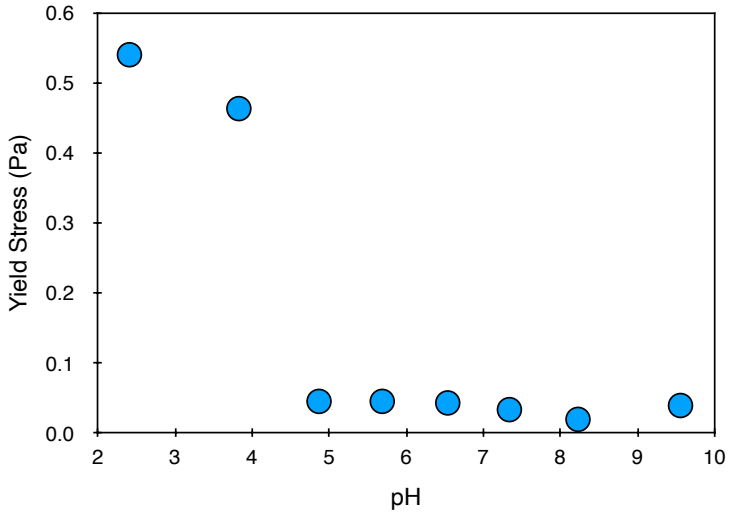

Figure 4.16: Changes to the yield stress of EPS from AGS as a function of pH. The EPS was extracted in the lab using sludge obtained from the wastewater treatment plant in Utrecht. The total dried solids (TS) were recorded as being approximately 3% w/w for all samples. A clear increase to the yield stress is noticeable below a pH ~ 5 to suggest the formation of hydrogen bonds within the sample.

Table 4.12: Protocol for the pilot scale extraction of extracellular polymeric substances (EPS) from aerobic granular sludge (AGS).

Step No.	Label	Remarks
1	Reactor Tank Filling	Reactor tank filled with AGS from treatment plant.
2	Reactor Tank Heating	Contents of tank heated to 80 °C using high pressure steam generator.
3	Alkalinisation	pH adjusted between 9-11 using 25 % w/w KOH solution.
4	Decanter Separation	Flow rate = 1.5 m^3/hr, RPM = 4560 ± 15. Undissolved solids separated from dissolved EPS.
5	Cooling	Overnight cooling of EPS sample.
6	Acidification	pH adjusted to 2.3 using 30% w/w HCl solution.
7	Disc Centrifugation	Flow rate = 1.5 m^3/hr, RPM = 6186 ± 200. Acidic EPS gel separated from acidic centrate.

Table 4.13: Average concentration of all 33 analytes from ICP – OES analysis.

Analyte	Conc (% w/w of TS) in "Untreated" sample	Conc (% w/w of TS) in "Dialysed-Blank" sample	Conc (% w/w of TS) in "Washed-No Added KCl" sample	Conc (% w/w of TS) in "Washed-Added KCl" sample
Calcium	0.438	0.548	0.078	0.044
Copper	0.040	0.045	0.040	0.035
Iron	3.086	3.513	3.437	3.388
Potassium	3.017	4.409	0.411	1.134
Magnesium	0.095	0.117	0.019	0.015
Sodium	0.137	1.976	0.039	0.013
Silver	0.001	0.001	0.001	0.001
Barium	0.012	0.013	0.013	0.011
Beryllium	-	-	-	-
Molybdenum	0.001	0.001	0.002	0.001
Lead	0.011	0.011	0.012	0.012
Rubidium	-	-	-	-
Aluminium	0.290	0.310	0.321	0.311
Boron	0.007	-	-	-
Cadmium	0.001	-	-	-
Cobalt	0.002	0.001	0.001	0.001
Chromium	0.004	0.004	0.004	0.004
Manganese	0.004	0.004	0.001	-
Nickel	-	-	-	-
Phosphorous	2.972	2.452	2.986	2.895
Sulphur	1.052	1.170	1.230	1.120
Selenium	-	-	-	-
Silicon	0.171	0.189	0.189	0.162
Tin	0.002	0.002	0.002	0.002
Zinc	0.039	0.044	0.016	0.013
Arsenic	-	-	-	-
Cerium	-	-	-	-
Lithium	0.001	-	-	-
Lanthanum	0.001	-	-	-
Zirconium	-	-	-	-
Strontium	0.006	0.006	0.002	0.001
Tungsten	-	-	-	-
TItanium	0.008	0.010	0.010	0.009

REFERENCES

[1] R. Geyer, J. Jambeck, and K. Law. "Production, use, and fate of all plastics ever made". In: *Science Advances* 3 (2017), e1700782. DOI: https://doi.org/10.1126/sciadv.1700782.

[2] T. More, J. Yadav, S. Yan, R. Tyagi, and R. Surampalli. "Extracellular polymeric substances of bacteria and their potential environmental applications". In: *Journal of Environmental Management* 144 (2014), pp. 1–25. DOI: https://doi.org/10.1016/j.jenvman.2014.05.010.

[3] S. Felz, S. Al-Zuhairy, O. Aarstad, M. van Loosdrecht, and Y. Lin. "Extraction of structural extracellular polymeric substances from aerobic granular sludge". In: *Journal of Visualized Experiments* 115 (2016), e54534.

[4] T. Seviour, B. Donose, M. Pijuan, and Z. Yuan. "Purification and conformational analysis of a key exopolysaccharide component of mixed culture aerobic sludge granules". In: *Environmental Science & Technology* 44 (2010), pp. 4729–4734. DOI: https://doi.org/10.1021/es100362b.

[5] N. Kim, N. Mao, R. Lin, D. Bhattacharyya, M. van Loosdrecht, and Y. Lin. "Flame retardant property of flax fabrics coated by extracellular polymeric substances recovered from both activated sludge and aerobic granular sludge". In: *Water Research* 170 (2020), p. 115344. DOI: https://doi.org/10.1016/j.watres.2019.115344.

[6] S. Felz, H. Kleikamp, J. Zlopasa, M. van Loosdrecht, and Y. Lin. "Impact of metal ions on structural EPS hydrogels from aerobic granular sludge". In: *Biofilm* 2 (2020), p. 100011. DOI: https://doi.org/10.1016/j.bioflm.2019.100011.

[7] S. Felz, P. Vermeulen, M. van Loosdrecht, and Y. Lin. "Chemical characterization methods for the analysis of structural extracellular polymeric substances (EPS)". In: *Water Research* 157 (2019), pp. 201–208. DOI: https://doi.org/10.1016/j.watres.2019.03.068.

[8] S. Velasquez Posada. "Extracellular Polymeric Substances from Aerobic Granular Sludge: Implications for Agricultural Use in Foliar Fertilization". Masters' Thesis. Delft University of Technology, 2023. URL: http://resolver.tudelft.nl/uuid:7d522b72-6d56-48f6-9b2d-50c312ca9a75.

[9] N. Bahgat, P. Wilfert, S. Eustace, L. Korving, and M. van Loosdrecht. "Phosphorous speciation in EPS extracted from Aerobic Granular Sludge". In: *Water Research* 262 (2024), p. 122077. DOI: https://doi.org/10.1016/j.watres.2024.122077.

[10] N. Bahgat, P. Wilfert, L. Korving, and M. van Loosdrecht. "Integrated resource recovery from aerobic granular sludge plants". In: *Water Research* 234 (2023), p. 119819. DOI: https://doi.org/10.1016/j.watres.2023.119819.

[11] D. Sobeck and M. Higgins. "Examination of three theories for mechanisms of cation-induced bioflocculation". In: *Water Research* 36 (2002), pp. 527–538. DOI: https://doi.org/10.1016/S0043-1354(01)00254-8.

[12] N. Dietrich. "Physico-chemical characterization of the extracellular polymer matrix of biofilms in membrane filtration systems". Doctoral Dissertation. Delft University of Technology, 2020. DOI: https://doi.org/10.4233/uuid:a6c6ee3d-55a0-4a2a-8ac9-b6e837e4862e.

[13] J. Li, X. Hao, M. van Loosdrecht, and Y. Lin. "Understanding the ionic hydrogel-forming property of extracellular polymeric substances: Differences in lipopolysaccharides between flocculent and granular sludge". In: *Water Research* 268 (2024), p. 122707. DOI: https://doi.org/10.1016/j.watres.2024.122707.

[14] L. De-Bashan and Y. Bashan. "Recent advances in removing phosphorus from wastewater and its future use as fertilizer (1997–2003)". In: *Water Research* 38 (2004), pp. 4222–4246. DOI: https://doi.org/10.1016/j.watres.2004.07.014.

[15] P. Wilfert, P. Kumar, L. Korving, G.-J. Witkamp, and M. Van Loosdrecht. "The relevance of phosphorus and iron chemistry to the recovery of phosphorus from wastewater: a review". In: *Environmental Science & Technology* 49 (2015), pp. 9400–9414. DOI: https://doi.org/10.1021/acs.est.5b00150.

[16] B. Cade-Menun and C. Liu. "Solution phosphorus-31 nuclear magnetic resonance spectroscopy of soils from 2005 to 2013: A review of sample preparation and experimental parameters". In: *Soil Science Society of America Journal* 78 (2014), pp. 19–37. DOI: https://doi.org/10.2136/sssaj2013.05.0187dgs.

[17] H.-L. Zhang, W. Fang, Y.-P. Wang, G.-P. Sheng, R. Zeng, W.-W. Li, and H.-Q. Yu. "Phosphorus removal in an enhanced biological phosphorus removal process: roles of extracellular polymeric substances". In: *Environmental Science & Technology* 47 (2013), pp. 11482–11489. DOI: https://doi.org/10.1021/es403227p.

[18] M. Rubinstein and R. Colby. *Polymer Physics*. Oxford, UK: Oxford University Press, 2003.

[19] T. Osswald and N. Rudolph. *Polymer Rheology: Fundamentals and Applications*. Munich, Germany: Carl Hanser Verlag GmbH, 2015.

[20] M. Agarwal, S. Sharma, V. Shankar, and Y. Joshi. "Distinguishing thixotropy from viscoelasticity". In: *Journal of Rheology* 65 (2021), pp. 663–680. DOI: https://doi.org/10.1122/8.0000262.

[21] J. Mewis and N. Wagner. "Thixotropy". In: *Advances in Colloid and Interface Science* 147 (2009), pp. 214–227. DOI: https://doi.org/10.1016/j.cis.2008.09.005.

[22] A. Raja, P. Wilfert, and S. Picken. "Charge mediated changes to the intrinsic viscosity of biopolymer systems". In: *Polymers* 16 (2024), p. 2894. DOI: https://doi.org/10.3390/polym16202894.

[23] F. Millero, R. Feistel, D. Wright, and T. McDougall. "The composition of Standard Seawater and the definition of the Reference-Composition Salinity Scale". In: *Deep Sea Research Part I: Oceanographic Research Papers* 55 (2008), pp. 50–72. DOI: https://doi.org/10.1016/j.dsr.2007.10.001.

[24] S. Felz, T. Neu, M. van Loosdrecht, and Y. Lin. "Aerobic granular sludge contains Hyaluronic acid-like and sulfated glycosaminoglycans-like polymers." In: *Water Research* 169 (2020), p. 115291. DOI: https://doi.org/10.1016/j.watres.2019.115291.

[25] Y. Wu, J. Luo, Q. Zhang, M. Aleem, F. Fang, Z. Xue, and J. Cao. "Potentials and challenges of phosphorus recovery as vivianite from wastewater: A review". In: *Chemosphere* 226 (2019), pp. 246–258. DOI: https://doi.org/10.1016/j.chemosphere.2019.03.138.

[26] W. Patrick Jr, S. Gotoh, and B. Williams. "Strengite dissolution in flooded soils and sediments". In: *Science* 179 (1973), pp. 564–565. DOI: https://doi.org/10.1126/science.179.4073.564.

[27] N. Bahgat, A. Siddiqui, P. Wilfert, L. Korving, and M. van Loosdrecht. "FePO4. 2H2O recovery from acidic phosphate-rich waste streams". In: *Water Research* 260 (2024), p. 121905. DOI: https://doi.org/10.1016/j.watres.2024.121905.

[28] S.-Y. Yoon, C.-G. Lee, J.-A. Park, J.-H. Kim, S.-B. Kim, S.-H. Lee, and J.-W. Choi. "Kinetic, equilibrium and thermodynamic studies for phosphate adsorption to magnetic iron oxide nanoparticles". In: *Chemical Engineering Journal* 236 (2014), pp. 341–347. DOI: https://doi.org/10.1016/j.cej.2013.09.053.

[29] R. Cornell and U. Schwertmann. *The iron oxides: structure, properties, reactions, occurrences, and uses*. Weinheim, Germany: Wiley-vch, 2003.

[30] T. Aragaw, F. Bogale, and B. Aragaw. "Iron-based nanoparticles in wastewater treatment: A review on synthesis methods, applications, and removal mechanisms". In: *Journal of Saudi Chemical Society* 25 (2021), p. 101280. DOI: https://doi.org/10.1016/j.jscs.2021.101280.

[31] Y. Yang, C. Zhang, and Z. Hu. "Impact of metallic and metal oxide nanoparticles on wastewater treatment and anaerobic digestion". In: *Environmental Science: Processes & Impacts* 15 (2013), pp. 39–48. DOI: https://doi.org/10.1039/C2EM30655G.

[32] R. Liu and R. Lal. "Synthetic apatite nanoparticles as a phosphorus fertilizer for soybean (Glycine max)". In: *Scientific Reports* 4 (2014), p. 5686. DOI: https://doi.org/10.1038/srep05686.

[33] M. Okada and T. Matsumoto. "Synthesis and modification of apatite nanoparticles for use in dental and medical applications". In: *Japanese Dental Science Review* 51 (2015), pp. 85–95. DOI: https://doi.org/10.1016/j.jdsr.2015.03.004.

5

YIELDING OF JAMMED DEFORMABLE HYDROGEL SUSPENSIONS

Jammed deformable hydrogel suspensions (JDHS) represent a set of emergent soft fluids that are important for 3D / 4D bioprinting, as well as for developing biopolymers with hydrogel forming characteristics. However, the influence of the hydrogel particle morphologies, as well as the solids content, on the overall rheological properties remains underexplored. Therefore, oscillatory strain amplitude sweep measurements spanning 6 orders of magnitude (SAOS to LAOS, or vice versa) were performed on a diverse, but arguably representative set of samples: alginate hydrogels, tomato ketchup, and extracellular polymeric substances (EPS) from wastewater. Trends that were observed in the resultant curves are systematically presented, alongside a discussion that compares the noted yielding phenomena with well-studied systems such as colloidal gels, yield stress fluids, as well as other jammed gel suspensions. In general, all JDHS systems studied here present a consistent set of trends that include extreme sensitivity to small oscillatory strain amplitudes (10^{-4} or less), and the presence of multiple yield stresses over a wide range of strain amplitudes. These results therefore challenge trends previously observed within non-macromolecular colloidal gels that show a single linear viscoelastic modulus plateau / yield stress. The presence of multiple yield stress levels is attributed to interparticle interlocking, possibly related to a change in the effective particle shape. The pragmatic appeal of relevant "ideal" and "fast" friction dominated self-healing mechanisms within JDHS is also discussed, alongside relevant applications as self-healing materials in the biomedical, soft robotics and the food industries.

At the time of finalising this thesis, this chapter is under review for publication in *Soft Matter* as: A. Raja and S.J. Picken, "The Dynamic Yielding Phenomena of Jammed Deformable Hydrogel Suspensions at Very Small Strain Amplitudes".

5.1. INTRODUCTION

The term jammed deformable hydrogel suspensions (JDHS) can be used to describe colloidal or non-colloidal jammed suspensions that are formed by deformable hydrogel granules (or flocs). As such, these suspensions are relevant for emergent biomedical applications [1], with a particularly high relevance for applications involving 3D / 4D bioprinting [2, 3] and tissue engineering [4]. In light of growing concerns surrounding the use of conventional polymer materials [5], and owing to the fact that the hydrogel particles may be formed using biopolymer materials [6], there is the added incentive to develop such systems for a larger variety of engineering applications. Thus, research conducted on JDHS is equally important for the applicability of emergent and sustainable bio-macromolecular hydrogel suspensions such as extracellular polymeric substances (EPS) from wastewater. [7].

So far, selective rheological studies have been conducted on JDHS with somewhat well-defined particle morphologies, with the effort being focussed on describing viscoelastic properties such as storage and loss moduli [2–4]. However, these studies do not observe trends in jammed state as a result of variations in the packing of neighbouring particles. Expectedly, sharp changes can be expected in the viscoelastic properties of JDHS by altering their concentration [8]. JDHS with no regularity in particle morphologies are also ubiquitous in a wide range of practically relevant applications in food science [9], including food products that use rheology modifiers [10], and equally relevant for separation, transport and homogenisation of concentrated suspensions [11, 12]. In particular, EPS (the system of current interest) are also made up of irregularly shaped polydisperse particles [7]. Further, EPS have been noted to have highly complicated chemical (or macromolecular) structure(s), with limited [13, 14] and partial [15, 16] insights available from the combined use of several analytical techniques. Despite this, it has been possible to establish structure-property relationships of EPS, by drawing relevant comparisons to well-studied biopolymer systems such as alginate [17] and gelatin [18]. Given the relevance of these relationships for applications, the ability to show tuneability in their properties, similar to a wide variety of known JDHS, successfully contributes towards their utility.

There is also an equal opportunity to develop the existing understanding about the viscoelastic properties of colloidal gels [19, 20] to cover JDHS. These widely cited literature sources on colloidal gels cover changes to the storage modulus and linear viscoelastic strain limit, due to changes in the volume fraction, as well as the stiffness of interparticle links. However, as they focus on non-macromolecular particles, they may not be successful in describing observations made using macromolecular gel systems. The deformability of particles within JDHS equally offers the possibility to test the rigorously developed understanding about yield stress fluids [21]. Although ubiquitous dilatant shear thickening JDHS, such as corn starch suspensions, remain widely cited in literature [22], very little explanation is provided for the potential mechanisms of shear thinning within JDHS. Unlike corn starch suspensions, or even JDHS with regularly shaped particle morphologies [8], considerable deformability

and irregularly in the shape of the hydrogel particles further implies their inability to function as the archetypical "hard spheres" system in the jammed state.

Therefore, this study covers experimentally observable changes to the storage modulus due to both, changes in the (mass) concentration, as well as the particle morphology. In the former case, the morphology of the particles are voluntarily varied to cover trends that may be observed across a wide range of JDHS. In the latter case, the analysis is limited to well mixed systems, attempting to avoid the effects of syneresis, and thus changes to the mass concentration as much as possible. It is worth mentioning that in both these cases, this study strictly confines itself to a concentration range where jamming was observed. This is because unjammed hydrogel suspensions are not directly relevant for the applications discussed above, and are otherwise thoroughly studied in the literature sources cited thus far. To aid a more thorough understanding of the results, consistency in the yielding phenomena are closely studied and suitably categorised. These trends are then compared to other systems cited in literature, such as colloidal gels, yield stress fluids, as well as other jammed gel suspensions. Collectively, this information may then be used to extend the overall general rheological understanding of hydrogel systems, with the hopes of developing them further for a growing list of relevant applications. These applications include the use of JDHS as self-healing materials within the biomedical, the food industry, and also for soft robotics [23]. Finally, an outlook is also provided to stimulate relevant and potential future research on JDHS.

5.2. MATERIALS AND METHODS

To investigate the effects of concentration, 4 different systems were chosen to cover a wide range of particle morphologies: hydrogen bonded alginate suspensions with irregularly shaped particles, calcium alginate suspensions with spheroidal particles, tomato ketchup with multiple types of particles, and EPS with irregularly shaped floccular particles. In all these cases, the medium (or solvent) is frequently a close to Newtonian fluid (water), and does not exhibit shear thinning to a major extent. Thus, yielding is expected to occur due to changes to the particle shape (or aspect ratio), as well as changes to the interactions between neighbouring particles.

To further elucidate the choice of materials under investigation, both the hydrogen bonded alginate suspension, as well as the EPS, are expected to form a jammed, "sticky", aggregated fractal like network spanning multiple length scales. These aggregated networks are expected to undergo breakup (or rearrangement) under shear, with potential (re)attachment of the "sticky" particles. By contrast, the calcium alginate hydrogel particles possess a (more) well-defined morphology upon crosslinking, with "non-sticky" and non-dynamic interactions between neighbouring particles. Therefore, yielding in this case is the result of the jamming constraint release through the favourable rearrangement of the deformable particles. Finally, ketchup is a jammed suspension of refined biomass particles possessing different

particle morphologies, composition and interactions. Thus, yielding in the case of ketchup is due to the breakdown of the sterically jammed lattice like network that may also show dynamic particle interactions. A single Alginate - Gluconic acid hydrogel system was also chosen to specifically investigate the effects of morphology. As the addition of the gluconic acid leads to the formation of hydrogen bonds within alginate, the morphology of the network (upon mechanical refinement - see below) is analogous to the hydrogen-bonded alginate and EPS systems described earlier.

A detailed account of the sample preparation, as well as the methodology adopted for rheology tests is provided below. Optical microscopy images, that qualitatively capture the morphological features described above, are available in Supplementary Material Subsection 5.6.1.

5.2.1. HYDROGEN BONDED ALGINATE SUSPENSION (H-ALGINATE)

A 10% w/w solution was prepared by dissolving sodium alginate (Na-Alginate, CAS number: 9005-38-3) from Sigma-Aldrich (product number: W201502, Zwijndrecht, The Netherlands) in Milli-Q water. To ensure complete dissolution, the solution was stirred within a sealed conical flask for 24 hours at 293 K and 50% RH. The polymer was subsequently crosslinked by reducing the pH to 2 (± 0.1) using a 1 M HCl solution. The contents of the flask were transferred to a beaker and homogenised using an IKA T18 digital Ultra-Turrax homogeniser operated at 15000 rpm (~ 1571 rad/s). The beaker was placed within an ice bath during the homogenisation process to mitigate the risk of thermal degradation. The homogeniser unit was discontinuously operated for a total run time of 1200 s, as it was occasionally halted to suitably repack the suspension within the beaker, as well as to replenish the ice bath. Owing to solvent loss and changes to the packing of hydrogel particles during homogenisation, the concentration of total solid substances was verified using thermogravimetric analysis (TGA). The Perkin Elmer TGA 8000 device was equipped with ceramic crucibles (Perkin Elmer - part no. N5370464) and operated at 378 K until no changes to the mass was observed. Finally, the pH and conductivity of the homogenised suspension was recorded, and suitable dilutions of the suspension were prepared using a $1x10^{-2}$ M HCl - $3x10^{-1}$ M NaCl solution. The presence of NaCl ensured that the ionic strength of the system was maintained despite dilution. The samples were refrigerated at 277 K until they could be tested further.

5.2.2. CALCIUM ALGINATE SUSPENSION (CA-ALGINATE)

The 10% w/w Na-Alginate solution was diluted to a concentration of 3.5% w/w using Milli-Q water. Next, a 0.5 M $CaCl_2$ solution was prepared by dissolving the desired amount of $CaCl_2$ in 200 cm^3 (or mL) of Milli-Q water (293 K, 50% RH). The $CaCl_2$ solution was subsequently filtered through a Whatman® filter paper to clarify the solution. The filtered salt solution was transferred to a crystallisation dish. Approximately 90 cm^3 of the Na-Alginate solution was transferred into an atomiser bottle, and the contents of the bottle were completely emptied by spraying

the polymer solution into the $CaCl_2$ solution. A schematic representation of this process is available in Supplementary Material Subsection 5.6.2. The dish was sealed using a watch glass and its contents were stirred for 1 hour. This process was carried out in an effort to suspend any aggregated hydrogel microparticles within the salt solution. Next, any large noticeable hydrogel chunks were meticulously removed, and the suspension was washed repeatedly to rinse out the remaining salt within the solution. The washing was carried out through the gross dilution of the suspension using Milli-Q water, followed by centrifugation (2000 g, 300 s, 298 K). The centrifugation process was carried out repeatedly, for a total of 4 runs, until the conductivity of the suspension dropped below 200 μS/cm ($2x10^{-2}$ S/m). Finally, one last centrifugation run was carried out to jam the suspension at the bottom of the tube, and to decant the clear supernatant (see Supplementary Material Subsection 5.6.2). Once again, the concentration of solid substances was verified using TGA, and subsequent dilutions of the suspension were made using Milli-Q water. The samples were refrigerated at 277 K until they could be tested further.

5.2.3. TOMATO KETCHUP

A 250 g (220 cm^3) bottle of commercially available Heinz tomato ketchup (batch number: 22841924TK3, The Netherlands) was procured for rheological measurements. The ketchup was tested approximately 14 months prior to its "best before" date. The ketchup has a reported salt content of 1.8% w/w, a carbohydrate content of 23.2% w/w (22.8% w/w sugars - assumed to be non-polymeric), 1.2% w/w proteins, and 0.1% w/w fats. Again, the concentration of total solid substances was verified using TGA. Subsequently, upon recording the pH and conductivity of the sample, dilutions were made using a $2x10^{-4}$ M HCl - $2x10^{-1}$ M NaCl solution in Milli-Q water. The samples were refrigerated at 277 K until they could be tested further.

5.2.4. EPS

The EPS was extracted using the first full scale domestic extraction plant of its kind located in Epe, The Netherlands [24]. Consistent with the information reported in this source, the EPS was extracted by initially dissolving the macromolecular content using KOH (expected pH ~ 9 to 11), and subsequent acidification using an HCl solution (pH ~ 2 to 3). For a more detailed overview of the typical extraction protocol, the reader is asked to refer to the information provided in Figure 1 of this source [24]. Owing to the low viscosity (or moduli) of the stock EPS suspension, the sample was repeatedly centrifuged (3880 g, 600 s, 298 K) for a total of 3 runs to increase the concentration of total solids. This was later measured using TGA, alongside the pH and the conductivity. The suspension was subsequently diluted using a $7x10^{-3}$ M HCl - $3x10^{-1}$ M NaCl solution in Milli-Q water. The samples were refrigerated at 277 K until they could be tested further.

5.2.5. ALGINATE - GLUCONIC ACID HYDROGEL SYSTEM

A fresh 50 cm^3 batch of the 3.5% w/w alginate solution was prepared similar to the methodology highlighted above (for 10% w/w sample). This was done to

replenish the 3.5% w/w solution. Subsequently, 0.25 M of NaCl was dissolved within the polymer solution to have ionic strength levels comparable with the H-Alginate system. The solution was then ultrasonicated at 293 K, 50% RH for a period of 300 s to remove any dissolved air bubbles within the sample. The pH within the Na-Alginate solution was regulated using D-(+)-gluconic acid δ-lactone (GDL, CAS number: 90-80-2) from Sigma-Aldrich (product number: G4750, Zwijndrecht, The Netherlands). As GDL readily hydrolyses to gluconic acid upon dissolution [25], it lowered the pH of the Na-Alginate solution over time, and therefore aided the formation of hydrogen bonded crosslinks within the entire sample. A GDL concentration of 13.04% w/w was selected to reach pH values close to 2.6 ± 0.01 (see Supplementary Material Subsection 5.6.3). It is worth noting that when compared to other (hydro) gelator systems [26], a relatively larger concentration of GDL was needed to reach the desired pH value. This is attributed to the buffering capacity of the polymer itself.

All preparatory steps were carried out at 293 K and 50% RH. Approximately 10 cm^3 of the sonicated Na-Alginate solution was poured into an inverted Petri dish cover until the entire surface of the cover was uniformly coated (see Supplementary Material Subsection 5.6.3). Next, the required amount of GDL (~ 1.5 g) was added and stirred gently until all visible particles of GDL were completely dissolved. This was typically achieved within 300 s. Care was taken not to introduce air bubbles within the sample. Following this, the Petri dish (bottom surface) was gently placed on the free surface of the sample. This was done to achieve parallel top and bottom surfaces with minimal skewness. The setup was also covered using a glass beaker with sealed edges in an effort to regulate the moisture level within the sample (see Supplementary Material Subsection 5.6.3). The sample was left undisturbed for 4 hours to reach the desired pH value.

In total three samples were prepared in the same fashion. In the case of the first sample (henceforth called "monolithic"), the beaker was removed after 4 hours, and the free edges of the Petri dish setup were carefully sealed using all-purpose laboratory film. The sample was immediately refrigerated at 277 K. Before rheological testing, the Petri dish was slowly released from the top surface of the sample. A suitable (unskewed) spot was selected, and a 21 mm hole punch was used to obtain a disc shaped gel sample for rheology. Once tested, the "monolithic" sample(s) was again homogenised using the Ultra-Turrax device (see above) operated at 13,800 rpm (~ 1445 rad/s) for a total of 10 minutes (293 K, 50% RH). This yielded a JDHS sample (henceforth called "granular" - see Supplementary Material Subsection 5.6.3) that could be tested further for its rheological properties.

In the case of the second sample (henceforth called "mosaic" sample - see Supplementary Material Subsection 5.6.3), the beaker was removed at the end of 4 hours, and the entire setup was flash frozen (or quenched) by immersing the sample into liquid nitrogen for 600 s. Care was taken not to crack the Petri dish or its cover by exposing them to the liquid nitrogen first for approximately 5 s. It is worth noting that

over the course of the 600 s, the "mosaic" sample, together with the Petri dish cover, became detached from the Petri dish itself. The sample was eventually recovered from the bottom of the liquid nitrogen dewar using a pair of tongs, without damaging the top surface of the sample. Once recovered, the Petri dish setup was again reattached, and the free edges were carefully sealed using all-purpose laboratory film. Once done, the sample was brought into contact with a water bath maintained at 293 K for 30 minutes to allow the ice crystals to thaw within the sample. The quick cooling and heating produced characteristic "mosaic" like cracks within the sample. A disc shaped sample was again recovered using the hole punch for rheological testing.

In the case of the third sample (henceforth called "foam" sample), the beaker was removed at the end of 4 hours, and the Petri dish cover was carefully released from the top surface. Three disc shaped "foam" samples, consistent in their (macroscale) appearance with the "monolithic" sample, were produced using the 21 mm hole punch and they were transferred into a separate, sealed Petri dish. The sealed Petri dish and its contents were frozen at 253 K for 18 hours to aid the formation of relatively large ice crystals within the sample. These ice crystals should not contain any polymer so that the macromolecular part of the system ultimately is confined between the ice crystals. After this, the sealed Petri dish was also brought into contact with the 293 K water bath for 30 minutes to thaw the ice crystals, thereby obtaining a macromolecular foam with water inside the voids. The best foam sample was then tested further for its rheological properties.

5.2.6. RHEOLOGY

Oscillatory strain amplitude sweep measurements were performed to study the transition from the small amplitude oscillatory shear regime to the large amplitude oscillatory shear regime (SAOS to LAOS), or vice versa and therefore, the yielding of the hydrogel systems. All measurements were carried out at 298 K using a TA Instruments Discovery Hybrid Rheometer 3 (DHR-3) with the help of a solvent trap. A 20 mm sandblasted stainless steel flat plate geometry and a 40 mm sandblasted stainless steel bottom plate were used to perform the measurements. All measurements were carried out at a frequency of 1 Hz (~ 6.28 rad/s), between strain amplitude values of $1x10^{-5}$ (m/m) and $1x10^{1}$ (m/m), and at a rate of 10 points per decade (for strain). Although the intended strain amplitude measurements cover six orders of magnitude, the measurement window was clipped if one (or more) of the following phenomena was observed: noise in the sinusoidal curves at lower strain amplitudes, large deviations from the sinusoidal response at higher strain amplitudes, exceedingly low storage modulus values (< $1x10^{-2}$ Pa), and sample expulsion from the geometry gap. The H-Alginate, Ca-Alginate and Alginate - Gluconic Acid systems were tested using ramp up measurements (low to high strain amplitudes). This was due to the risk of sample expulsion at high strain amplitudes (See Figure 5.1). By contrast, the tomato ketchup and EPS samples were tested using ramp down measurements (high to low strain amplitudes).

In the case of the H-Alginate and Ca-Alginate systems, an initial "patty" shaped

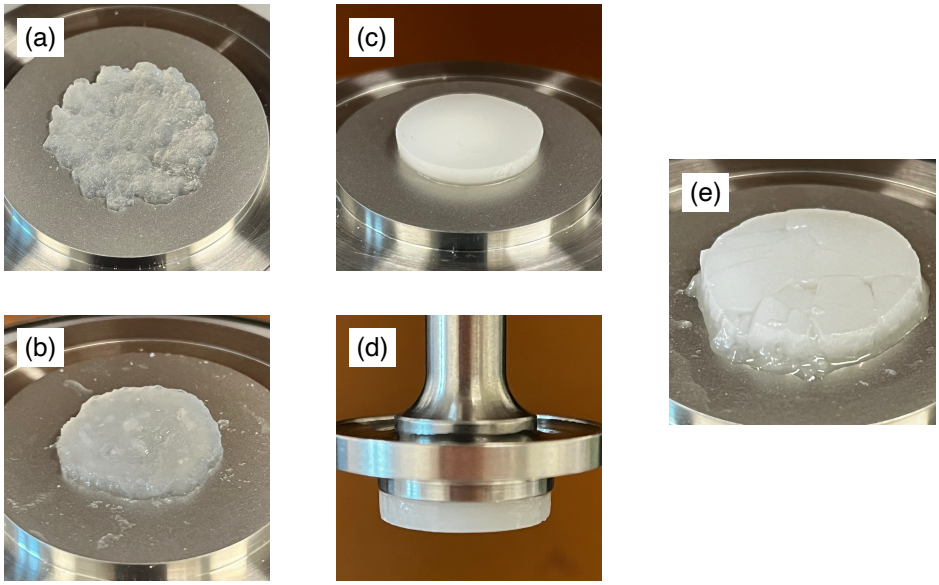

Figure 5.1: Relevant photographs from rheology measurements (a) a "patty shaped" Ca-Alginate sample during sample loading highlighting the potential underfilling due to the lack of a well-defined circular edge, (b) the well-defined circular edge of a Ca-Alginate sample after measurement highlighting that the initial underfilling was addressed, (c) the lack of a clearly discernible water layer to suggest syneresis within the "monolithic" sample, (d) the adhesion between the "foam" sample and the sandblasted geometry highlighting capillary action due to the presence of voids within the sample, and (e) a clearly discernible water layer on the surface of the "mosaic" sample to suggest syneresis within the sample.

sample was loaded onto the surface of the bottom plate (Figure 5.1 a). Next, the geometry was manually lowered until contact was made with the patty shaped sample. Care was taken not to exceed a compressive axial force of 0.1 N during the lowering process. This protocol, in combination with a variable measurement gap between 1500 and 2000 μm, mitigated the potential for syneresis. Subsequently, the geometry shaft was locked by prescribing a rotation velocity of 0 rad/s, and under-filled sections within the measurement gap were filled using additional sample (Figure 5.1 b). Prior to measurement, the samples were rested at zero strain for 100 s to aid complete recovery following the loading process. Post measurement, the gel samples were recollected, mixed with the remaining volume of the respective JDHS system, and reused for measurements. A total of 3 runs were performed for all H-Alginate and Ca-Alginate systems in an effort to obtain representative measurements at each concentration. A constant measurement gap of 1750 μm was used for all tomato ketchup and EPS samples. The required sample volume was loaded onto

the surface of the bottom plate and the geometry was lowered to the measurement gap. Prior to measurement, the tomato ketchup and EPS samples were pre-sheared using a 100 s^{-1} shear rate for 30 s to clear all sample history. Post measurement, these sample were reused for a total of 3 runs, with a 100 s rest time between each run.

A measurement gap of 2800 μm, 3300 μm , 3300 μm, and 1750 μm was used for the "monolithic", "foam", "mosaic", and "granular" samples respectively. Owing to the irrecoverable fracture within the "monolithic", "foam" and "mosaic" samples at high strain amplitudes, these three samples were measured only once. The "granular" sample was measured repeatedly for 3 runs. Once again, a 100 s rest time preceded each measurement for the "granular" sample. Although a slight overfilling was inevitable due to the use of a slightly larger hole punch, this equally ensured that defects created within the outer edges of the sample during the punching process remained outside the geometry gap. Additional features that were observed during measurement have also been presented in Figure 5.1. For instance, the "monoithic" sample presented very minimal syneresis during sample loading (Figure 5.1 c). By contrast, a water layer, with a thickness of a few microns, was present on all free surfaces of the "foam" sample. This has been attributed to the capillary action due to formation of voids within the sample. In combination with the high wettability of the geometry's sandblasted surface, this resulted in adhesion of the sample to the geometry after measurement (Figure 5.1 d). The water layer was also noted within the "mosaic" sample (Figure 5.1 e). However, no adhesion was noted between the "mosaic" sample and the geometry's surface.

5.3. RESULTS

The results from the amplitude sweep measurements are shown in Figures 5.2 - 5.6. Figures 5.2 - 5.5 shows the effect of concentration for the H-Alginate, Ca-Alginate, tomato ketchup and EPS systems respectively; whilst Figure 5.6 shows the effect of morphology for the Alginate - Gluconic Acid system. The loss modulus curves of all systems are presented in the Supplementary Material Subsection 5.6.4. The repeated testing of the same sample, over multiple runs, has the potential to yield time dependent evolution of rheological properties. However, given the variability associated with sample loading times, as well as the results shown in Figures 5.2 - 5.6, the absence of a time-dependent evolution of the rheological properties suggests that rheological characterisation can be performed repeatedly and is representative for the mechanics of the samples at hand.

Figures 5.2 - 5.5 highlight trends that can be observed across multiple JDHS. In most cases, suspensions with the largest concentration show a single linear viscoelastic regime (Figures 5.2 - 5.4). However, upon dilution, multiple yielding events can in fact be observed within the same amplitude sweep curves (Figure 5.2 - 9.5% w/w, Figure 5.3 - 1.8% w/w, Figure 5.4 - 21.9% w/w, Figure 5.5 - all concentrations). In other cases, a further reduction to the concentration results in a power law behaviour for the amplitude sweep curves (Figure 5.2 - 7.6%

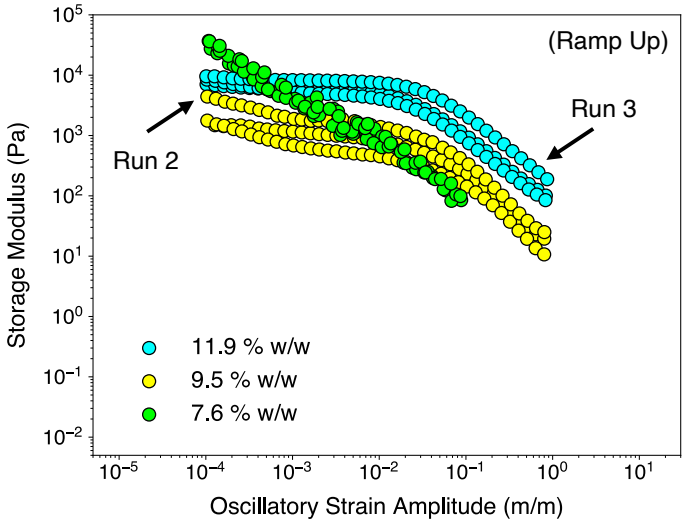

Figure 5.2: Oscillatory strain amplitude sweep curves of the H-Alginate system. Labels are provided to identify experimental runs with distinguishable amplitude sweep curves.

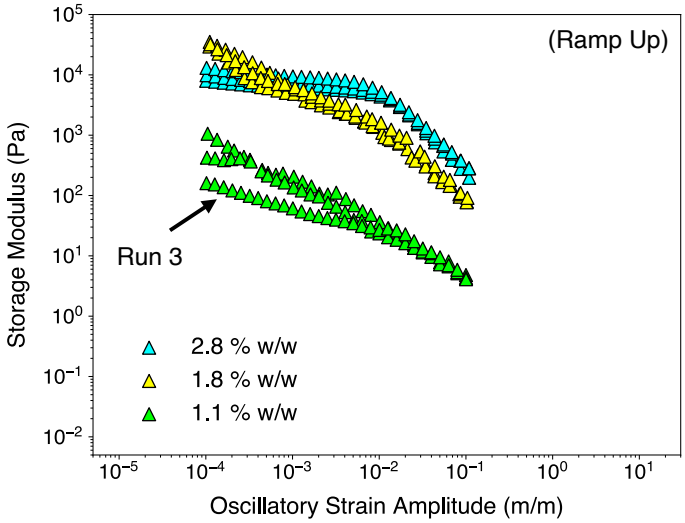

Figure 5.3: Oscillatory strain amplitude sweep curves of the Ca-Alginate system. Labels are provided to identify experimental runs with distinguishable amplitude sweep curves.

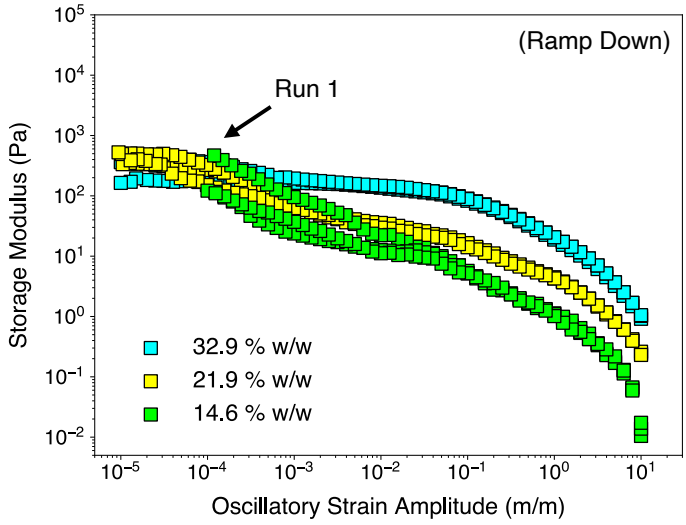

Figure 5.4: Oscillatory strain amplitude sweep curves of the tomato ketchup system. Labels are provided to identify experimental runs with distinguishable amplitude sweep curves.

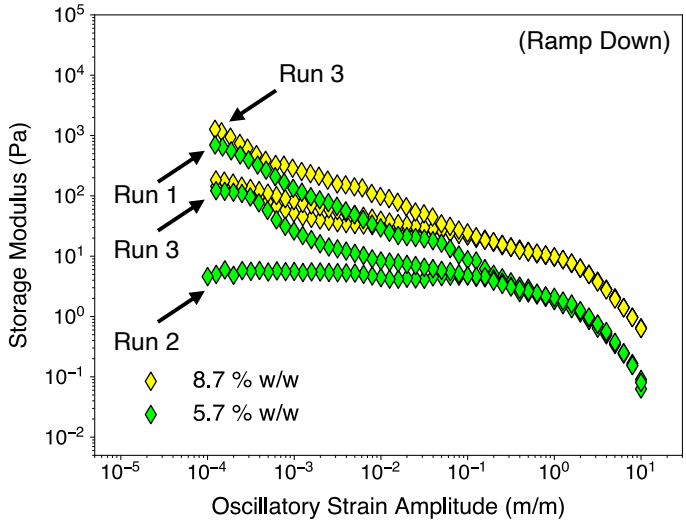

Figure 5.5: Oscillatory strain amplitude sweep curves of EPS. Labels are provided to identify experimental runs with distinguishable amplitude sweep curves.

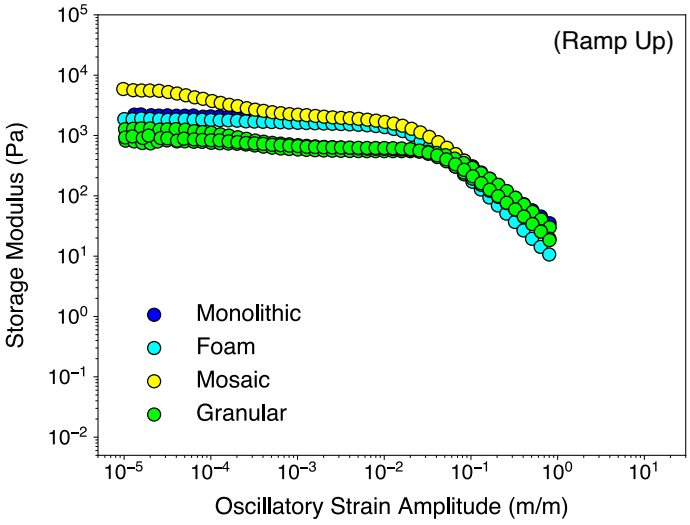

Figure 5.6: Oscillatory strain amplitude sweep curves of the Alginate - Gluconic Acid system.

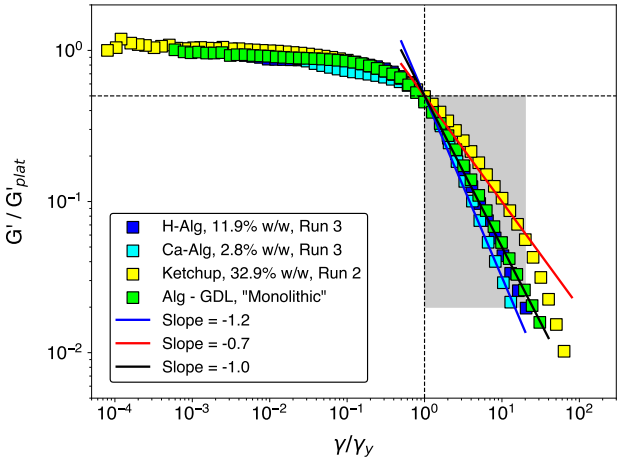

Figure 5.7: Strain amplitudes (γ) and storage moduli (G') rescaled for curves with a single linear viscoelastic regime, using the yielding strain amplitude (γ_y) and estimated pleateau moduli (G'_{plat}) respectively. The shaded region represents the domain where a good agreement is observed between (most of) the experimental data and the approximated slope values.

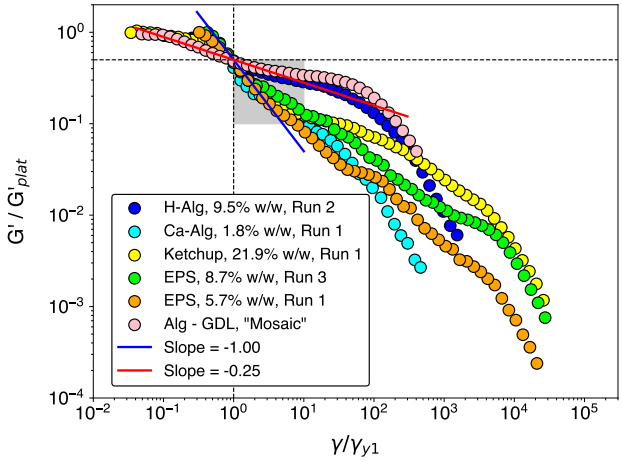

Figure 5.8: Strain amplitudes (γ) and storage moduli (G') rescaled for curves with multiple yielding regimes, using the first yielding strain amplitude (γ_{y1}) and estimated pleateau moduli (G'_{plat}) respectively. The shaded region represents the domain where a good agreement is observed between (most of) the experimental data and the approximated slope values.

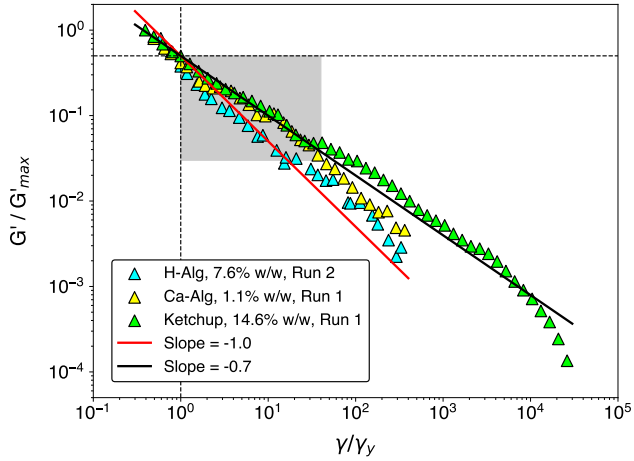

Figure 5.9: Strain amplitudes (γ) and storage moduli (G') rescaled for curves exhibiting a power law behaviour, using the yielding strain amplitude (γ_y) and the maximum observed storage moduli (G'_{max}). The shaded region represents the domain where a good agreement is observed between (most of) the experimental data and the approximated slope values.

w/w, Figure 5.3 - 1.1% w/w, Figure 5.4 - 14.6% w/w). In some cases, the storage modulus of relatively dilute suspensions is greater than (or comparable to) the more concentrated samples at lower strain amplitudes (Figures 5.2 - 5.5). As such, it seems counterintuitive that less densely packed suspensions (although jammed) are capable of having a greater storage modulus than more densely packed suspensions. It is also worth noting that the strain amplitude curves transition to power law like yielding at substantially different mass fraction of the particles. The estimated concentrations for these transitions are as follows: 8.6% w/w for H-Alginate, 1.6% w/w for Ca-Alginate, 12% w/w for tomato ketchup, and possibly around 4% w/w for EPS. It is worth acknowledging that, as these concentrations are estimated using limited sets of experimental runs, they only provide a crude approximation by virtue of having large uncertainties in their values (up to 5% w/w or more in the case of ketchup). Finally, in only two cases, the most dilute suspensions display an overall lower storage modulus (Figure 5.3 - 1.1% w/w, Figure 5.5 - 5.7% w/w, Run 2). It is also worth highlighting that the trends observed here appear to be independent of the methodology adopted (e.g. ramp up vs. ramp down measurements).

Certain trends are clearly discernible as a result of sample morphology in Figure 5.6. In general, the samples that lack a fragmented structure display a single linear viscoelastic regime ("monolithic" and "foam" samples). However, samples with gel fragments display sensitivity to small strains ("mosaic" and "granular" samples), as well as multiple yielding events ("mosaic" sample). As the "monolithic" sample lacks voids within its morphology, it expectedly has an overall larger storage modulus compared to the "foam" and "granular" samples. Finally, the relatively larger storage modulus values of the "mosaic" sample has been attributed to the increase in solid concentration post syneresis (See Supplementary Material Subsection 5.6.3).

In an effort to closely examine the yielding strain amplitudes, as well as the slopes made by the curves after yielding, representative oscillatory measurements have been rescaled and plotted in Figures 5.7 - 5.9, which represent the three cases discussed above - curves with a single linear viscoelastic regime (Figure 5.7), curves with multiple yielding events (Figure 5.8), and curves exhibiting a power law behaviour of storage modulus vs. oscillatory strain amplitude (Figure 5.9). The strain amplitude (γ) of all curves in Figures 5.7 - 5.9 were scaled using either the strain amplitude at which yielding was observed (γ_y), or using the first strain amplitude at which yielding was observed for curves with multiple yielding events (γ_{y1} - see Figure 5.8). These are represented using dashed vertical lines in Figures 5.7 - 5.9. Similarly, the storage modulus values (G') of all curves in Figures 5.7 - 5.9 were scaled using either an estimate for the linear viscoelastic storage modulus value (G'_{plat}), or using the maximum observed storage modulus value in the case of curves with a power law behaviour (G'_{max} - see Figure 5.9). It is worth reporting that for all systems shown in Figures 5.7 - 5.9, the yield point was estimated as being 50% of the G'_{plat} or G'_{max} value, where a clear departure from the linear viscoelastic response was noted for all systems [21]. These values are represented using the dashed horizontal lines in Figures 5.7 - 5.9. Owing to

the fact that measurements were carried out at discrete strain amplitudes, both γ_y and γ_{y1} correspond to the first oscillatory strain amplitude value where G' < 0.5 x G'_{plat} or G' < 0.5 x G'_{max}. These values are tabulated in Table 5.1 for the sake of clarity.

Table 5.1: Estimated yielding strain amplitude of JDHS shown in Figures 5.7 - 5.9.

System	Yielding Strain Amplitude
H-Alg, 11.9% w/w, Run 3	4.21 x 10^{-2}
Ca-Alg, 2.8 % w/w, Run 3	8.37 x 10^{-3}
Ketchup, 32.9% w/w, Run 2	1.25 x 10^{-1}
Alg-GDL, "Monolithic"	2.61 x 10^{-2}
H-Alg, 9.5% w/w, Run 2	5.21 x 10^{-4}
Ca-Alg, 1.8% w/w, Run 1	2.22 x 10^{-4}
Ketchup, 21.9% w/w, Run 1	3.06 x 10^{-4}
EPS, 8.7% w/w, Run 3	2.89 x 10^{-4}
EPS, 5.7% w/w, Run 1	3.78 x 10^{-4}
Alg-GDL, "Mosaic"	2.60 x 10^{-4}
H-Alg, 7.6% w/w, Run 2	2.33 x 10^{-4}
Ca-Alg, 1.1% w/w, Run 1	2.75 x 10^{-4}
Ketchup, 14.6% w/w, Run 1	3.03 x 10^{-4}

The shaded regions of Figures 5.7 - 5.9 correspond to domains where a good fit was obtained between (most of) the experimental data and the approximated slope values. As a general observation, this region extends to at least one decade above both γ_y and γ_{y1} (γ/γ_y , $\gamma/\gamma_{y1} \geq$ 1 x 10^1), and at least half a decade below both 0.5 x G'_{plat} and 0.5 x G'_{max} (G'/G'_{plat} , $G'/G'_{max} \leq$ 1 x 10^{-1}). This has been noted as the limits of the respective JDHS to retain their dynamic microstructure after yielding. From Table 5.1, and Figures 5.2 - 5.6, 5.8, and 5.9, it is clear that JDHS are capable of yielding even at oscillatory strain amplitudes in the order of 10^{-4}. Therefore, deviations from the approximated slope value outside the shaded regions in these two cases, can be explained by the fact that the underlying microstructure is highly sensitive to the oscillatory strain amplitudes that are ~ 10^{-4}. Despite this, there appears to be an overall consistency in the slope value in Figure 5.9, with the slopes all curves falling between (-0.7) and (-1). However, there is a clear lack of consistency in the slopes of Figure 5.8. This can be explained by the fact that above γ_{y1}, these systems are rapidly (or dynamically) transitioning from one microstructure to another between individual yielding events. Therefore, the slopes span a broad range of values from (-0.25) to (-1). The slope values noted in terminal regions of Figure 5.8 were also approximated, and are reported in Supplementary Material Subsection 5.6.5. Except in the case of the "mosaic" sample, the terminal slopes are much greater than (-1) and fall within the range of (-1.34) to (-1.48). Finally, the "classical" viscoelastic response curves of Figure 5.7 clearly highlight the fact that the slopes of all curves are within the somewhat narrow range of (-0.7) to (-1.2), with there being a reasonably good agreement with the slope value of (-1) for half of the

curves.

5.4. DISCUSSION

5.4.1. COMPARISONS TO EXISTING LITERATURE

Based on the traditional definition provided by Shih et al. [19], colloidal gels exhibit a single linear strain limit and a well-defined storage modulus plateau. However, it is clear from the results presented in Figures 5.2 - 5.6, that neither a single linear strain limit, nor a single storage modulus plateau exist within all JDHS. Depending on the concentration, some systems also exhibit multiple yield stresses spanning a wide range of strain values. Equally, Shih et al. hypothesise that both the linear strain limit, as well as the plateau value of the storage modulus, scale as power law functions with respect to the particle volume fraction. Changes to the overall shape of the amplitude sweep curves at different concentrations (Figures 5.2 to 5.5) confirm changes to the particle volume fraction for the JDHS described here (even with deformable jamming). Despite this, the studied JDHS systems with different particle volume fractions display comparable storage modulus values at different concentrations, and more importantly, do not always display a clear storage modulus plateau over a wide range of strain values, as would be suggested by the scaling arguments.

Shih et al. also suggest that the origin of the solid like gel structure, and therefore the stiffness, is governed by the rigidity of interparticle links between neighbouring flocs over multiple length scales. However, their results were limited to a specific subset of colloidal gels. In the systems presented within this study, attractive interactions between neighbouring particles are not expected in all cases. As shown earlier, neighbouring particles within the Ca-Alginate and the tomato ketchup systems do not necessarily possess "sticky" interactions. Thus, the stiffness of a particular JDHS need not be the result of dynamic or reversible interparticle links.

More recently, Shewan et al. [8] clearly highlight the importance of interparticle frictional forces in governing the jamming of hydrogel suspensions. Based on the explanation provided in this source, the surface roughness of the particles considerably contributes towards the constrained jamming of a colloidal / non-colloidal hydrogel suspension. In addition, the Ca-Alginate system shows that in the deducible absence of surface roughness features (see Supporting Infromation Section 5.6.1), there is clearly still a coalescence of suitable particle morphologies, thereby producing solid like structures that contribute towards the overall stiffness of the suspension. Certainly, based on the results shown in Figures 5.2 - 5.6 , the moduli of all systems are somewhat comparable, and fall within 3 orders of magnitude under low strains (10^2 to 10^5 Pa); without any clear correlation with the nature of the underlying system. Although, it can be seen that the volume fractions (or mass concentrations) at which the various types of rheological behaviour are revealed can vary substantially between the systems. For instance, Ca-Alginate has a clear plateau

and slope at 2.8% w/w, whereas tomato ketchup only reveals such features at 32.9% w/w.

Using the typical definition provided for polymer solutions [27], and a broader definition provided for a range of relevant rheological systems [21], shear thinning may be described as a loss of flow resistance due to the compliant rearrangement of a material in the direction of the shearing force. For polymer solutions particularly, the macromolecular chains exhibit a "rolling over and stretching" effect, due to the combined rotational and translational degrees of freedom [27]. Similarly, Shewan et al. suggest that oscillatory strains are sufficient to mobilise the interlocking rolling constraints of a hydrogel suspension [8]. Thus, in the case of JDHS studied here, yielding is a result of the particles' ability to rearrange themselves, by rolling over one another, and deforming at 45° with respect to the direction of the applied oscillatory load.

In an effort to assess the precedence for sensitivities to oscillatory strain amplitudes in the order of 10^{-4}, comparisons are made with jammed bisamide (BA) organogel suspensions [28]. Upon closely examining the results presented for the 5BA gel system (Figure 9a of this publication), it is clear that the storage modulus drops from its original value of 3 x 10^{6} Pa at a strain amplitude of 1 x 10^{-5}, and displays signs of yielding at a strain amplitude of 2 x 10^{-4}, where the storage modulus has dropped to a value of 1.5 x 10^{6} Pa. However, as no loss modulus curves are provided in this source, it is unclear if the system has completely deviated from linearity at this strain amplitude. Based on a more conservative approach, it is clear that upon reaching a strain amplitude of 7 x 10^{-4}, the storage modulus curve approaches a power law type behaviour and has definitely deviated from linearity by this point. Therefore, the BA system too displays signs of yielding at strain amplitudes in the order of 10^{-4}, and is successful in establishing that jammed deformable gel suspensions in general, display heightened sensitivities to small oscillatory strain amplitudes. Further, similar to the JDHS described here, the (optimal) storage modulus of the BA suspensions appear to be inversely proportional to width of the linear viscoelastic limit (storage modulus plateau); although a clear plateau for the storage modulus is observable in all cases for the BA system.

5.4.2. HYPOTHESIS FOR THE YIELDING BEHAVIOUR

Based on the trends observed in Figures 5.2 - 5.9, as well as Table 5.1, it appears that the ability of the jammed systems to rearrange themselves, strongly influences both; the sensitivity of JDHS to very small oscillatory strain amplitudes (~ 10^{-4}), as well as their yielding behaviour.

At a sufficiently high mass concentration (depending on the system under consideration), the rearrangement of neighbouring particles is constrained due to either, "sticky" / friction dominated soft interparticle interactions, or steric jamming effects (such as might be the case for ketchup). Therefore, they tend to behave like a

solid viscoelastic structure with a single yielding strain. However, a slight reduction to the mass concentration is successful in producing free space between particles, thereby providing the particles the opportunity to suitably rearrange themselves upon the application of a shearing strain. At these intermediate concentrations, the changing microstructure potentially allows the system to form a new, more favourable network, which exhibits a second (or multiple) storage modulus plateau(s). Thus, the JDHS are no longer "highly jammed" and are expected to behave as a "labile" system capable of displaying multiple yield stresses. Table 5.1 highlights the fact that this rearrangement already begins at strain amplitudes ~ 10^{-4}. In addition, Figures 5.6 and 5.8 particularly suggest that suitable rearrangement, and the accompanying formation of new constraints can occur across a wide range of length scales, as multiple yielding was also observed within the "mosaic" sample.

Upon reaching a critically low concentration, the presence of additional free volume permits the gel particles to freely arrange themselves into a fractal like network. As found from the experimental results, this network seems to be able to produce a structure which is stiffer than the "highly jammed" network of gel particles at higher mass concentrations. Given the locally heterogeneous structure of the system, consisting of more rigid particles with interfaces of relatively higher compliance, it is unavoidable to conclude that the inter particle regions will be exposed to much higher strain values than the externally applied strain amplitude (strain magnification at the interfaces). If this local strain exceeds a certain limit, the network connectivity will fail at those locations, thus reducing the stiffness of the network. This will proceed further with increasing externally applied (macro) strain amplitude, which explains the extreme sensitivity of the system to very small strains. This cascade of network disruptions with increasing strain amplitudes would plausibly explain the observed power law dependence of the network elasticity.

The lack in regularity of the underlying microstructure makes it difficult to draw meaningful interpretations about the effective aspect ratio and moduli of JDHS in this study. Therefore, considerable further research will be required to confirm the (re)arrangement and the nature and diversity of soft interactions between irregularly shaped gel particles. An examination of the coalescence of these particles below the critical concentration, and their ability to produce optimally stiff structures (albeit sensitive) at close to zero strain, is also called for. Additionally, exploring the concept of a fractal like network to explain power indices that are observed in Figures 5.7 - 5.9, would seem to be a reasonable working hypothesis. The development of a model to describe the fractional power indices in this way by the authors, however, has not been successful. Thus, further research will be required to obtain a fairly accurate estimation of the storage modulus using the fractal network approach. What follows below however, is an idealised interpretation of the curves exhibiting a slope value of (-1) in Figures 5.7 - 5.9.

In cases where a plateau is observed for the storage modulus, a linear dependence between the oscillatory stress and the oscillatory strain is successful in capturing the

increase in stress levels with the strain amplitude:

$$\sigma = G'\gamma \tag{5.1}$$

Here, σ is the oscillatory stress amplitude, G' is the storage modulus, and γ is the oscillatory strain amplitude. This linear dependence is represented using slope 1 curves in Figure 5.10, and using storage moduli plateaus in Figure 5.11. Once the critical yield stress is achieved however, the JDHS is susceptible to a rate independent plastic yielding at the constant yield stress value of σ_y. This plastic yielding regime is represented using the plateau regions in Figure 5.10. Owing to the continuous transitions from the linear elastic regime to the plastic yielding regime, Equation 5.1 may be rewritten in terms of σ_y to obtain a relationship for the strain dependent storage modulus (or indeed the secant modulus) in the yielding regime:

$$G'(\gamma) = \sigma_y \gamma^{-1} \tag{5.2}$$

This inverse linear relationship is used to construct the yielding regimes of the strain amplitude storage moduli curves in Figure 5.11. As such, the somewhat asymptotic stress vs. strain curves in Figure 5.10 are not entirely idealised and can be observed within solid materials such as lead or lead-tin alloy based solders [29, 30]. Additionally, it is worth noting that that the transition to the (-1) slope yielding regime might involve a multitude of plateau values (larger than the 2 shown in Figures 5.11). Likewise, although all 4 idealised curves shown were not obtained for any individual JDHS system studied above, they may be expected upon increasing the number of concentration steps for all systems.

5.4.3. IMPACT FOR ENGINEERING APPLICATIONS

As such, the properties of the JDHS studied here find relevance within emergent fields of materials science. The success in popularising self-healing materials can be attributed to the development of a set of healing mechanisms that are implementable within a wide range of mechanical, thermal and chemical systems [31, 32]. In turn, there have been more attempts at defining relevant terminology surrounding the healing approaches from an pragmatic perspective [33, 34]. In particular, Garcia [33] is successful in expressing that in extreme cases, a self-healing material that completely restores the initial performance may be termed as "ideal". Similarly, Azevedo et al. [34] are successful in describing that self-healing events may be termed "fast" (in the context of biological systems), if they occur within the span of a few minutes, although a precise, quantitative definition for the term "few" is not provided.

For the systems described here, there has been no attempt to traverse the proposed self-healing routes for mechanical systems [31]. Despite this, JDHS appear to be both "ideal" and "fast" self-healing materials. As reported earlier within the Materials and Methods section (Section 5.2), the same samples were repeatedly tested over multiple runs during rheological measurements. At least in cases where ramp up measurements were performed, the homogeneous macrostructure of the jammed

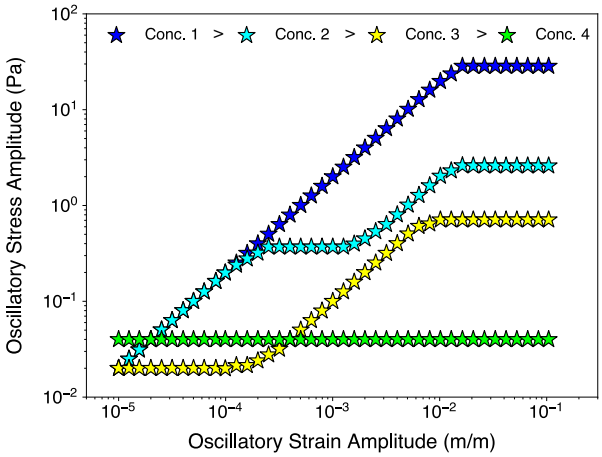

Figure 5.10: An idealised set of oscillatory stress amplitude vs. oscillatory strain amplitude curves (see Equation 5.1). Conc. 1 - Single slope, Conc. 2 - Dual slopes, Conc. 3 - Single intermediate slope, and Conc. 4 - Power law yielding. Note that the slopes of all curves are parallel to each other as a result of using a slope value of 1.

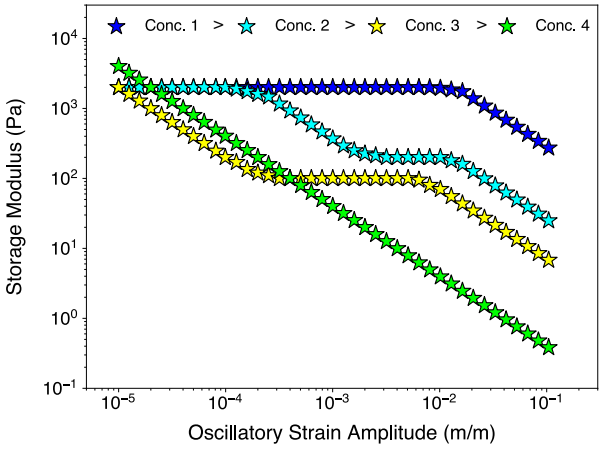

Figure 5.11: An idealised set of the resulting oscillatory strain amplitude sweep curves from Figure 5.10 (see Equation 5.2). Conc. 1 - Single plateau, Conc. 2 - Dual plateau, Conc. 3 - Single intermediate plateau, and Conc. 4 - Power law yielding. Note that the terminal slopes of all curves are parallel to each other as a result of using a slope value of -1.

gel system was fractured during testing, the gel fragments were recollected, and were remixed to form a homogeneous sample once again. Despite this, the samples recover their initial storage modulus in a large number of cases (see Figures 5.2, 5.3 and 5.6). These results are consistent with the definition of "ideal" self-healing materials. Also, as most of these recovery events occur within the span of 100 s or less, they are equally consistent with the definition provided for "fast" self-healing materials.

From a practical perspective, these "ideal" and "fast" mechanisms serve to reinforce the relevance of JDHS for biomedical applications such as bioprinting and tissue engineering, where the quick recovery of the original properties is desirable. Equally, they may also be appealing for emergent applications within the field of soft robotics [35], where the ease of deformability, combined with the quick recovery of the actuating system is highly desirable. A strategy to realise the implementation of these systems, however, is a subject of ongoing research [23]. Additionally, JDHS remain relevant even within the food industry, where an accurate assessment of the yield stress [21], and the associated sensory texture due to the rheology of the JDHS governs the successful adoption of the final product [9]. The ability to quickly recover the yield stress is appealing, to preserve the sensory texture despite continuous deformation within the mouth while chewing. Finally, similarities that may be highlighted in the yielding phenomena of existing JDHS, and emergent hydrogels such as *aquafaba*, further facilitates the development of vegan and vegetarian food products [10], thereby ensuring successful replacements of one ingredient for the other.

5.5. CONCLUSIONS

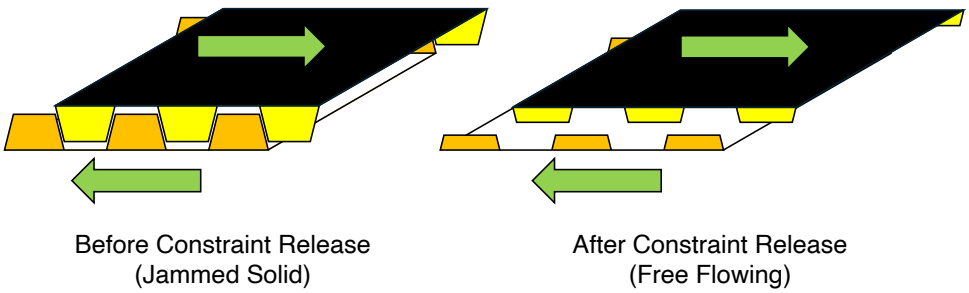

Figure 5.12: Idealised "washboard" surface features that may be created on the surface of spherical particles in JDHS. Through birefringence analysis, the deformation of these features may be observed using rheo-optical techniques [36], and comparisons can be to existing theoretical approximations [8].

An effort was made to highlight the specific influence of particle morphology, and

mass concentration, on the yielding of jammed deformable hydrogel suspensions (JDHS). Although it is difficult to carry out rheological measurements on such materials using a single experimental methodology, it is still possible to classify the trends observed within a wide variety of JDHS.

This study, however, limits itself to this classification, with the sole purpose of highlighting trends that were previously not observed within systems such as colloidal gels. In view of the pragmatic relevance of JDHS, an extensive study that probes the mechanisms of deformation between neighbouring particles is encouraged. As such, it is possible to theoretically predict interfacial frictional forces for jammed, smooth, monodisperse spherical particles. Thus, spherical particles, with suitable surface morphologies such as dendrites or "washboard" features (see Figure 5.12), can be created on the surface of these particles to promote interlocking and jamming. The distribution of the stress, as well as the interfacial deformation between particles may then be suitably studied using rheo-optical techniques that were not directly available during the time of this study. These techniques are targeted at capturing the birefringence of gel particles, and providing a suitable assessment of the stresses using the stress-optic law. Through such idealised systems, it is possible to highlight the impact of specific interfacial features on the rheology of JDHS.

Finally, despite repeated testing, it is clear that JDHS are capable of recovering their original storage modulus. As discussed above, these "ideal" and "fast" self-healing events remain relevant for applications within the biomedical, soft robotics and the food industry.

5.6. DATA AND SUPPLEMENTARY MATERIAL

The data from the oscillatory strain amplitude sweep measurements, as well as the unprocessed optical microscopy images, is publicly accessible using the following link: https://doi.org/10.4121/bf496cc6-c205-4451-9dcb-f921eff8cb2d.

5.6.1. OPTICAL MICROSCOPY IMAGES

The size and morphologies of the H-Alginate, Ca-Alginate, tomato ketchup, EPS, and "granular" Alginate - Gluconic Acid systems were evaluated using brightfield optical microscopy. All observations were carried out using a Nikon Eclipse E600 POL optical microscope, equipped with a Nikon DS-Ri1 camera. Observations were made using a Nikon 5x / 0.15 NA - LU Plan, a Nikon 10x / 0.30 NA - LU Plan, and a Nikon 20x / 0.35 NA - L Plan objective lenses. All samples were observed in their hydrated state, by diluting them down to a concentration of 0.10 - 0.15% w/w, with the exception of the tomato ketchup system, which was diluted down to a concentration of 5.12% w/w. A plastic cover slip with a refractive index of 1.54 and a thickness of 0.18 mm was also used to cover the samples.

Relevant images of the sample were taken with the help of the camera and using the Nikon Imaging Software (NIS) - Elements AR (version 3.0). These are shown in Figures 5.13 - 5.18. Auto white balancing, along with suitable adjustments to the exposure and contrast, was carried out before capturing the relevant features within the sample. Images of a 10 μm and a 100 μm scale bar were also taken (for calibration purposes) at different magnifications in the same fashion. The images were further post-processed for their colour balance, brightness and contrast levels using the ImageJ software (version 1.54g). Finally, a calibrated scale bar was added using ImageJ, and the images were exported in the TIFF format to preserve their resolution.

5.6.2. SAMPLE PREPARATION: CA-ALGINATE

Figure 5.19 shows the preparatory steps for the Ca-Alginate system.

5.6.3. SAMPLE PREPARATION: ALGINATE - GLUCONIC ACID SYSTEM

Figure 5.20 shows the preparatory steps for the Gluconic-Acid system.

5.6.4. LOSS MODULUS CURVES

Figures 5.21 - 5.25 show the loss modulus curves for all systems shown in Figures 5.2 to 5.6 respectively.

5.6.5. TERMINAL SLOPE VALUES

The terminal slope values of the curves shown in Figure 5.8 are reported in Table 5.2 .

Table 5.2: Terminal slope values of the curves shown in Figure 5.8

System	Terminal Slope Value
H-Alg, 9.5% w/w, Run 2	-1.41
Ca-Alg, 1.8% w/w, Run 1	-1.34
Ketchup, 21.9% w/w, Run 1	-1.46
EPS, 8.7% w/w, Run 3	-1.48
EPS, 5.7% w/w, Run 1	-1.41
Alg-GDL, "Mosaic"	- 1.02

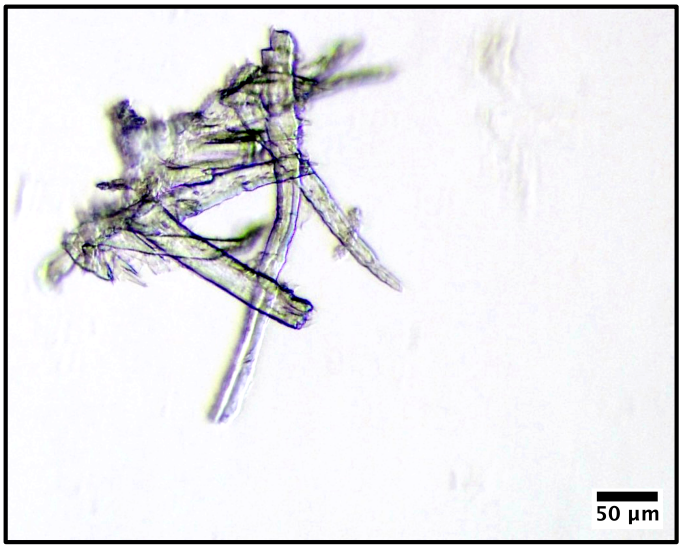

Figure 5.13: Optical microscopy image showing the presence of fibrillated gel particles within the H-Alginate system following the homogenisation process (20x magnification, 0.35 field aperture).

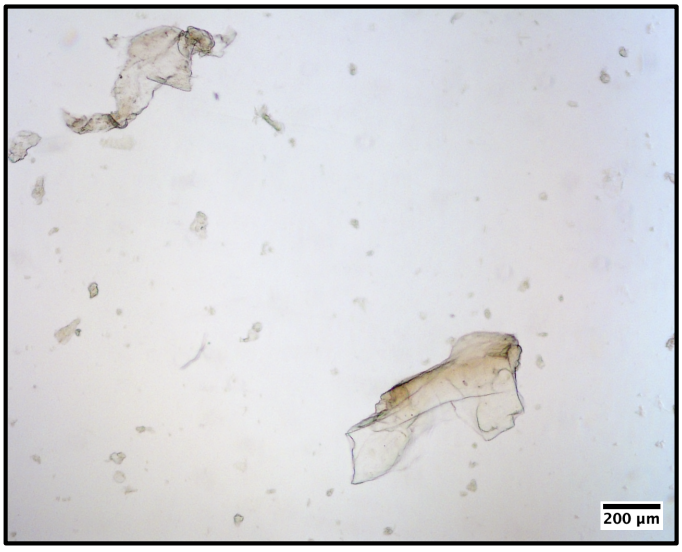

Figure 5.14: Optical microscopy image showing the presence flake like particles within the H-Alginate system (5x magnification, 0.15 field aperture).

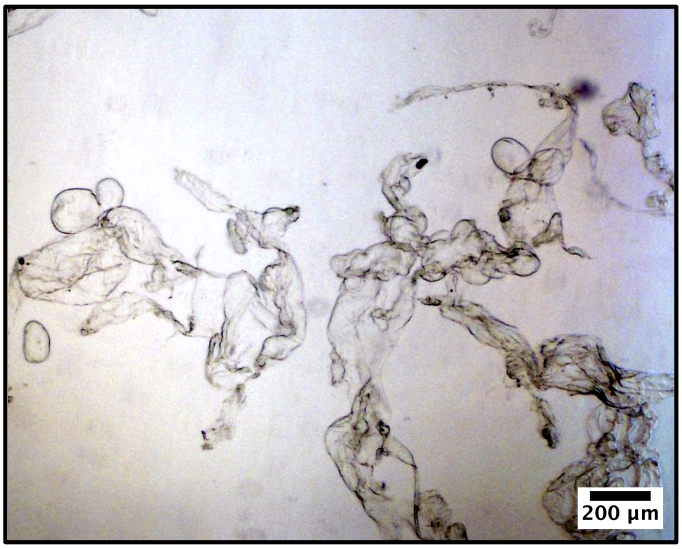

Figure 5.15: Optical microscopy image showing the coalescence of spheroidal particles with elongated "tail" sections following the aerosolization of the Ca-Alginate system (5x magnification, 0.15 field aperture).

Figure 5.16: Optical microscopy image showing the presence of tomato skin fragments (red lattice like structure) within the ketchup system, as well as other fibrillated and floccular structures from within tomato pulp (5x magnification, 0.07 field aperture).

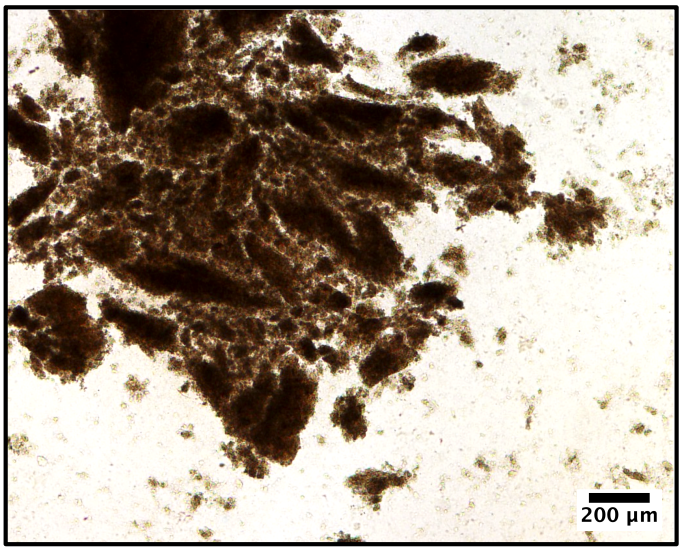

Figure 5.17: Optical microscopy image showing the coalescence of floccular gel like particles with "fuzzy" edges within EPS (5x magnification, 0.15 field aperture).

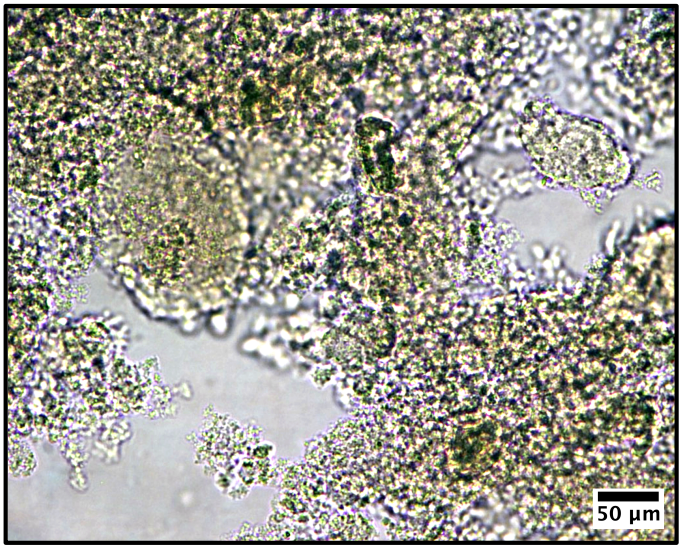

Figure 5.18: Optical microscopy image showing the coalescence of gel particles with multiple particle sizes with the "granular" Alginate - Gluconic acid system (20x magnification, ~ 0.00 field aperture).

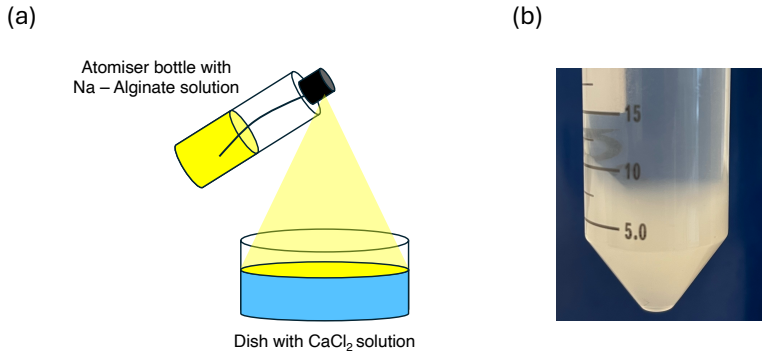

Figure 5.19: (a) A schematic representation of the atomisation process to ensure spheroidal hydrogel particles, and (b) the centrifugation of the suspended hydrogel particles in an effort to jam the suspension and decant the supernatant.

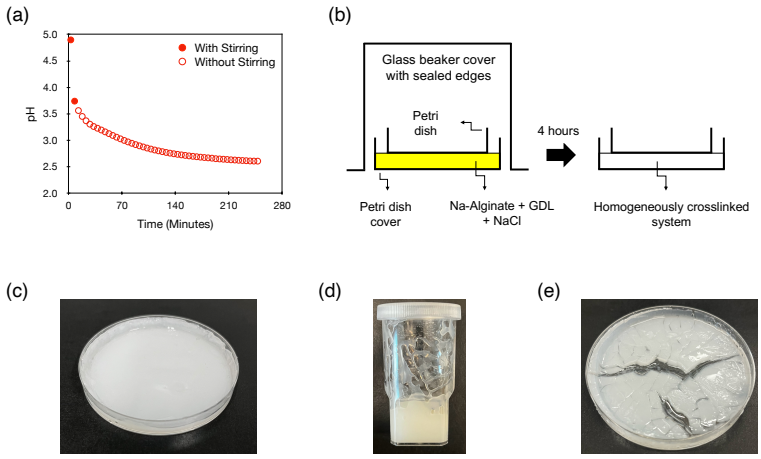

Figure 5.20: (a) The pH of the hydrogel system as a function of time, (b) the Petri dish setup used to produce samples for rheological testing, (c) the "monolithic" hydrogel sample with no voids (d) the "granular" jammed deformable hydrogel suspension (JDHS), and (e) the "mosaic" hydrogel sample produce by flash freezing and thawing.

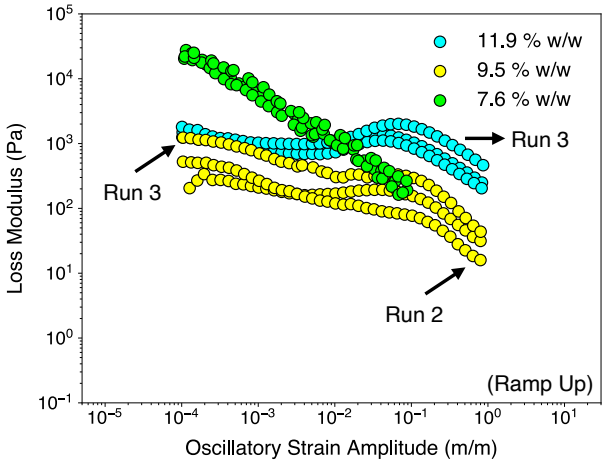

Figure 5.21: Loss modulus curves of the H-Alginate system. Labels are provided to identify experimental runs with distinguishable amplitude sweep curves.

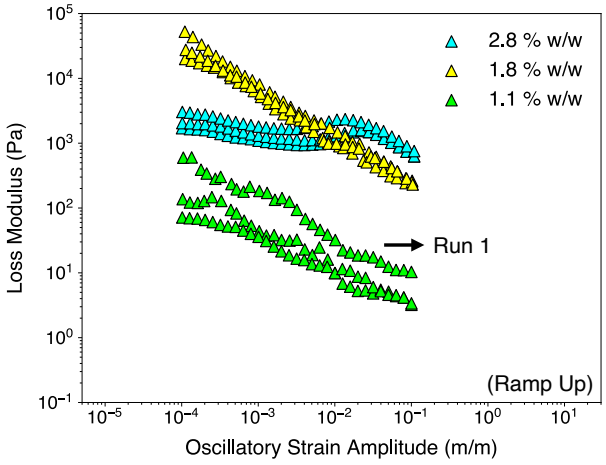

Figure 5.22: Loss modulus curves of the Ca-Alginate system. Labels are provided to identify experimental runs with distinguishable amplitude sweep curves.

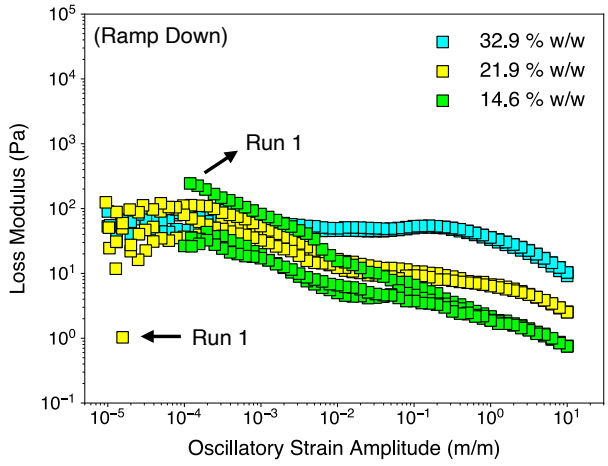

Figure 5.23: Loss modulus curves of the tomato ketchup system. Labels are provided to identify experimental runs with distinguishable amplitude sweep curves.

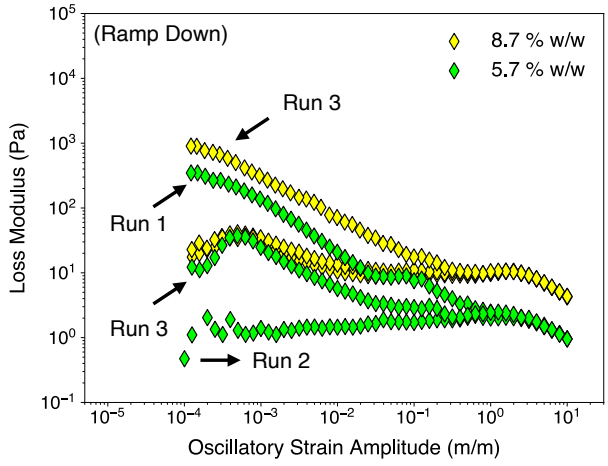

Figure 5.24: Loss modulus curves of EPS. Labels are provided to identify experimental runs with distinguishable amplitude sweep curves.

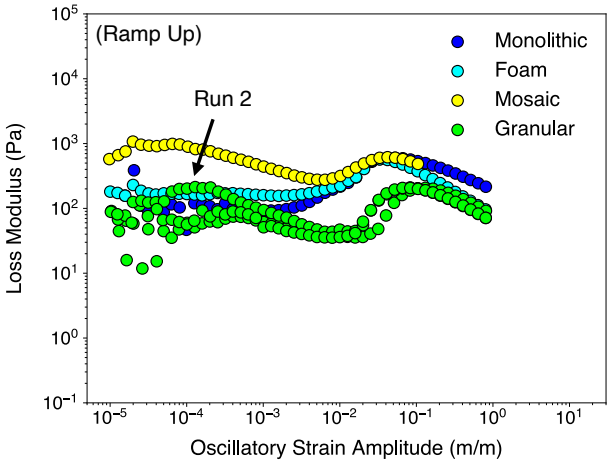

Figure 5.25: Loss modulus curves of the Alginate - Gluconic acid system. Labels are provided to identify experimental runs with distinguishable amplitude sweep curves.

REFERENCES

[1] A. Daly, L. Riley, T. Segura, and J. Burdick. "Hydrogel microparticles for biomedical applications". In: *Nature Reviews Materials* 5 (2020), pp. 20–43. DOI: https://doi.org/10.1038/s41578-019-0148-6.

[2] C. Highley, K. Song, A. Daly, and J. Burdick. "Jammed microgel inks for 3D printing applications". In: *Advanced Science* 6 (2019), p. 1801076. DOI: https://doi.org/10.1002/advs.201801076.

[3] A. Ding, O. Jeon, D. Cleveland, K. Gasvoda, D. Wells, S. Lee, and E. Alsberg. "Jammed micro-flake hydrogel for four-dimensional living cell bioprintings". In: *Advanced Materials* 34 (2022), p. 2109394. DOI: https://doi.org/10.1002/adma.202109394.

[4] L. Riley, L. Schirmer, and T. Segura. "Granular hydrogels: emergent properties of jammed hydrogel microparticles and their applications in tissue repair and regeneration". In: *Current Opinion in Biotechnology* 60 (2019), pp. 1–8. DOI: https://doi.org/10.1016/j.copbio.2018.11.001.

[5] R. Geyer, J. Jambeck, and K. Law. "Production, use, and fate of all plastics ever made". In: *Science Advances* 3 (2017), e1700782. DOI: https://doi.org/10.1126/sciadv.1700782.

[6] V. Muir and J. Burdick. "Chemically modified biopolymers for the formation of biomedical hydrogels". In: *Chemical Reviews* 121 (2020), pp. 10908–10949. DOI: https://doi.org/10.1021/acs.chemrev.0c00923.

[7] S. Felz, S. Al-Zuhairy, O. Aarstad, M. van Loosdrecht, and Y. Lin. "Extraction of structural extracellular polymeric substances from aerobic granular sludge". In: *Journal of Visualized Experiments* 115 (2016), e54534.

[8] H. Shewan, G. Yakubov, M. Bonilla, and J. Stokes. "Viscoelasticity of non-colloidal hydrogel particle suspensions at the liquid–solid transition". In: *Soft Matter* 17 (2021), pp. 5073–5083. DOI: https://doi.org/10.1039/D0SM01624A.

[9] Q. Chen, D. Schott, and J. Jovanova. "Determination of ketchup sensory texture acceptability and examination of determining factors as a basis for product optimization". In: *International Journal of Food Properties* 18 (2015), pp. 660–669. DOI: https://doi.org/10.1080/10942912.2013.853186.

[10] Y. He, V. Meda, M. Reaney, and R. Mustafa. "Aquafaba, a new plant-based rheological additive for food applications". In: *Trends in Food Science & Technology* 111 (2021), pp. 27–42. DOI: https://doi.org/10.1016/j.tifs.2021.02.035.

[11] K. Landman and L. White. "Solid/liquid separation of flocculated suspensions". In: *Advances in Colloid and Interface Science* 51 (1994), pp. 175–246. DOI: https://doi.org/10.1016/0001-8686(94)80036-7.

[12] M. Ungarish. *Hydrodynamics of suspensions: fundamentals of centrifugal and gravity separation*. Berlin, Germany: Springer Science+Business Media, 2013.

[13] S. Felz, P. Vermeulen, M. van Loosdrecht, and Y. Lin. "Chemical characterization methods for the analysis of structural extracellular polymeric substances (EPS)". In: *Water Research* 157 (2019), pp. 201–208. DOI: https://doi.org/10.1016/j.watres.2019.03.068.

[14] S. Felz, T. Neu, M. van Loosdrecht, and Y. Lin. "Aerobic granular sludge contains Hyaluronic acid-like and sulfated glycosaminoglycans-like polymers." In: *Water Research* 169 (2020), p. 115291. DOI: https://doi.org/10.1016/j.watres.2019.115291.

[15] N. Bahgat, P. Wilfert, S. Eustace, L. Korving, and M. van Loosdrecht. "Phosphorous speciation in EPS extracted from Aerobic Granular Sludge". In: *Water Research* 262 (2024), p. 122077. DOI: https://doi.org/10.1016/j.watres.2024.122077.

[16] T. Páez-Watson, S. Tomás-Martínez, R. de Wit, S. Keisham, H. Tateno, M. van Loosdrecht, and Y. Lin. "Sweet Secrets: Exploring Novel Glycans and Glycoconjugates in the Extracellular Polymeric Substances of "Candidatus Accumulibacter"". In: *ACS ES&T Water* 4 (2024), pp. 3391–3399. DOI: https://doi.org/10.1021/acsestwater.4c00247.

[17] S. Felz, H. Kleikamp, J. Zlopasa, M. van Loosdrecht, and Y. Lin. "Impact of metal ions on structural EPS hydrogels from aerobic granular sludge". In: *Biofilm* 2 (2020), p. 100011. DOI: https://doi.org/10.1016/j.bioflm.2019.100011.

[18] S. Espíndola. "Biopolymer nanocomposites: lessons from structure-property relationships". Doctoral Dissertation. Delft University of Technology, 2023. DOI: https://doi.org/10.4233/uuid:7d3d4287-271d-4bbb-9b73-39674a0af60f.

[19] W.-H. Shih, W. Shih, S.-I. Kim, J. Liu, and I. Aksay. "Scaling behavior of the elastic properties of colloidal gels". In: *Physical Review A* 42 (1990), p. 4772. DOI: https://doi.org/10.1103/PhysRevA.42.4772.

[20] C. Rueb and C. Zukoski. "Viscoelastic properties of colloidal gels". In: *Journal of Rheology* 41 (1997), pp. 197–218. DOI: https://doi.org/10.1122/1.550812.

[21] A. Malkin, V. Kulichikhin, and S. Ilyin. "A modern look on yield stress fluids". In: *Rheologica Acta* 56 (2017), pp. 177–188. DOI: https://doi.org/10.1007/s00397-016-0963-2.

[22] A. Fall, N. Huang, F. Bertrand, G. Ovarlez, and D. Bonn. "Shear thickening of cornstarch suspensions as a reentrant jamming transition". In: *Physical Review Letters* 100 (2008), p. 018301. DOI: https://doi.org/10.1103/PhysRevLett.100.018301.

[23] Q. Chen, D. Schott, and J. Jovanova. "Model-Based Design of Variable Stiffness Soft Gripper Actuated by Smart Hydrogels". In: *Soft Robotics* 11 (2024), pp. 924–934. DOI: https://doi.org/10.1089/soro.2023.0185.

[24] N. Bahgat, P. Wilfert, L. Korving, and M. van Loosdrecht. "Integrated resource recovery from aerobic granular sludge plants". In: *Water Research* 234 (2023), p. 119819. DOI: https://doi.org/10.1016/j.watres.2023.119819.

[25] D. Adams, M. Butler, W. Frith, M. Kirkland, L. Mullen, and P. Sanderson. “A new method for maintaining homogeneity during liquid–hydrogel transitions using low molecular weight hydrogelators”. In: *Soft Matter* 5 (2009), pp. 1856–1862. DOI: https://doi.org/10.1039/B901556F.

[26] V. Lakshminarayanan, C. Chockalingam, E. Mendes, and J. van Esch. “Gelation Kinetics-Structure Analysis of pH-triggered Low Molecular Weight Hydrogelators”. In: *ChemPhysChem* 22 (2021), pp. 2256–2261. DOI: https://doi.org/10.1002/cphc.202100276.

[27] T. Osswald and N. Rudolph. *Polymer Rheology: Fundamentals and Applications*. Munich, Germany: Carl Hanser Verlag GmbH, 2015.

[28] E. Ghanbari, Z. Chen, P. Padmanabhan, S. Picken, and J. van Esch. “Supramolecular arrangement and rheological properties of bisamide gels”. In: *Langmuir* 39 (2023), pp. 10913–10924. DOI: https://doi.org/10.1021/acs.langmuir.3c01100.

[29] P. Christiansen, J. Hattel, N. Bay, and P. Martins. “Physical modeling and numerical simulation of V-die forging ingot with central void”. In: *Proceedings of the Institution of Mechanical Engineers, Part C: Journal of Mechanical Engineering Science* 228 (2014), pp. 2347–2356. DOI: https://doi.org/10.1177/0954406213517878.

[30] J. Blanche, M. Strickland, R. Knight, P. Lall, R. Jaeger, J. Suhling, and M. Rahim. “Reliability of flip chip assemblies subjected to extreme low temperatures”. In: *Thermal and Thermomechanical Proceedings 10th Intersociety Conference on Phenomena in Electronics Systems, 2006* (2006), pp. 1379–1389. DOI: https://doi.org/10.1109/ITHERM.2006.1645506.

[31] R. Wool. “Self-healing materials: a review”. In: *Soft Matter* 4 (2008), pp. 400–418. DOI: https://doi.org/10.1039/B711716G.

[32] Y. Yang and M. Urban. “Self-healing polymeric materials”. In: *Chemical Society Reviews* 42 (2013), pp. 7446–7467. DOI: https://doi.org/10.1039/C3CS60109A.

[33] S. Garcia. “Effect of polymer architecture on the intrinsic self-healing character of polymers”. In: *European Polymer Journal* 53 (2014), pp. 118–125. DOI: https://doi.org/10.1016/j.eurpolymj.2014.01.026.

[34] S. Azevedo, A. Costa, A. Andersen, I. Choi, H. Birkedal, and J. Mano. “Bioinspired ultratough hydrogel with fast recovery, self-healing, injectability and cytocompatibility”. In: *Advanced Materials* 29 (2017), p. 1700759. DOI: https://doi.org/10.1002/adma.201700759.

[35] G. Whitesides. “Soft robotics”. In: *Angewandte Chemie International Edition* 57 (2018), pp. 4258–4273. DOI: https://doi.org/10.1002/anie.201800907.

[36] Y. Yokoyama, S. Ichihara, and Y. Tagawa. “High-speed photoelastic tomography for axisymmetric stress fields in a soft material: temporal evolution of all stress components”. In: *Optics and Lasers in Engineering* 178 (2024), p. 108224. DOI: https://doi.org/10.1016/j.optlaseng.2024.108224.

6

OUTLOOK

Benjamin Franklin performed a beautiful experiment using surfactants; on a pond at Clapham Common, he poured a small amount of oleic acid, a natural surfactant which tends to form a dense film at the water-air interface. He measured the volume required to cover all the pond. Knowing the area, he then knew the height of the film, something like three nanometers in our current units. This was to my knowledge the first measurement of the size of molecules.

In our days, when we are spoilt with exceedingly complex toys, such as nuclear reactors or synchrotron sources, I particularly like to describe experiments of this Franklin style to my students.

Pierre-Gilles de Gennes

6.1. INTRODUCTION

In Chapters 2-5, multiple types of measurement were used to highlight the dependence between a biopolymer's rheological properties, and the presence of specific ions in solution. Additionally, Chapters 4 and 5 demonstrate that other analytical techniques, such as ICP-OES, NMR and optical microscopy, can be used in parallel to rheology, to aid the interpretation of structure-property relationships. As shown in literature [1], it is also possible to integrate spectroscopic and optical techniques to conduct *rheo-NMR* or *rheo-optics* measurements respectively. Typically, these coupled measurements help in understanding changes to the (chemical) structure during deformation, and therefore aid in interpreting the observed rheological response; especially within complex multiphase systems. Although these coupled measurements are useful in establishing relevant structure-rheology relationships, access to such advanced techniques, as well as the ease of *on site* implementation, remains fairly limited. In part, these shortcomings are due to the costs associated with the procurement, operation, and maintenance of commercial rheology equipment. Therefore, it is advantageous from a practical perspective, to reduce the dependence on rheology, by grossly simplifying the critical experiments needed for *on site* processes such as quality control.

In light of these requirements, what is shown here is that a simple assessment of the Herschel-Bulkley parameters, may already highlight quantitative differences between samples. In general, this is possible due to the understanding gained by studying multiple biopolymer systems in Chapters 2-5, where a dataset of useful rheological measurements is readily available to facilitate such comparisons. Therefore, in an attempt to leverage the existing data, Section 6.2 focuses on the understanding that can be gained by quantifying Herschel-Bulkley parameters for extracellular polymeric substances (EPS). However, the methods described here are certainly extendable to a wide variety of commercially relevant biopolymer systems. Additionally, Section 6.3 discusses the quantification of the Herschel-Bulkley parameters using *low cost* methods, whereby the limitations highlighted above are overcome even further. Finally, the open challenges relating to both, the measurement of the Herschel-Bulkley parameters, and the collective work carried out in Chapters 2-5, is discussed in Section 6.4.

6.2. EPS MEASUREMENTS

A case study was performed using two samples of acidic EPS that were extracted using the aerobic granular sludge (AGS) from Epe, The Netherlands. The first sample is EPS that was extracted using the typical extraction protocol (see Chapter 4), i.e. dissolution under alkaline conditions, followed by acidification to precipitate the gel sample (using a centrifuge). By contrast, a ceramic membrane with a pore size of 0.2 μm, was used to separate the second sample (in place of the final centrifugation step). The pH and the conductivity of the samples were recorded, before the samples were diluted to a final concentration of 4.5 % w/w using a 2.5 x 10^{-4} M HCl solution. To

ensure complete screening, the conductivity of the samples was maintained above 2 S/m using NaCl. The final pH and conductivity of the sample are reported in Table 6.1.

Table 6.1: pH and conductivity of the samples after adjusting the TS to 4.5% w/w.

Sample	pH	Conductivity (S/m)
Centrifuge	2.18	2.13
Membrane	2.65	2.60

Similar to the earlier chapters, a stress-controlled TA Instruments Discovery Hybrid Rheometer 3 (DHR-3), operated at 298K, was used to carry out the rheology measurements. The Herschel-Bulkley parameters were evaluated using a single stress controlled flow ramp (ramp time = 60s, final value = 0 Pa), using a sandblasted cone (40 mm, 0.035 rad) on sandblasted plate (40 mm) setup to mitigate slip. An initial conditioning step (100 s^{-1}, 30 s) was carried out to erase the sample history. Table 6.2 documents the fitted Herschel-Bulkley parameters for both samples.

Table 6.2: The Herschel-Bulkley parameters of both EPS samples. (± Standard Deviation)

Sample	Yield Stress - σ_0(Pa)	Consistency Index - K(Pa)	Flow Index - n
Centrifuge	0.328 ± 0.003	0.035 ± 0.001	0.735 ± 0.004
Membrane	0.338 ± 0.003	0.060 ± 0.001	0.692 ± 0.003

Based on the discussion provided in Chapter 2, direct comparisons of the coil size (using viscosity data) is permissible, as long as screening mediated interactions are comparable for all systems. From Table 6.2, the lowest conductivity value of 2.13 S/m corresponds to a Na^+ concentration of ~ 0.21 M. At this concentration, the Debye screening length is ~ 0.66 nm at 298 K. As such, this value is suitable to completely screen both, polysaccharides as well as polypeptides (see Chapter 2, [2, 3]). Thus, both systems presented here are completely screened (as intended), and therefore permit discussions of the size. Upon comparing the consistency index values in Table 6.2, it is clear that the consistency index of the EPS extracted using the membrane is ~ 1.7 times larger than the EPS extracted using the centrifuge, and therefore suggests that the former sample has a larger macromolecular gel complex.

Further, as shown in Chapter 3, it is possible to collapse trends in the consistency index of biopolymer systems onto a set of universal curves. Thus, despite carrying out a single measurement in the overlapped regime, the best fit curves from Chapter 3 can be used to estimate the macromolecular gel complex size. As both EPS systems are hydrogen bonded, a lower bound and an upper bound estimation for the size is provided using the slope = 4 and slope = 3 curves respectively (see Chapter 3). The expected range of intrinsic viscosities are summarised in Table 6.3.

Table 6.3: Estimated range of intrinsic viscosities ([η]) for the extracted EPS using the best fit curves from Chapter 3.

Sample	[η] **(m^3/kg)**
Centrifuge	0.075 - 0.136
Membrane	0.078 - 0.163

It is clear from Table 6.3, that the size of EPS extracted using the membrane, is slightly larger than the size of EPS extracted using the centrifuge. As such, these results can be explained using the fact that the membrane lacks the ability to retain particles that are smaller than 0.2 μm. Therefore, the average size of the individual gel fragments (or gel complexes) within the membrane extracted sample, is potentially larger than the gel fragments within the centrifuge extracted sample. Based on the results provided in Chapter 4, it is equally likely that the EPS extracted using the membrane may also have a larger inorganic content, as this leads to the formation of bigger complexes. However, due to the lack of quantitative data confirming changes to the inorganic content, the latter hypothesis may only be confirmed with additional measurements for both EPS samples.

From Table 6.2, it is clear that both samples have comparable yield stresses. As elucidated in Chapter 5, the presence of a yield stresses within jammed deformable hydrogel suspensions such as EPS highlights the ability of neighbouring hydrogel particles to dynamically "stick" to each other. Therefore, it appears that by adopting the membrane filtration setup, no detrimental changes were made to the inherent ability of the gel particles to adhere with one another.

6.3. LOW COST METHODS

Throughout this thesis, measurements of the Herschel-Bulkley parameters was carried out using a stress-controlled rheometer. However, to facilitate the ease of estimating the Herschel-Bulkley parameters *on site*, alternative *low cost* methods can be used [4, 5] to atleast quantify the yield stress. Some of these methodologies were developed in parallel to the studies carried out here (in collaboration with van der Vaart [4]), and a brief description of these methods is described further. It is worth remarking that these *low cost* methods are consistent with analogous practices for paints and lubricants, concrete, food products [6–8], etc. Therefore, they find their relevance within multiple industries, and aid the processing of commercial products.

As shown in Figure 6.1, commercially available laboratory equipment was used to measure the yield stress of xanthan gum solutions. In all cases, the mass density (ρ) of the fluid retained either on the surface of the plate, or inside the funnel / capillary tube, can be used in combination with a critical dimension (d_c), to calculate the yield stress under gravitational loading:

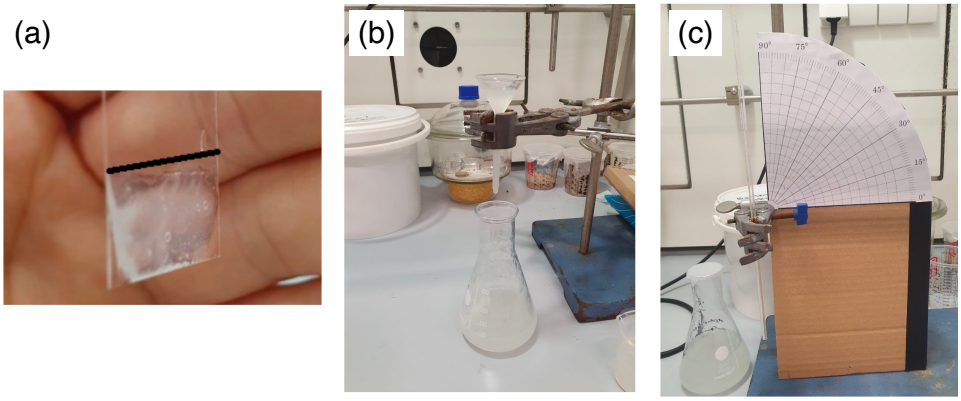

Figure 6.1: *Low cost* methods used to determine the yield stress of xanthan gum solutions [4]: (a) using a roughened (glass) plate, (b) using a funnel, and (c) using a capillary tube.

$$\sigma_0 = \rho g d_c \tag{6.1}$$

Here, g corresponds to the acceleration due to gravity (~ 9.81 m/s^2). In case a plate is used to calculate the yield stress, d_c corresponds to the thickness of the fluid film on the surface of the plate. It is worth noting that good adhesion between the plate and the fluid film is important to guarantee accuracy of results (see Figure 6.1 a). In case a funnel or capillary tube is used to calculate the yield stress, d_c corresponds to the critical diameter at which the fluid stops flowing. As shown in Figure 6.1 c, the angle (θ) made by the capillary tube with respect to the horizontal plane can be changed further to control the resolution of the gravitational loading force. In such cases, Equation 6.1 becomes:

$$\sigma_0 = \rho d_c \cdot g sin(\theta) \tag{6.2}$$

Based on the observations reported by van der Vaart, the use of capillary tubes yielded results within an error margin of ~ 20% when compared to the rheometer. However, it is worth noting that a significant yield stress was needed (~ 10 Pa) to ensure these levels of accuracy. In general, the limited sensitivity of these *low cost* methods is attributable to the dimensions and tolerances of standard laboratory equipment. As an alternative, these components can be produced specifically for yield stress measurements, as they are still appealing, *low cost* alternatives to a commercial rheometer.

6.4. OPEN CHALLENGES

The challenges from the Herschel-Bulkley measurements discussed in this chapter may be summarised as follows:

1. In the particular example of EPS, the Herschel-Bulkley parameters are unsuccessful in providing clarity about the inorganic vs. organic (or non-macromolecular vs. macromolecular) content. In cases where gross differences are not expected for the (macromolecular) composition, this is not a limitation, and these parameters may be instruments in providing insight about the molar mass. Although, as the lack of changes to the composition cannot be guaranteed in all cases, the development of additional techniques that simplify the *on site* inorganic analysis is highly encouraged. As such, a comprehensive guide, outlining a great number of spot tests for inorganic analysis, is readily available [9]. However, given that the development of spot tests remains fairly outdated, and that biopolymers in solutions can exhibit great selectivity in binding with particular ions, there is an impetus that encourages the development of these tests specifically for biopolymer systems.

2. Although yield stresses may be meaningfully evaluated using the gravity driven capillary tube setup, the estimations of other Herschel-Bulkley parameters using this setup needs careful consideration. This is because, the capacity of fluids to undergo shear thinning, appears to be sensitive to the height of the fluid column within the capillary tube [4]. Other effects, such as the wall roughness, slip, and improper wetting can also be expected to influence the accuracy of measurements. As these effects were not studied in detail, a closer understanding of this dependence is certainly possible, and is therefore earmarked as a task for future work in this direction. If successful viscosity measurements can be carried out, by closely controlling the shear rates, it is possible to unify the collective findings within this thesis, in combination with a convenient and widely adoptable measurement technique, to characterise a variety of relevant biopolymer systems *on site*.

The open challenges from the broader context of this thesis may be summarised as follows:

I. **Advancing Polymer Physics**: Chapter 1 of this thesis specifically outlines the lack of physical models that capture the structure-rheology relationships of weak polyelectrolytes such as biopolymers. As a result, Chapters 2-5 try to capture the impact of parameters such as pH and ionic strength. However, there is sufficient scope to integrate the understanding gained by modifying these two parameters, with the traditional understanding that is based on temperature / thermal energy ($k_B T$). As such, it is useful to model the dependence on temperature for specific biopolymer systems such as proteins, where the secondary structures may be denatured to yield an *athermal* solution [10–12]. In this case, temperature is simply used to increase the *excluded volume* between oppositely charged monomers of a polypeptide chain [12]. By contrast, what is being highlighted here, is the limited scope with which charge mediated interactions can be modelled using *virial coefficients*. Not only can these *virial coefficents* explain the trends observed for the Herschel-Bulkley consistency index (see Chapter 3), but they may also be successful in unifying

osmotic pressure measurements with viscosity measurements. In turn, this would provide a means of correlating the second *virial coefficient* term with the Huggins coefficient, thereby overcoming a critical knowledge gap in the field of *(bio)polymer physics* [13, 14].

II. **Abstracting Complexity**: Based on the studies carried out in Chapters 2-5, it appears that the structure-rheology relationships of a significant number of polysaccharides, proteins / polypeptides, and glycoproteins can now be explained using a simplified and abstracted charged structure. Despite these well intended efforts, it is worth noting that nature has the capacity to evade such simple descriptions, and can present complex biopolymers that pose a new set of challenges. Chapter 2 already describes the difficulty in quantifying charge mediated swelling / shrinkage in the coil size of ampholytic polypeptides. As if to complicate matters further, it is possible to identify a subset of glycoproteins called *proteoglycans*, that have polysaccharides known as *glycosaminoglycans* [15]. These *glycosaminoglycans* can have multiple charged functional groups, thereby increasing the structural complexity of charged molecules even further. The molar mass of these *glycosaminoglycans* is also much larger than the mono-, di- or oligosaccharides typically found in other glycoproteins [15]. This poses additional constraints to the persistence length, as well as the conformation freedom of *proteoglycan* coils. Therefore, while it has been possible to unify a significant number of biopolymer systems under the same collective rheological framework, it is encouraged that the work carried out in this thesis be extended to definitively cover known *proteoglycans*. This would assist in developing the structure-rheology relationships of a wider variety of relevant biopolymer systems.

III. ***High-Performance* Biopolymer Solutions**: Although this thesis tries to provide a comprehensive list of structure-rheology relationships that are relevant for a wide variety of engineering applications, it does not focus on any particular engineering problem that may be solved using biopolymers. Indeed, depending on the stringency of constraints, unique properties such as (ultra) high strength, (relatively) high stiffness / modulus, or flame retardancy may become desirable. In a typical setting, such *high-performance* characteristics are exploited by fabricating composite materials that specifically meet these design requirements [16]. However, it is worth recognising that such highly specific design requirements have already been addressed by biopolymer systems found in nature. For example, *Sequoia sempervirens* (California redwood), are amongst the tallest known trees in the world, and can reach heights of up to 130 m [17]. Despite being made of wood, the trunk section close to the ground, can easily support the weight of the entire tree above it without undergoing buckling. Therefore, it is an example of a high strength biopolymer composite material. Analogously, nacre (*mother of pearl*) is a naturally occurring biocomposite material that is capable of exhibiting moduli values comparable to metals such as aluminium (~ 70 GPa) [18]. This is an order of magnitude higher than the moduli of the synthetically produced polymer glasses, or indeed

plasticised semi-crystalline polymers [16]. Finally, polysaccharides such as alginate can exhibit thermo-mechanical stability up to a temperature of 160 °C (433 K) [19]. This makes them ideal, to be combined with materials such as nanoclay, and form nanocomposite foams that are capable of exhibiting excellent flame retardant and heat deflection capabilities [20]. These examples barely scratch the surface of what is possible using biopolymers, and do not cover for instance, *extremophilic* systems that are capable of surviving some of the harshest natural environments in terms of pH, salinity, temperature, radiation, vacuum, etc. [21]. It is clear then that biopolymers may also be particularly useful in circumstances that do not permit the use of conventional engineering materials. Thus, as a reiterative message that encourages retention, the ability to grow engineering applications using novel biopolymers, may only be limited by the imagination and effort needed to identify systems with relevant structure-property relationships.

REFERENCES

[1] R. Kádár, S. Spirk, and T. Nypelo. "Cellulose nanocrystal liquid crystal phases: Progress and challenges in characterization using rheology coupled to optics, scattering, and spectroscopy". In: *ACS Nano* 15 (2021), pp. 7931–7945. DOI: https://doi.org/10.1021/acsnano.0c09829.

[2] C. Lopez. "Entanglement of semiflexible polyelectrolytes: Crossover concentrations and entanglement density of sodium carboxymethyl cellulose". In: *Journal of Rheology* 64 (2020), pp. 191–204. DOI: https://doi.org/10.1122/1.5127015.

[3] R. Corey and L. Pauling. "Fundamental dimensions of polypeptide chains". In: *Proceedings of the Royal Society B: Biological Sciences* 141 (1953), pp. 10–20.

[4] M. van der Vaart. "Yield Stress Estimation of Biopolymers: Testing different methods on the reproducibility and accuracy". Bachelors' Thesis. Delft University of Technology, 2022.

[5] P. Wilfert, M. van Loosdrecht, S. Velasquez Posada, S. Picken, C. Chassagne, Y. Lin, A. Raja, G. Kleine, A. Shajimon, L. Chen, *et al.* "Kaumera Methods Manual: A comprehensive guide to lab extraction and characterization methods for extracellular polymeric substances (EPS)". Delft University of Technology, 2024.

[6] A. C. Gaquere-Parker, N. A. Doles, and C. D. Parker. "Chemistry and art in a bag: an easy-to-implement outreach activity making and painting with a copper-based pigment". In: *Journal of Chemical Education* 93 (2016), pp. 152–153. DOI: https://doi.org/10.1021/acs.jchemed.5b00364.

[7] Colad. *Mixing Cups*. URL: https://www.colad.com/en_gb/painting/paint-preparation/mixing-cups/mixing-cups.

[8] C. F. Ferraris and F. de Larrard. "Modified slump test to measure rheological parameters of fresh concrete". In: *Cement, Concrete, and Aggregates* 20 (1998), pp. 241–247. DOI: https://doi.org/10.1520/CCA10417J.

[9] F. Feigl and V. Anger. *Spot tests in inorganic analysis*. Amsterdam, The Netherlands: Elsevier, 2020.

[10] D. Nelson, M. Cox, and A. Hoskins. *Lehninger Principles of Biochemistry*. New York, NY, USA: Macmillan Learning, 2021.

[11] K. te Nijenhuis. "On the nature of crosslinks in thermoreversible gels". In: *Polymers Bulletin* 58 (2007), pp. 27–42. DOI: https://doi.org/10.1007/s00289-006-0610-7.

[12] M. Rubinstein and R. Colby. *Polymer Physics*. Oxford, UK: Oxford University Press, 2003.

[13] R. Sayko, M. Jacobs, and A. Dobrynin. "Quantifying properties of polysaccharide solutions". In: *ACS Polymers Au* 1 (2021), pp. 196–205. DOI: https://doi.org/10.1021/acspolymersau.1c00028.

[14] J. Pathak, S. Nugent, M. Bender, C. Roberts, R. Curtis, and J. Douglas. "Comparison of Huggins coefficients and osmotic second virial coefficients of buffered solutions of monoclonal antibodies". In: *Polymers* 13 (2021), p. 601. DOI: https://doi.org/10.3390/polym13040601.

[15] G. Moss. "IUPAC-IUB Joint Commission on Biochemical Nomenclature (JCBN). Nomenclature of glycoproteins, glycopeptides, and peptidoglycans". In: *Eur. J. Biochem., 159, 1-6 (1986); Glycoconjugate J., 3, 123-124 (1986); J. Biol. Chem., 262, 13-18 (1987); Pure Appl. Chem., 60, 1389-1394 (1988); Royal Society of Chemistry Specialist Periodical Report, 'Amino Acids and Peptides', vol. 21, p. 329 (1990); ref. 2, pp. 84-89.* (2025).

[16] M. F. Ashby and D. Cebon. "Materials selection in mechanical design". In: *Le Journal de Physique IV* 3.C7 (1993), pp. 1–9. DOI: https://doi.org/10.1051/jp4:1993701.

[17] G. W. Koch, S. C. Sillett, G. M. Jennings, and S. D. Davis. "The limits to tree height". In: *Nature* 428 (2004), pp. 851–854. DOI: https://doi.org/10.1038/nature02417.

[18] A. Jackson, J. Vincent, and R. Turner. "The mechanical design of nacre". In: *Proceedings of the Royal society of London. Series B. Biological sciences* 234 (1988), pp. 415–440. DOI: https://doi.org/10.1098/rspb.1988.0056.

[19] J. Zlopasa. "Exploring the Structure, Properties, and Applications of Highly Ordered Bionanocomposites". Doctoral Dissertation. Delft University of Technology, 2017. DOI: https://doi.org/10.4233/uuid:e47bfa54-4d58-4c82-829f-3cb2ceb6cfc7.

[20] A. Raja. "Cellular Solids Based on Biopolymer Nanocomposites: For Hypersonic Heat Shields Aboard Sounding Rockets". Masters' Thesis. Delft University of Technology, 2020. URL: http://resolver.tudelft.nl/uuid:1b4598f6-124d-40f8-9228-d98f8aba31cc.

[21] L. J. Rothschild and R. L. Mancinelli. "Life in extreme environments". In: *Nature* 409 (2001), pp. 1092–1101. DOI: https://doi.org/10.1038/35059215.

ACKNOWLEDGEMENTS

"Scientific breakthroughs do not happen in isolation; progress depends on the collective contributions of many."

David Baker, Nobel Prize banquet, 2024

Dear Stephen, if my observations are astute, then we do not fit the traditional labels of *mentor* and *protégé*. In many ways, this joint journey has provided me with the opportunity to question my fundamental ideologies about life. Indeed, it would have been naive on my part to have worked with biopolymers, and not to have ruminated about the metaphysical fabric of my existence. With your help, I was equally successful in imbibing important virtues such as patience, stoicism, and humility. I credit these virtues as being the factors that have helped my thought, and my faculties to develop this far. Therefore, I am forever grateful for your ability to lead by example, and for the numerous life lessons that you have given me.

Dear Philipp, typically, it is said that "two's company, and three's a crowd". Yet, our fruitful collaborations with Stephen has proven this wrong on numerous occasions. I imagine that we are the exception due to your unique ability to look past the triviality of things. Despite me being rough around the edges, you have meticulously helped me reinforce my strengths and my abilities. In part, this is because you abandoned all formality, and treated me as your friend; even when you had the newfound responsibility of fathering your own child. In return, I promise to uphold my end of the bargain, and will continue to return the countless favours that I owe you.

If my PhD candidacy is a journey, then Kaumera® is definitely its point of origin. This single word has brought me in touch with numerous people, all of whom are specialists in their own right. **Mark, Yuemei, Claire, Leon, Nouran, Lemin, Gijs, Adarsh, Waqas, Basem, Sofia, and Bart**, thank you for your fruitful collaborations over the years. Without you all, I would have never had the opportunity to discover the encyclopaedia of useful experimental techniques. I am equipped to traverse all future journeys within the scientific landscape thanks to the expertise you all have provided me. **Jure** and **Suellen**, although our collaborations have been of a different nature, I would say that the two of you have co-authored a very useful book that complements this encyclopaedia: "Surviving in Academia - For Dummies" ☺. Thank you, for all the undocumented supervision that the you have provided me over the years. I could not have overcome the steep learning curves without the two of you.

Moving on to the positive workforce that I encountered during my day-to-day activities. **Jan, Eduardo, Wolter, Rienk, Laura, and Veby**, thank you for being such wonderful members of staff within ASM. In the wake of growing concerns surrounding social safety, I can affirmatively say that ASM is successful in hosting an open minded work environment that welcomes people from all walks of life. **Aleksandra, Sietse, Marcel, Stephen Eustace, Duco, Xiaohui, and Bart Boshuizen**, through first hand experience from having to manage the rheology lab, I can declare undoubtedly, that the contributions of technicians is severely overlooked within academic circles. Collectively, you represent the foundation of all successful experiments within ASM. Therefore, I sincerely acknowledge the support that I have received from all of you. **Bowen, Peggy, Yu, Jianan, Bohang, Reece, Sarah, Benjamin, Irene, Guotai, Hendrik, Benni, Anastasiia, Elmira, Ardeshir, Mark Kwakernaak, Juncheng, Tamar, Jacqueline, Daniel, Andrey, and Dnyandevi**, individuals are only as smart as the people they surround themselves with. Thank you for all the engaging conversations, the amazing parties, as well as the ASM cricket match. If I am a smart man, it is because I have learnt a great deal about a diverse set of cultures, and about science itself from all of you. A special thanks to **Min**, who very kindly donated multiple 10 mm tubes on short notice, thereby assisting my NMR measurements. **Pouyan and Valeria**, despite our limited interactions, you have contributed greatly to my academic trajectory. I thank the two of you for helping me establish myself as an independent rheologist. **Georgy**, you are a strong and beautiful force of nature that ushers a wave of positivity into everyone's lives. I would like to return the favour by saying that, if a third person is reading this, please send him the coolest microscopes that you may have. **Adarsh, Jasmeen, Christel, Sophie, Sven, Henri, Dominik, Kalani, and Margareth**, thank you for letting me shoulder your burdens as a fellow PhD Council member. The happy moments we have spent together represents a great deal of positive change that we have brought about within the ChemE department. To **Dennis, Tessel and Mark de Geus**, I welcome you to ASM, and wish that you have successful tenures in TU Delft. We deserve more young and dynamic minds like the three of you.

Maartje, Menno, and Anne, you were all grade A BEP students, and rightfully deserve to have successful professional lives. Thank you for providing me with the opportunity to mentor you. I would like to particularly acknowledge **Wanyu Dong**. As a mentor, I can only hope to leave a lasting and positive impression in my students' mind. But as Andy Dufresne said, "hope is a good thing, maybe the best of things, and no good thing ever dies". Although I was never your primary supervisor, we have shared some wonderful exchanges about rheology following your graduation. I am grateful for all the messages that I have received from you, and wish you the very best with your career.

Ajo, the two of us have come a long way in life. I can always sleep easy knowing that I have your support through thick and thin. Just like me, I know that great things are waiting for you right around the corner, as you rightfully deserve all the good things that come your way. **Push, Moonmoon, Deus Vult, Rajajinagar Robin, Leon from Sweden, and Ballapur**, the cringy, over the top Whatsapp shenanigans is what has fuelled my dopamine spikes on dark and depressing mornings. I thank you for accommodating my unreason-

able and overbearing projections. Although I have contested grave battles in academia, it pales in comparison to the battles you have contested with your personal lives. Despite that, you have continued to support me, and proven to me that you are wonderful human beings. Godspeed. **Rammohan Sir and Shrikanth Sir**, I am crossing this finish line, only because the two of you continued to believe in my abilities. I wish that every other student in India finds teachers just like the two of you. **Lars and Esmée**, thank you for providing me with a home when I needed it the most. Van Lodensteynstraat, and all the wonderful moments that we have spent there, will live on forever as cherished memories for the rest of my life.

This thesis would have been impossible without the support of some people that matter more than everyone else. **Mummy, Papa, and Jaideep**, I am so happy to have found a new home away from home in Chembur. I am forever grateful that you chose to accept me as a member of your family. In the very limited time that we have known each other, you have accepted me for who I am, and have already gone out of your way to support me in my endeavours. In return, I promise to always support you, as a son would support his own family. **Amma, Appa, Adi and Paati**, ever since I embarked on my personal journey to the Netherlands, you have contended with a lot of battles without my support. Some of these include deeply emotional battles due to personal losses, and due to my prolonged separation from the rest of you. In trying times like these, I am happy that we have always found the strength to overcome our problems, and tried to achieve things that puts an end to our struggles. This PhD is a mark of victory, for all the battles you have fought in the background without me.

To my dear wife Janani, there are a great deal of things that I have planned for in life. Yet, the best companion that I have ever received is an unplanned surprise. When I think about us, I am always reminded about the first video call that I had with Roger Federer's sister. Although I was tired and isolated due to the COVID-19 infection, you somehow managed to put a smile on my face, and touched my heart with your sincerity. Ever since then, you have always put my dreams first, and travelled half way across the world, just so that I may complete my thesis. Although I am flawed in so many aspects, you somehow look past those flaws and continue to cherish me for who I am. Jannu ma, even if I planned my every move, I could not have found a partner that loves me, or cares for me, as much as you do. I strive to become a better husband in every fleeting second that we spend together, and am forever indebted to you. Which is why I dedicate this thesis solely to you.

Anand Raja

April 2025,
Delft, The Netherlands.

Curriculum Vitæ

Anand Raja

30/12/1995	Born in New Delhi, India.
08/2014 - 05/2018	**Bachelor of Technology - Mechanical Engineering** PES University - Bengaluru, India *Specialisation*: Engineering Design (Continuum Mechanics) *Minor degree*: Computer Science and Engineering *Thesis*: Computational Challenges of Multifunctional Composites *Supervisor*: Prof. dr. Rammohan Bhanumurthy
09/2018 - 11/2020	**Master of Science - Materials Science and Engineering** Delft University of Technology - Delft, The Netherlands *Specialisation*: Aerospace Structures and Materials *Thesis*: Cellular Solids Based on Biopolymer Nanocomposites *Supervisor*: Prof. dr. Stephen J. Picken
04/2021 - 04/2025	**PhD Candidate** Advanced Soft Matter Group, Department of Chemical Engineering, Faculty of Applied Sciences, Delft University of Technology - Delft, The Netherlands
05/2025 - 07/2025	**Research Engineer** Kaumera Sales & Services BV - The Netherlands

Notable Achievements

2017	2nd Position, TEAM 3 – PACE Global Annual Forum
2018	10/10 – Bachelors' Thesis
2019	1st Position, Formula Student Netherlands
2023	Best Oral Presentation Award – IHE PhD Symposium
2024	Successful Test Flight of SHEAR – REXUS 32 Campaign

List of Publications

1. M. Valibeknejad, F. Heidari, S. M. Mihaila, R. Alizadeh, S.M. Abdoli, **A. Raja**, P.E. Boukany, J. Quodbach, A. Raoof. "Intestinal villi as micro static mixers: Experimental and numerical investigation on a chip". (*In Preparation* - 2025)

2. **A. Raja**, P. Wilfert and S. Picken. "Investigating the properties of extracellular polymeric - cation complexes from aerobic granular sludge." Submitted to: *Bioresource Technology* (2025)

3. **A. Raja** and S. Picken. "The dynamic yielding phenomena of jammed deformable hydrogel suspensions at very small strain amplitudes". Under review: *Soft Matter* (2025)

4. **A. Raja**, P. Wilfert and S. Picken. "Charge mediated changes to the intrinsic viscosity of biopolymer systems". In: *Polymers* 16 (2024), p. 2894. DOI: https://doi.org/10.3390/polym16202894

5. **A. Raja**, P. Wilfert and S. Picken. "Using the Herschel–Bulkley consistency index to characterise complex biopolymer systems – The effect of screening". In: *Polymers* 16 (2024), p. 2822. DOI: https://doi.org/10.3390/polym16192822

6. P. Wilfert, M. van Loosdrecht, S. Velasquez Posada, S. Picken, C. Chassagne, Y. Lin, **A. Raja**, G. Kleine, A. Shajimon, L. Chen, *et al.*. "Kaumera Methods Manual: A comprehensive guide to lab extraction and characterization methods for extracellular polymeric substances (EPS)". Delft University of Technology, 2024.

7. E. Menting, J. Huiskes, **A. Raja**, and S. Picken. "The Implementation of the alginate montmorillonite nanocomposite foam into heat shields". In: *Proceedings of the International Astronautical Congress, IAC* C2 (2021)